Department of Structural, Geotechnical and Building Engineering

Master's degree in civil engineering

Experimental investigation on the rheological behavior of bentonite slurries for SS-TBM excavation

Supervisors

Prof. Daniele Peila
Prof. Carmine Todaro
Eng. Alfio Di Giovanni

Candidate

Gabriele Destefanis

A.Y. 2024/2025

5th December 2025

Abstract

Slurry Shield Tunnel Boring Machines (SS-TBM) are soil machines widely employed for underground excavation in urban environments, where excavation at shallow depths in soft, unconsolidated and water bearing-soil, poses major challenges related to face stability and ground settlement. These machines use a bentonite-based slurry to maintain counter pressure, prevent groundwater inflow, and ensure the stability of the excavation face. However, the rheological properties of bentonite slurries can be significantly affected by mechanical degradation during excavation, which may lead to viscosity reduction, problems in pressure transmission and filter cake formation, potentially leading to face instability or slurry losses.

This research investigates the rheological behavior of eight different bentonites, used to prepare slurries at varying concentrations, subjected to controlled mechanical stress in order to simulate, at laboratory scale, the stresses at which the slurries are subjected during SS-TBM excavation.

A preliminary characterization was performed through swelling index, to identify the main physical properties and classify bentonites based on objective parameters, providing a useful framework for interpreting the rheological results.

Subsequently, rheological measurements were performed on both unstressed and mechanically stressed slurries using the Marsh cone test, viscometer, and density and temperature assessments. In addition, a basic evaluation of the slurry-soil interaction was carried out, by investigating filter cake formation and quality, to study the influence of the rheological properties on its development. The study focuses on evaluating how the rheological behavior of bentonite slurries evolves under shear stress, highlighting the relationship between viscosity variation, bentonite type, concentration and applied mechanical stress. These results contribute to a better understanding of bentonite behavior under operational conditions and provide useful guidance for optimizing slurry management in tunnelling applications.

Index

List of figures

List of tables

1 Introduction

How many times in life do we hear the words: “Face problems and don't beat around the bush?” This same idea has driven humans during history to face one of the most challenging construction activities: excavating rocks to build passages and tunnels. The metaphor between everyday struggles and tunnel construction is quite fitting, in both cases there is something that a person needs to face, an obstacle that requires perseverance and determination to overcome. For engineers, the obstacle is represented by technical challenges, for people, by the problems of everyday life.

The necessity of passing through something to create a more efficient, fast and clean way to reach a certain destination has always led the minds of constructors and engineers to improve the excavation method. Research and study, over time, were the key in finding new technical ways and better materials, to define optimal methods for tunnel excavation through all ground conditions, from the hardest rock to the softest soil.

The first excavated tunnel in Italy dates back to 500 years ago, the so called “*Buco di Viso*” excavated in two years, between 1478 and 1480. The tunnel had a total length of 80 meters and a maximum diameter of 2.5 m, located at an altitude of 2880 m a.s.l (figure 1.1). The tunnel was wanted by Ludovico II, from Vasto, Marquis of Saluzzo, to intensify the international traffic of goods. Thanks to the tunnel was possible to pass by walk from Italy to France, avoiding the steep Traversette pass, just higher up in altitude, but a lot harder to cross due to fog and snow in winter season. The tunnel excavation technique adopted was rudimental, using pickaxes, workers created small cracks in the rocks, then pour hot water mixed with vinegar into these fissures and lit controlled fires. This method slightly softened the rock, allowing them to advance easily with the pickaxes. (*Il Buco di Viso: il primo traforo delle Alpi,* Torinostoria, 2025).

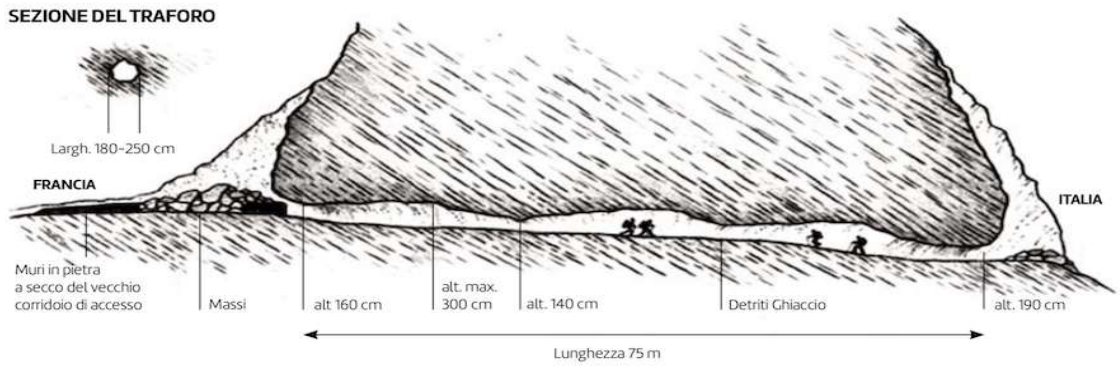

Figure 1.1 - Horizontal section of the “Buco di Viso” (Torinostoria)

From this first walkable tunnel, the progress in excavation began to increase exponentially. A lot of events in history push forward the study of underground construction. Starting from the world wars, soldiers built trenches at the front and underground tunnels to move safely without being exposed to the enemy. On Mount Grappa (1775 m a.s.l.), the "*Vittorio Emanuele III*" tunnel system was rapidly constructed using innovative excavation techniques. The complex consisted of numerous branches and tunnels; it housed a lot of artillery, starting from cannons, machine guns, as well as food storage areas and a lot of other space, with accommodation for 1500 soldiers. During the Second World War, further progress in underground construction was achieved, as bomb shelters spread in all cities across Europe, to protect the civilians from air raids.

In more recent years, globalization has increased the demand of new safe and faster transportation routes. This need for a global interconnection pushed governments to construct new tunnels allowing goods, people and information to move rapidly across borders, mountains and even under the sea. A lot of new tunnels have been constructed, shedding light on some of the most incredible engineering masterpieces, starting from the first important railway tunnel, the Fréjus tunnel, between Italy and France, constructed in 1871, the Gotthard base tunnel and the Eurotunnel, the latter connects France and England, with a rail tunnel under the Strait of Dover.

From the "*Buco di Viso*" built by pickaxes, technological progress has provided the means to meet these challenges. Research, study, and the development of innovative techniques have greatly advanced geotechnical and tunnelling knowledge. The most widely employed excavation technique is the traditional method, which involves the use of explosive and auxiliary support systems like steel arches, steel pipe umbrella, shotcrete or fiberglass, to keep the face and the crown safe. A revolution in the tunnel excavation method comes with the introduction of the Tunnel Boring Machine (TBM), which enabled faster and safer excavations even in complex geological conditions. This huge machine excavates full-face tunnel with incredible efficiency, thanks to their versatility has also made feasible projects that were previously unimaginable with traditional excavation methods.

The complexity of this new technology brings an incredible number of elements that must be analysed and understood, since behind each of them there may be potential issues if not properly investigated in advance. This highlights the fundamental importance of research, which allows us to identify and understand the characteristics, functions, and properties of each component, knowledge that can be crucial to improving performance in every field of engineering.

This research study presents an experimental investigation aimed at defining the rheological behavior of bentonite slurries used in Slurry Shield Tunnel Boring Machine (SS-TBM), in static conditions and when subjected to mechanical stress. Among the different types of soil TBM, SS-TBMs are a valid solution for tunnelling in geological context composed of soil that have not experienced high confinement stresses and are therefore soft, unconsolidated or weakly cohesive. These soils typically consist of sand and gravel, with low percentage of silt and clay, and are often saturated due to the high groundwater tables.

The main challenges in these geological conditions are groundwater inflow and settlement control. When tunnelling beneath urban areas, the induced settlement must be kept within limits compatible with the safety of buildings and any kind of surface infrastructure.

SS-TBM effectively addresses these challenges thanks to the counter-pressure applied at the tunnel face by means of bentonite-based slurry. The slurry, a mixture of water and bentonite, plays a fundamental role during excavation because its physical and rheological properties significantly impact tunnelling performance. Slurry forms a thin filter cake on the excavation front, preventing water inflow. In additions it is essential for stabilizing the tunnel face and keeping the excavated material in suspension, which is later extracted via a pumping mechanism.

Several influencing factors can lead to bentonite properties and behavior variation, leading to possible operational issues during excavation. One critical aspect is the change in rheological behavior when the slurry is subjected to mechanical stress. As will be discussed in the following chapter, during SS-TBM excavation, bentonite slurries are constantly exposed to mechanical stress, and their response under these conditions must therefore be controlled to prevent potential problems. An experimental campaign was carried out to analyzed how bentonite slurries react after being subjected to controlled mechanical stress applied through rotation using a laboratory mixer with its propeller. After a preliminary characterization of the bentonites through swell index, the rheological properties were measured both before and after the application of stress, using a Marsh cone and viscometer. The results were then analysed to evaluate how the rheological behavior varied according to bentonite type, concentration and applied mechanical stress.

2 Tunnel Boring Machine (TBM)

Tunnel boring machines are among the most important technical advancements in the history of tunnelling. They consist of long, cylindrical machines, with a cutterhead at the front, which, through rotation and pressure exerted on the tunnel face by their tools, are able to excavate in various underground conditions.

The first concept of a machine capable of excavating the rock, as a substitute for the unsafe hand mining method, was introduced in 1845, when the king of Sardinia, Charles Albert, commissioned to digging of the Fréjus rail tunnel between France and Italy, through the Alps. To accomplish this task, the Belgian engineer Henry Maus designed a machine composed of more than one hundred percussion drills mounted at the front of a locomotive and mechanically power-driven. Despite the effort invested in its construction and research, the revolution of 1848 affected the available funding, and the tunnel was completed ten years later using traditional and less expensive methods. From this initial attempt, the research in the field of TBM continues, leading in 1853 to the development of a TBM with mechanisms more like those employed today. The American inventor Ebenezer Talbot patented a TBM that used cutting discs mounted on rotating arms, which were then installed on a rotating head.

The evolution of TBM has led to the possibility of excavating tunnels rapidly and safely. Modern TBMs are now capable of operating in both hard and soft terrain, including saturated soil, by adapting the type of machines and equipment. Nevertheless, the drill and blast method or other conventional excavation techniques are still employed in certain cases, particularly when geological conditions are extremely challenging or when these methods prove to be more effective and cost-efficient.

The selection of the most suitable TBM for a specific case of study is based on several key parameters that characterize the ground and the influence of the excavation process.

- Geological and geotechnical parameters: lithology, UCS (in case of rock excavation), degree of fracturing and grain size distribution.
- Hydrogeological parameters: groundwater pressure, soil permeability.
- Design parameters: diameter, length and overburden.

By investigating the terrain conditions, focusing on the above-mentioned parameters, the most suitable TBM can be identified among the different types available. The first distinction is between rock TBMs and soft ground TBMs. Rock TBMs are further classified into open

and shielded, while soft ground TBMs are divided into Earth Pressure Balance (EPB) TBMs and Slurry Shield TBMs. Recent developments have led to the creation of new TBM technologies, as the Multi-mode TBM and the Variable-Density TBM, which are particularly valid for mixed ground conditions (Herrenknecht AG website). Each of these machine types will be discussed accurately in the following paragraph.
Although all these distinctions, some components are common to all TBMs, especially those elements related to the machine function and mechanical components:

- The cutterhead, whose characteristic depends on the TBM types and terrain to be excavated. It can be equipped with cutting discs for rock or scraper tools for soft soil
- The drive unit that enables the cutterhead to turn, composed of all electrical, hydraulic and mechanical components
- The main motors that provide propulsion to the entire system, usually composed of synchronous or asynchronous electric motors distributed around the cutterhead. The power can be of few hundred kW in a small TBM to several MW in large machines.
- Gearboxes, that enable to reduction of the speed to the required value of the cutterhead rotation.
- The main bearing, that is the most important structural component, enables the rotation of the cutterhead and transmits all the forces.

The supply of the tunnelling machine is provided in the back-up that brings the total length of the TBM up to 150 m. The back-up is made by the steel structures, and contains all hydraulic units, pumps, also control cabinets, ventilation system and laser measurement technology, in addition recreational areas, offices and rescue containers for tunnelling crew, and the handling equipment for transporting the segment to the site. All the information, data and important values for the tunnelling advancement come together in the central control container, where they are visualized on a monitor and provided to the machine operator, who can adjust every single parameter for a correct excavation if necessary.

2.1 Rock TBM

Rock TBMs are mainly used in hard rock ground conditions. Developed in 1956 from the idea of engineer James Robbins, their use rapidly expanded as they quickly demonstrated a significant advancement rate, also in challenging geological conditions. As previously mentioned, they are divided into open TBM and shielded TBM, although many characteristics are common between the two types.

The core component of a rock TBM is its circular rotating cutterhead, which can be manufactured in different diameters: from 4 meters, in micro tunnelling applications, up to 9-12 meters in large-scale projects designed to excavate tunnels for vehicles and high-speed railways.

On the cutterhead are mounted the disc cutters, circular steel discs, typically ranging from 432 to 483 mm in diameter, free to rotate around a pivot that connects them to the cutterhead. They can operate alone or in pairs, and are characterized by different possible ring profiles, depending on the rock type. Based on their position on the cutterhead, they are classified as centre cutter, face cutter or gauge cutter, the latter positioned on the periphery of the cutterhead, forming the overcutting device (figure 2.1). This system enlarges the excavation diameter beyond the outer dimension of the lining, thereby reducing friction between the machine and the surrounding ground and creating sufficient space for the installation of the tunnel lining. Another key element present on the cutterhead are the buckets, which collect the detached material during excavation and convey it toward a conveyor belt to transport the material outside the tunnel.

1- Gauge cutter
2- Bucket
3- Centre cutter
4- Face cutter

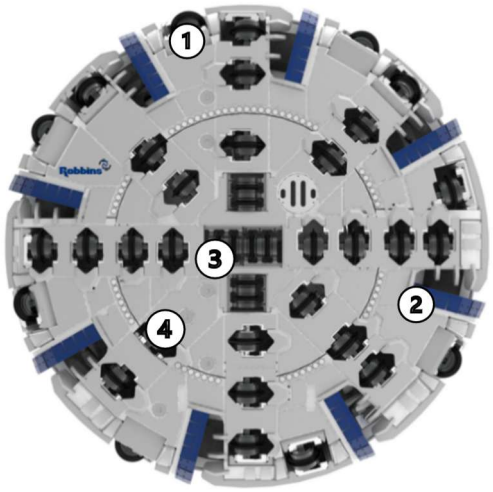

Figure 2.1 - Rock TBM cutterhead and his component (The Robbins company, 2025)

Rock TBM uses a thrust bearing to simultaneously provide both rotation to the cutterhead and the application of longitudinal thrust against the face. By concentrating the applied load on the small contact area of each cutter, fractures are induced in the rock through a process of chipping and spalling. The spacing between cutters is carefully designed to follow concentric paths at different radial distances from the centre in order to minimize wear and ensure uniform excavation. The distance between cutters should be sufficiently close to allow the connection of cracks generated by adjacent cutters, ensuring the detachment of rock chips from the tunnel face.

Cutterhead bucket collects the excavated material and channels it onto a conveyor belt that runs along the entire length of the TBM, which transports it towards the tunnel portal and eventually to a specified site outside the excavation area.

2.1.1 Open TBM

Open TBMs are a specific type of rock TBM not equipped with any protective shield. They are employed in ground conditions where there is no risk of collapse or rock detachment for a sufficient period after excavation. In such conditions, neither a shield nor any other immediate ground support is required, allowing equally safe and efficient excavation while reducing construction cost.

The main components are those described previously and are common to all rock TBM. The main difference, apart from the absence of any protective shield around the core of the machine, lies in the advancement mechanism.

The TBM is equipped with large gripper shoes, which are heavy steel pads that extend outward to press against the tunnel wall, providing stability during advancement. They can be single or double, depending on the required stability, and work in combination with a series of hydraulic jacks. The hydraulic jacks serve two functions: the first is to thrust the grippers against the tunnel wall, and the second is to push the cutterhead against the tunnel face to advance, generating counterforce through the grippers. Once the hydraulic jacks are fully extended, allowing the cutterhead to advance by approximately 1 to 1.5 m, the degripping phase begins. During this phase, the grippers are retracted from the tunnel wall, and a vertical hydraulic jack is deployed to keep the TBM horizontally in position. Subsequently, grippers are extended again, and the whole back-up of the machine is advanced by means of hydraulic jacks, and a new advancement phase can begin.

Two types of open TBM are used (figure 2.2): those with a simple-gripper scheme and those with a double-gripper scheme. In the simple-gripper scheme, the thrust for advancement is counteracted by a single pair of grippers, pressed against the tunnel wall on a single anchorage plane. As result, the advancement line of the machine is not strictly fixed but follows the excavation path and can be changed during excavation.

In the double-gripper scheme, the counterforce to the thrust of the hydraulic jack for advancement is provided by two pairs of grippers, a front and a back gripper, spaced a few meters apart. This type of anchorage is fixed at two points in space, creating the gripper carrier, the structure that guides the main beam. In this configuration, the advancement line of the TBM is rigidly fixed during excavation and can only be repositioned at the beginning of each excavation round (Tanzanini 2008).

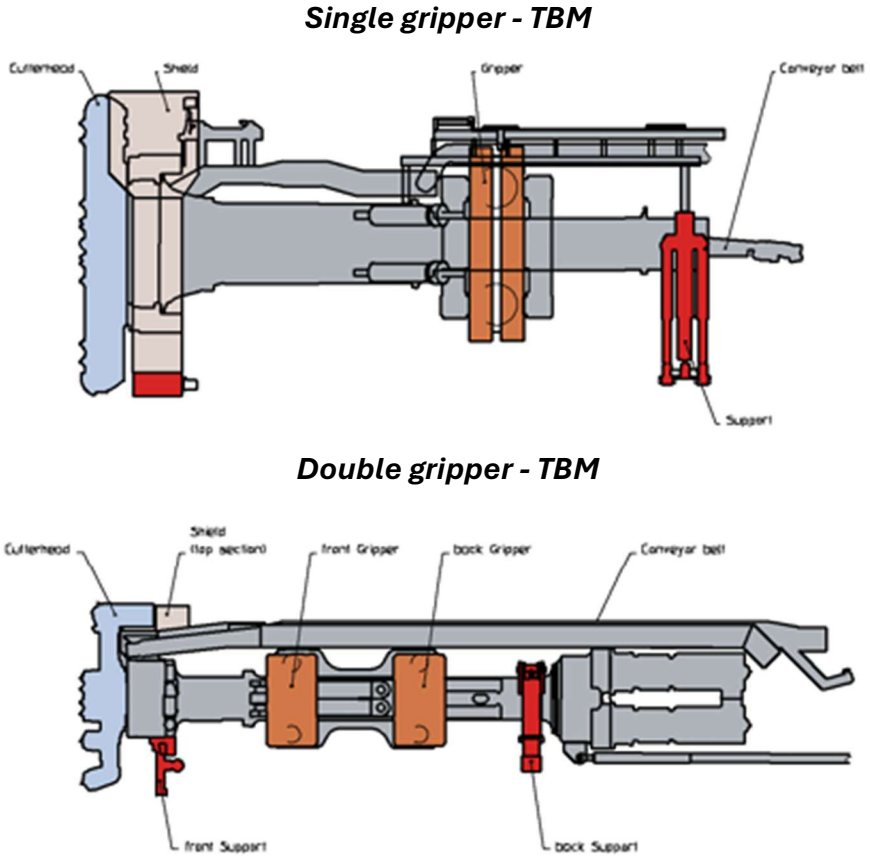

Figure 2.2 - Open TBM single and double gripper scheme (Herrenknecht AG)

The terrain where those types of TBM are usually employed does not need immediate support of the wall, so differently from what happens with other types of TBM, in the open one, usually are not provided with a ring erector, to set in place the prefabricated segment lining.

With open TBM excavation, the lining is completed sometimes after the excavation, using traditional methods like in situ concrete lining, cast using large travelling formwork, which advances step by step along the excavated tunnel.
In some cases, to be on the safer side, the open TBMs are also provided with a small shield that protects workers from possible detachment of rock. It is also possible, where needed, to prepare the installation of temporary sustains, like rock bolts or shotcrete, immediately behind the cutterhead support, being aware of not interfering with the grippers.

2.1.2 Single shield TBM

Rock subjected to physical, chemical and biological processes develops an important degradation that produces a huge fragmentation and instability. These rock conditions imply an enormous risk for workers where detachment of small to large rock portions is frequent and therefore open TBMs are not suitable.
To allow a safe advancement in this type of rock, single shield TBMs are used. This TBM type presents many characteristics common with all the other types, but with some peculiar additional components. The tunnel is driven under the protection of the shield skin, which serves as rock support, until the tunnel lining is installed. Lining made by precast concrete segment is installed within the shield, which protects the crew and TBM component during the whole procedure, from the surrounding rock mass. Each lining segment is picked up with a hydraulic manipulator, the so-called ring erector, and positioned to form a complete ring. Each ring is composed of a fixed number of precast segments, a number that depends on the tunnel diameter and remains equal for the whole tunnel, typically consisting of several regular segments and a key segment. During curve, the segment number remains the same as in a straight, only the relative position of each successive segment is adjusted to achieve the required curvature radius. Once the key segment is installed and a ring is completed, the next excavation phase can begin. Cutterhead and shield advance thanks to the hydraulic thrust cylinder that pushes against the ring. As soon as the shield is pushed forward in relation to the tunnel lining, an annular gap is created between the rock mass and the segment extrados. This gap is continuously filled, while the machine moves forward, to ensure good interlocking between the segment and the rock wall, preventing also the water inflow. Shielded TBMs are not equipped with grippers, the shield slides directly along the excavated surface. Once the advancement is completed, the ring erector resumes operation and during

each segment installation, the hydraulic thrust cylinders are retracted to their rest position, ready for the next advancement. To reduce vibration and stabilize the machine during advance, hydraulic stabilizers located in the front shield area are pressed against the tunnel wall (figure 2.3).

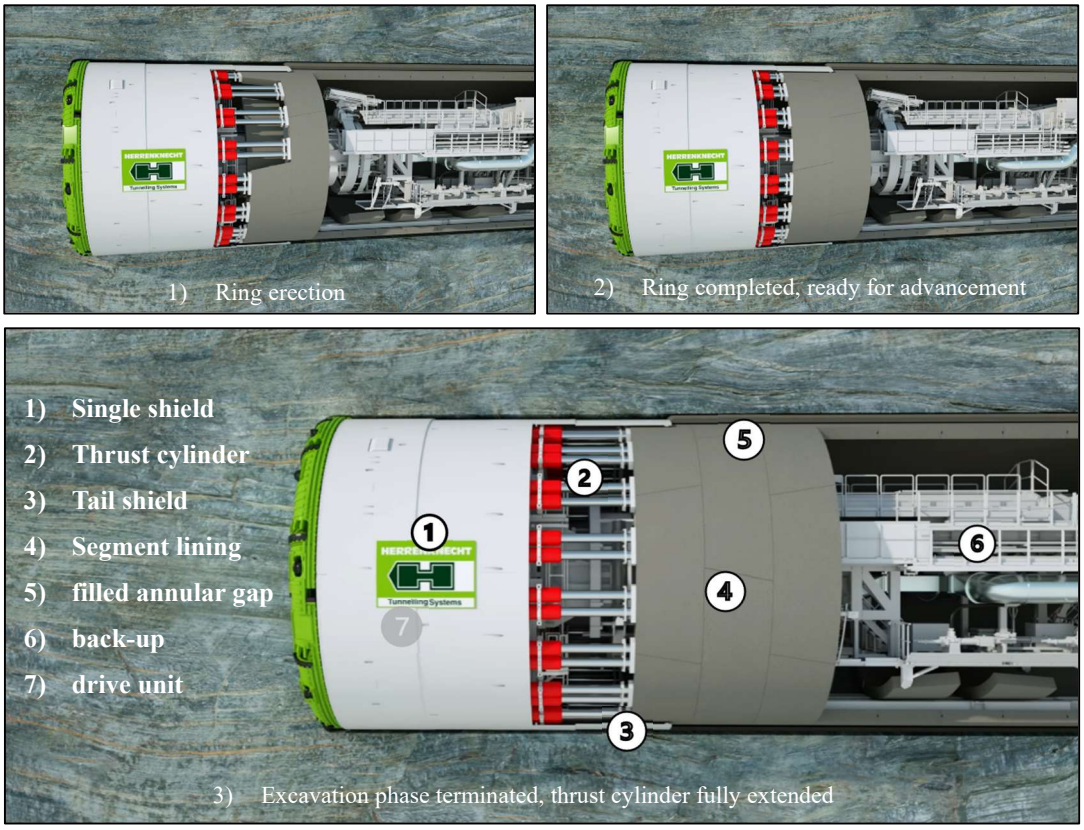

Figure 2.3 - TBM single shield scheme and the three different excavation phases (Herrenknecht AG, 2025)

Various drives are available for tunnelling with single shield TBMs. Depending on the diameter and project requirement, either a permanently installed drive with steering cylinders or a torque box drive is used. The drive unites composed by the torque box system (figure 2.4) allows infinitely variable horizontal and vertical adjustment of the drive, and the cutter head thrust force can be precisely monitored via hydraulic cylinders.

1) Excavation chamber
2) Drive unit and torque box
3) Main bearing
4) Cutterhead

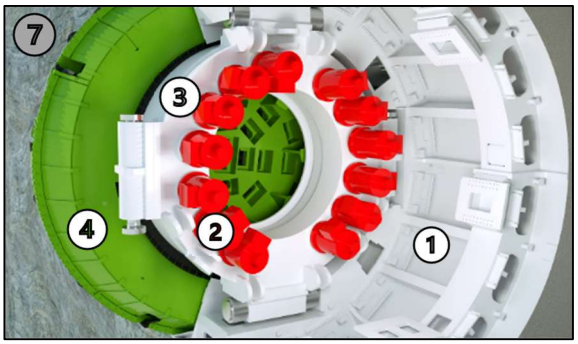

Figure 2.4 - Drive unit (Herrenknecht AG, 2025)

To extend the geological area of TBM applications, ground improvement can be performed safely during excavation. TBM machines are predisposed with drill ring, that means of injection drilling through the shield, for example to reduce the water ingress.

2.1.3 Double shield TBM

The main characteristic is the presence of two shields positioned consecutively behind the cutterhead, a front and a rear shield, forming the so-called split shield skin (figure 2.5). The rear shield is also known as the grip shield, houses the gripper unit, the auxiliary thrust cylinder and the tail skin. The main thrust cylinder located in the front shield connects the two shield sections with each other. A telescopic shield between them protects the thrust cylinders and the inner part of the shield from the tunnel walls.

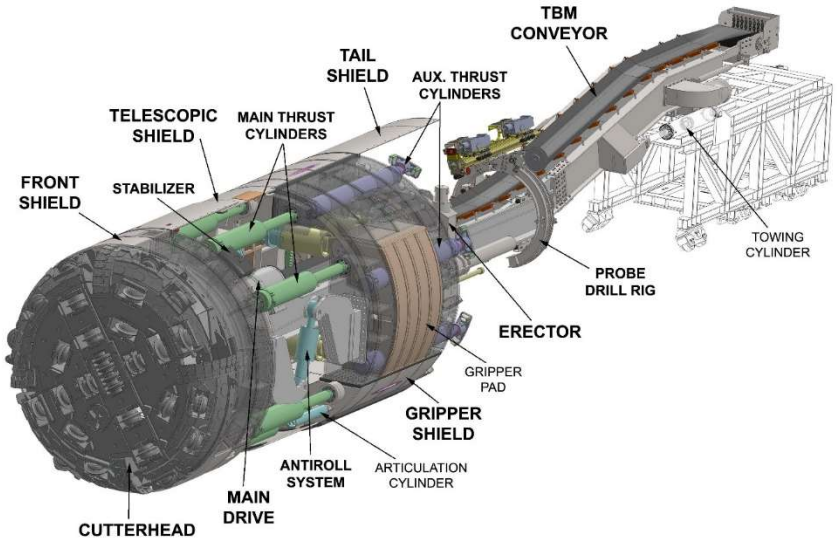

Figure 2.5 - Double shield TBM scheme (TunnelPro S.p.A, 2025)

During conventional tunnel, the machine extends the gripper to brace itself radially against the rock, and the front shield, thanks to the main thrust cylinder, can advance independently of the rear shield. In meanwhile, at the rear shield, the operation of ring erection can proceed in parallel, undisturbed, because differently from the single shield TBM, the reaction forces during boring are transferred to the rock by the gripper. The auxiliary thrust cylinders are used to secure the position of the installed segment. Once the advance cycle is completed, the gripper plates are retracted, the auxiliary thrust cylinder pushes the rear shield forward in the direction of the advance, and in parallel, the main thrust cylinders are closed (figure 2.6).

This repositioning phase lasts just a few minutes, enabling continuous tunnelling leading to an important time reduction in tunnel excavation with respect to the single shield.

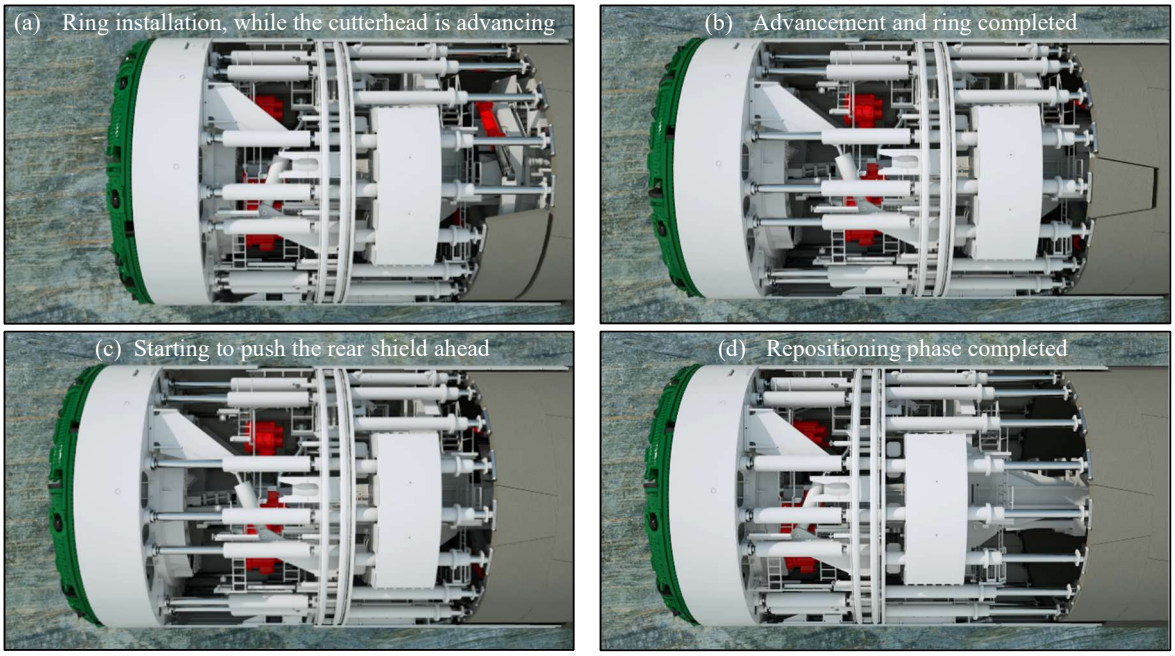

Figure 2.6 - Double shield TBM advancement phases (Herrenknecht AG, 2025)

The TBM can also work as a single unit, with the two shield moving together, like single-shied TBM, in case of tunnelling through an area characterized by with fault zone or low rock strength, where the gripper cannot be braced safely in the rock. In that case, the thrust is given only by the auxiliary cylinder, and the last ring built serves as an abutment for support. This possibility increases the geological area of application, gaining more versatility and the possibility to adapt in different conditions during excavation.

There are some cons to consider in the choice of double shielded TBMs. There is a huge increase in mechanical and electrical components that suffer malfunctions during excavation due to the hard conditions of work. Main problems can arise at the telescopic shield, that in condition of rock mass convergence, can bring to a complete stop of the machine. Also, the articulation and telescopic joints require careful maintenance and regular inspection to prevent malfunctions.

2.2 Soil TBM

Soft soil represents a major challenge for civil engineering. Tunnel excavation in soft ground is highly complex due to the unfavourable geomechanical properties of these materials: low mechanical resistance, high compressibility and high-water content.

An additional difficulty arises from the lack of self-supporting capacity of the ground and its natural tendency to move toward the tunnel, which implies volume loss and potential surface settlements. Tunnel excavation inevitably induces deformation in the surrounding soil mass, changing the stress distribution which results in a propagation of settlement up to the ground surface (figure 2.7). These conditions are typically encountered in urban environments, where tunnels are often constructed at shallow depths, sometimes with an overburden of less than 20 m. It has been proven that the overburden thickness plays a key role in the magnitude of the induced settlements, "maximum settlement at the ground surface induced by tunnelling is larger for shallower tunnels" (Zhao et al., 2019) (figure 2.8).

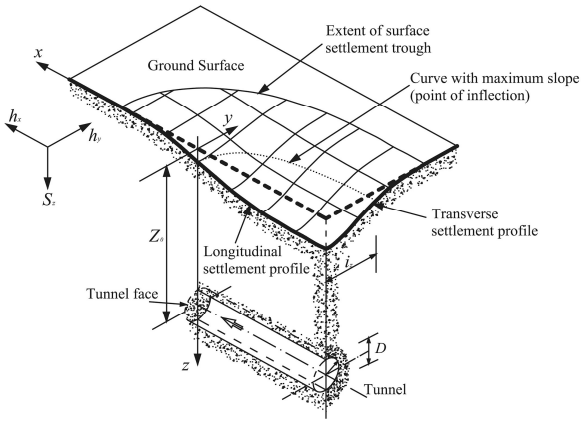

Figure 2.7 - Tunnelling induced surface settlement profile (Attwell et al., 1986)

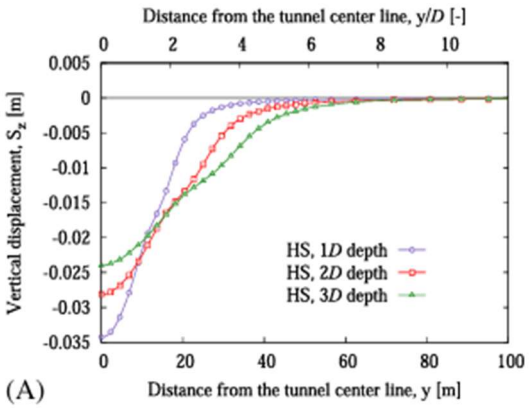

Figure 2.8 - Influence of tunnel overburden depth (Zhao et al., 2019).

Settlement control therefore becomes a priority in urban tunnelling projects to avoid structural deformations or damage to surface buildings and infrastructure. Moreover, soft soils, are usually characterized by high permeability and porosity due to their large number of voids within particle.

When the soil is saturated by high groundwater table, water inflow during excavation represents an additional and critical challenge for tunnelling operations. All these challenges can be well managed by adopting a particular type of TBM specifically designed for soil. These machines are the soil TBMs, further divided into two main categories: the Earth Pressure Balance (EPB) TBM and the Slurry Shield TBM (SS-TBM). Other types of TBMs

have also been employed in the past, such as the mechanical support shield TBM, which supported the tunnel face using a mechanical bulkhead, and the compressed air TBM, which applied air pressure in the excavation chamber to counterbalance the ground and water pressure. However, these technologies are no longer commonly used, mainly due to safety issues and operational limitations compared with modern pressurized TBMs. In more recent year new machines have been developed that combine two or more TBM technologies, the Multi-mode TBM and the Variable-Density-TBM, perfect for tunnelling in variable geology, they offer high flexibility in terms of support and excavation methods.

Soil TBMs generally share the same fundamental mechanical components already seen for Shielded TBMs, such as the cutterhead, shield, drive motors, gearboxes, thrust system and ring erector. The main difference lies in the excavation mode and face support system. Soil TBM supports the tunnel face applying counterpressure using different methodology. For this reason, they required additional components, as a pressurized excavation chamber, bulkhead sealing, pressure sensor and screw conveyor or slurry circuit for spoil removal.

The cutterhead design is completely different. The purpose of excavating soft soil no longer requires many strong disc cutters. In some cutterhead designs for very fine soil, the discs are entirely replaced by scrapers, flat blades and replaceable teeth such as rippers, breakers and loading or shoe tools (figure 2.9). Typically, the cutterhead rotation speed is higher to keep the excavated soil moving and homogeneous, while the required torque is lower. The open area ratio is significantly larger, between 30% and 50% in EPB machines and up to 70% in slurry TBMs, to allow a better flow of soil and slurry through the cutterhead openings.

1) Discs cutter
2) Openings
3) Scrapers/foam injection point
4) Bucket lips

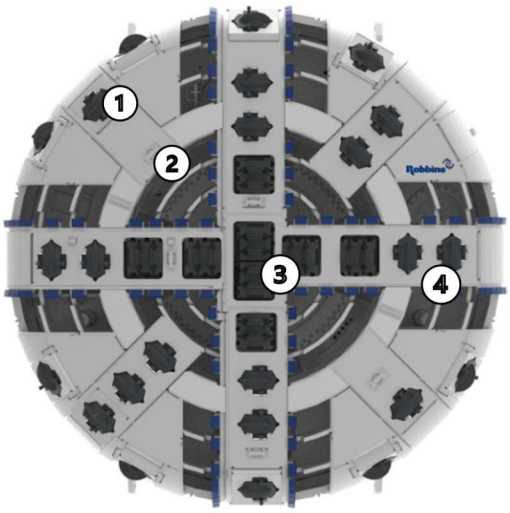

Figure 2.9 - EPB Cutterhead and his component (The Robbins company, 2025)

2.2.1 Earth Pressure Balance (EPB) TBM

The Earth Pressure Balance (EPB) excavation mode relies on the pressurization of the excavation chamber, where the tunnel face is supported by the excavated soil itself. This material, kept under control pressure, directly transmits the stabilizing pressure to the face (figure 2.10). The excavated material is then transported out of the pressurized chamber by a screw conveyor into the atmospheric-pressure zone of the tunnel. The screw conveyor, designed with an helicoidal geometry, is responsible for dissipating the pressure gradient between the two zone along its length. By adjusting its rotation speed and conveying capacity, the system maintains the desired face pressure and ensures controlled discharge of excavated soil.

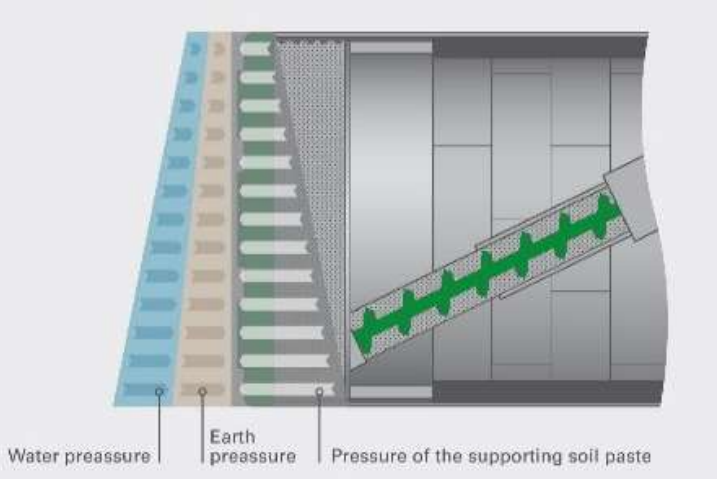

Figure 2.10 - Pressure balance at the tunnel face EPB TBM (Herrenknecht AG, 2025)

The general excavation mechanism is like that one of shielded TBMs, and in modern machines, to the double-shield configuration. The soil is excavated by the cutterhead, which is advanced through the thrust cylinders, reacting against the last installed lining ring. The material then entered the pressurized excavation chamber, which is enclosed by the bulkhead, a pressure resistant steel wall separating the pressurized section from the atmospheric-pressure zone inside the TBM (figure 2.11). The face support pressure is regulated by controlling the advancement rate and by using conditioning agent. Once the required advance is achieved, the segment installation phase begins, preparing the machine for the next excavation cycle.

1- Cutterhead
2- Excavation chamber
3- Pressure bulkhead
4- Thrust cylinder
5- Screw conveyor
6- Ring erector
7- Segment lining

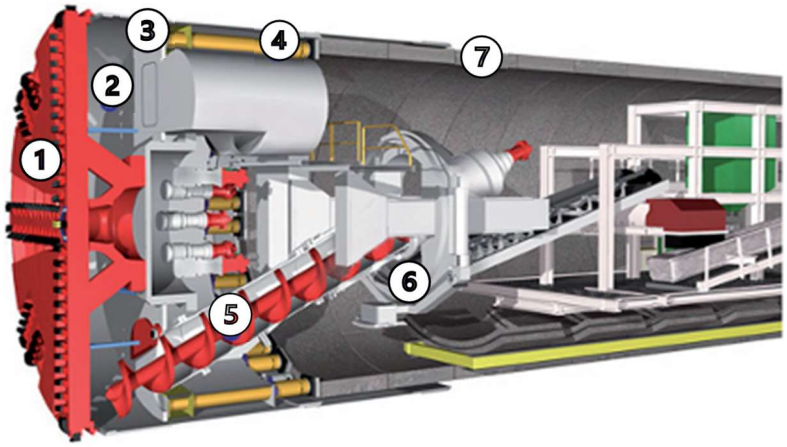

Figure 2.11 - EPB TBM components (Herrenknecht AG, 2011)

The EPBs are able of maintaining pressure of up to 6-7 bar, sufficient for operation in urban environment where, at a depth of 20-30 m, the groundwater pressure typically reaches similar values.

A fundamental element in the EPB tunnelling is the use of conditioning agents, which ensure efficient excavation and proper pressurization. Since the excavated soil is used as the supporting medium, its rheological behaviour must remain within specific limit, acting like a pasta like material: not too stiff, which would block the screw conveyor and not too fluid, which would reduce face pressure.

For this reason, conditioning agents are injected directly into the excavated soil within the chamber through dedicated injection points. The type and quantity of conditioning agent depend on the soil properties, particularly on parameters such as the plasticity index and the consistency index (figure 2.12).

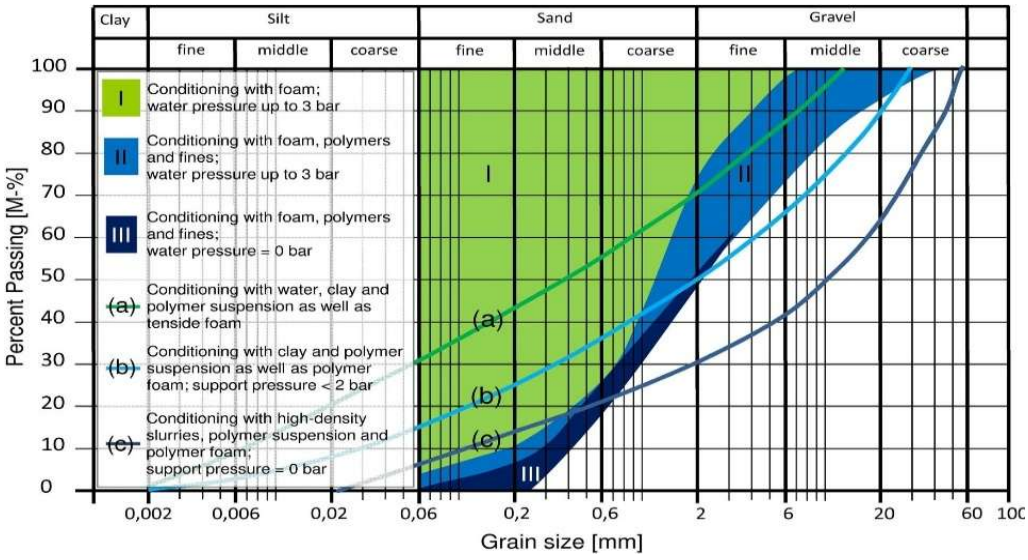

Figure 2.12 - Application range for EPB-shields depending on necessary soil conditioning (Budach & Thewes, 2015)

Different conditioning materials may be employed: foam, polymers, additives or fine filler, to change artificially the grain size curve, sometimes combined for better performance.
The main problem to be avoided is clogging, where sticky clay adheres to the mechanical components, reducing cutterhead rotation and advance rate, and in severe cases, causing complete stoppage.
The principal functions of conditioning agents include:

1. Internal friction reduction, lowering shear resistance and cutterhead torque.
2. Impermeabilization, reducing soil permeability and improving pressure retention at the face.
3. Plasticity increases, transforming the excavated soil into a homogeneous, plastic material capable of maintaining a uniform and continuous pressure.
4. Lubrification, improving soil flow through the screw conveyor and reducing wear on metallic parts.
5. Better and more controlled discharged of the excavated material from the chamber.

Control of face pressure has a significant influence on the mechanical performance parameters of the TBM, including torque, penetration rate and specific energy. A recent study (Bilgin & Copur, 2023) confirmed that increasing face pressure results in higher torque, thrust and specific energy value, while penetration decreases correspondingly. Up to approximately 2 bars, a slight increase in penetration was observed, likely due to the opening of fractures in the rock mass, after which it decreases as expected. Therefore, precise pressure control is fundamental not only to prevent ground deformation and machine blocking but also to optimize efficiency and overall cost.

2.2.2 Slurry Shield TBM (SS-TBM)

The other TBM technology used in soft ground is the slurry shield TBM (SS-TBM), widely employed in coarse soil like loose sand or gravel, especially under groundwater conditions. differently from the EPB excavation system, SS-TBM uses a mixture of water and bentonite, called slurry, injected under pressure into the excavation chamber to provide counterpressure. The slurry transmits reactive pressure against the earth and groundwater pressure, ensuring face stability.

Slurry effectively prevents water inflow. Due to its rheological properties, it slightly penetrates the tunnel face, and forms a thin layer known as filter cake, which reduces the ground permeability and maintains pressure equilibrium at the face (figure 2.13).

1) Feeding pump
2) Discharge pump
3) Fragmentation unit
4) Ring erector

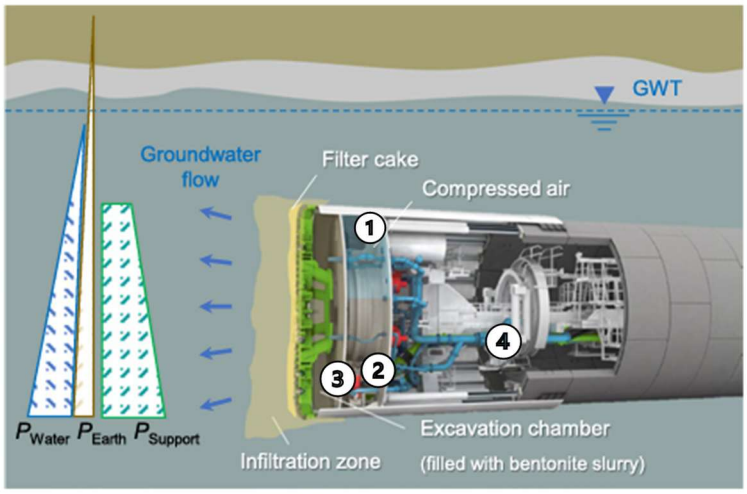

Figure 2.13 - Scheme of tunnel face support principle in front of a Slurry Shield TBM (Qin et al., 2023)

There are two possible methods to generate pressure in the excavation chamber of a SS-TBM:

- Hydraulic slurry pressurization – The excavation chamber is filled with slurry, which is pumped in under controlled pressure through a feed line. The mixture of slurry and excavated material is then extracted through a separate discharge line. The pressure within the excavation chamber is regulated by controlling the amount of slurry pumped in or extracted. Increasing the volume of slurry pumped into the chamber raises the pressure, while increasing the discharge flow reduces it.
- Air cushion pressurization – an air cushion chamber is introduced above the slurry level. Pressurized air is injected and regulated by a control valve, transmitting pressure to the slurry and hence to the tunnel face. In this case, a submerged wall separates the two zones: one fully filled with slurry and the other containing both air and slurry, each supplied through independent lines. The excavated slurry muck mixture is extracted as before. The pressure control in the excavation chamber is regulated by compressor and automatic control valves, which allow the air pressure to be increased or decreased as required to maintain a constant face pressure.

The air-cushion system is generally preferred because it requires a smaller volume of slurry and allows for finer control of the face pressure. In the full-slurry system, much larger quantities of slurry must be pumped and continuously adjusted, since its incompressibility

makes pressure regulation more difficult and can lead to instability at the face. From this point onward, all the research and discussion will focus on SS-TBM air-cushion system.
The SS-TBM excavation mechanism ed main components are similar to those of a shielded TBM, where a protective shield ensures the safety of the workers and the mechanical part until the final lining is completed. The cutterhead, characterized by a larger area opening ratio and equipped with soft soil excavation tools, advanced through the soil by the push of the main thrust cylinder, which reacts against the latest installed ring.
During the advancement, the bentonite slurry serves also to remove the material excavated by the cutterhead. Spoil remains suspended within the slurry and is extracted through a discharge valve located in the lower part of the excavation chamber. The mixtures of bentonite and excavated material are then pumped outside, to the separation plan for treatment and recycling. To prevent possible obstruction in the chamber, a fragmentation unit is usually installed just before the grid of the discharge pump. Its function is to crush oversized rock fragments, avoiding blockages and ensuring a continuous and efficient slurry flow through the excavation process.
Once the advancement is completed, the ring erector, protected by the tail shield, installs the concrete segment to form a new ring. After this phase, a new excavation cycle can begin. The bentonite slurry used during excavation follows a closed circuit from the tunnel face to the separation plant, to recover, if possible, part of the water to prepare new slurry for subsequent excavation cycles. (Qin et al., 2023)

2.2.2.1 Separation plant

When SS-TBM operates, it is important to ensure constant high quality of the bentonite suspension with the removal of the partially dispersed soil particles as completely as possible before reuse, keeping intact as much as possible its rheological properties. For this reason, the discharge slurry, which contains the excavated soil, is treated using expensive separation plant to recover part of the slurry and water. The possibility to recover slurry or water depends on different aspects, the used type of bentonite, and the chemical additive adopted during slurry treatment, which may prevent the reuse of slurry and water, or even hinder their safe disposal due to environmental impediments. The separation plant is therefore a fundamental component of Slurry Shield TBM, is located outside the tunnel due to the large component needed and consists of several units designed to perform a precise separation process. (Maidly et al., 2004)

The main components and phases of the slurry treatment circuit are (figure 2.14):

1. Bentonite mixing unit, where water and bentonite are mixed to prepare the slurry.
2. The storage tank, where the prepared slurry is kept and from which the feed pump draws the material to supply the excavation chamber.
3. During excavation, the used slurry mixed with soil is extracted from the chamber through a discharge pump and sent to the separation plant
4. In the first separation stage, coarser particles (larger than 4-5 mm) are removed using a vibrating sieve.
5. In the second stage, hydrocyclones separate medium-sized particles typically larger than 75 μm.
6. In the final stage, fine particles (< 75 μm) are removed in clarification tanks or filter presses, often assisted by the addition of flocculants for chemical separation and water depuration.

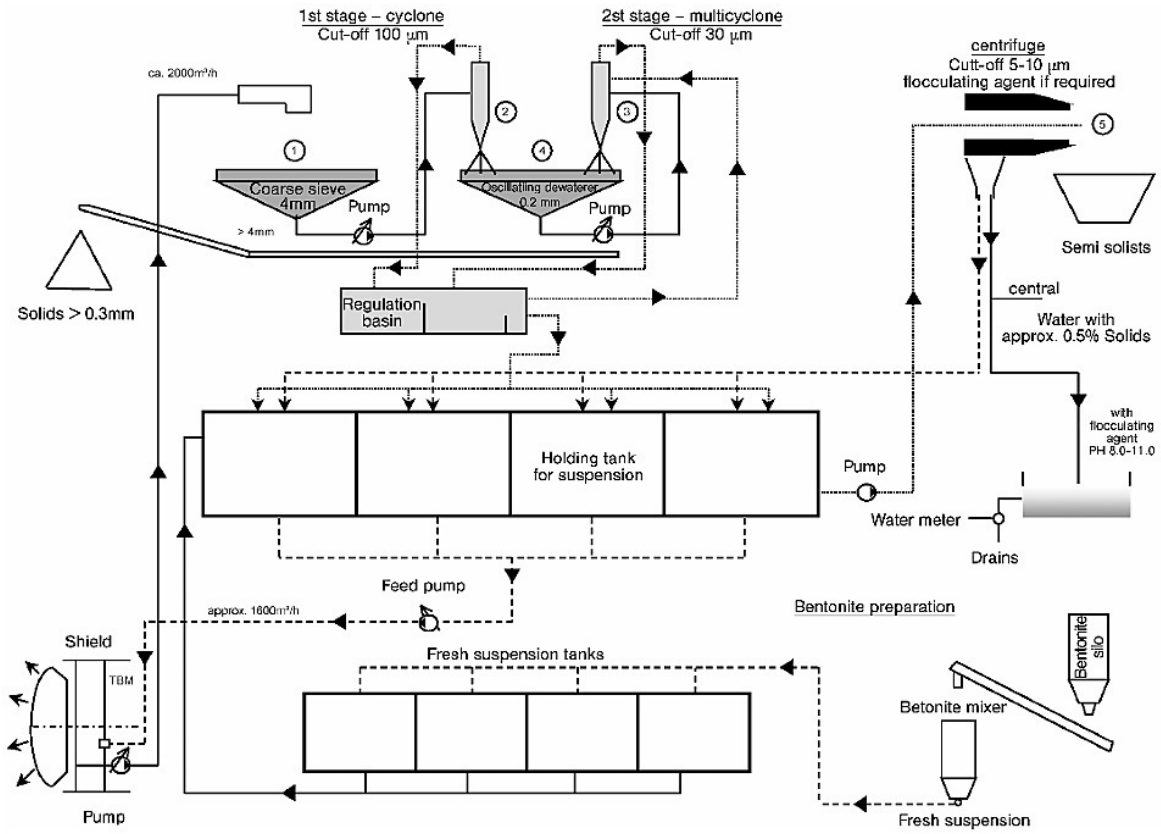

Figure 2.14 - Functional diagram of a slurry separation plant (Maidl et al, 2004)

Thanks to this process, part of the slurry, or almost 70% of water, can be recovered and reused, significantly improving the sustainability of the excavation procedure.

Vibrating sieves are used in the first stage to separate the coarse particles from the discharge slurry. They operate using big sieves that, by means of mechanical vibration, allow the fine material to pass through the mesh while retaining larger fragments.

The hydrocyclones are conical separators that are based on the use of centrifugal forces generated by the tangential entry of the slurry into the upper cylindrical part of the device (figure 2.15). Bentonite slurry is pumped at high velocity, from an overflow nozzle, creating a spiral movement, a vortex. Due to the centrifugal effect, the heavier and coarse particles are pushed outwards toward the wall of the cone and move downward, being discharged through the underflow outlet at the bottom. Finer particles and liquid phase remain on top and exit through the overflow outlet. The overflow, containing the finer bentonite suspension, moves further in the separation plant for additional treatment. Hydrocyclones are usually installed in parallel or series to increase treatment capacity. They offer continuous separation with no moving parts, low maintenance and fast operation. However, they are very expensive and for very fine particles, their efficiency decreases. A recent study by Wang et al. in 2024, and ongoing research in Polytechnic of Turin, describe the possibility of reusing part of the exhausted slurry produced during slurry shield tunnelling for backfilling applications. This represents a significant step forward in improving the sustainability of tunnelling projects that employ bentonite slurry system.

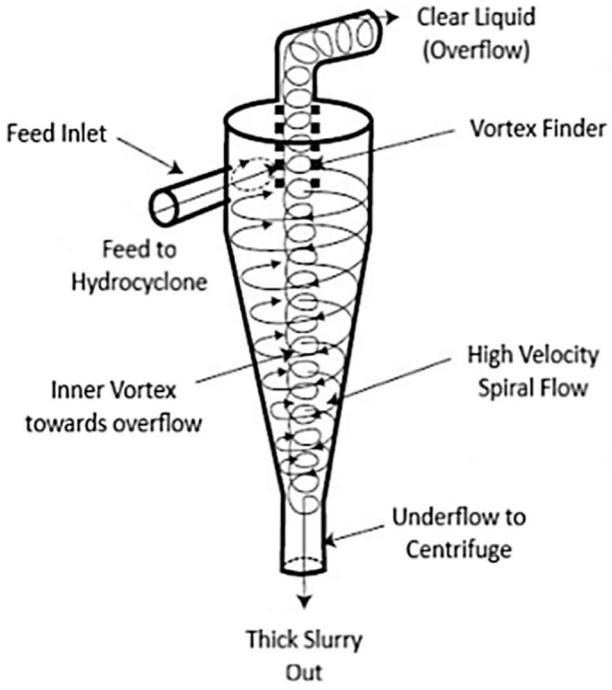

Figure 2.15 - Hydrocyclone scheme (Thermosag india Pvt Ltd, 2025)

The filter press operates by applying mechanical pressure that forces the slurry through a series of filter plates covered with permeable cloths, allowing the water to pass while retaining the solid particles (figure 2.16). Slurry coming from the cyclones is pumped into the filter press chamber. Here, while pressure increases, water is expelled through filter cloth, and the solid particles accumulate on the surface, forming a thin compact layer of material. Once the process is finished and the plates are opened, this layer is discharged for disposal and can be reused in other ways, for example as filler. The portion of the water collected during the process is tested to assess if it can be reused for new slurry preparation or safely discharge in compliance with environmental standards.

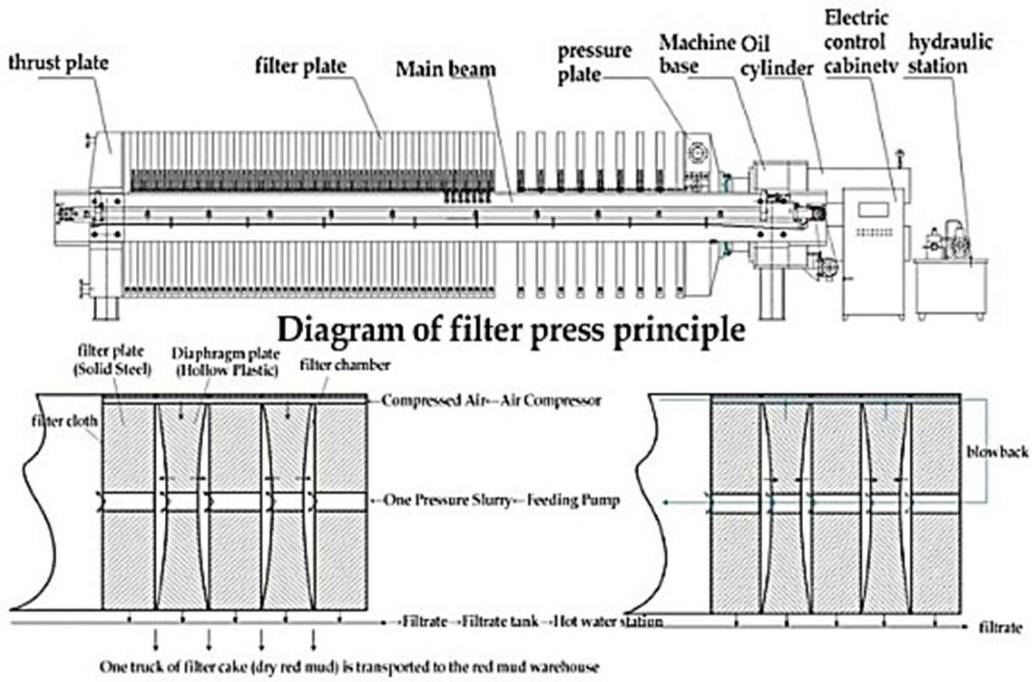

Figure 2.16 - Diagram of filter press principle (Kindle-Tech, 2024)

2.2.2.2 Problem related to Slurry Shield TBM

For each project that involves the use of Slurry Shield TBM, a fundamental aspect to control is to select the appropriate bentonite. As will be explained in the following chapter, bentonite behavior depends on several factors such as its typology, mineralogy composition, presence of additives and the concentration of soluble ions in the mixing water. These parameters strongly influence the rheological and physical behavior of the slurry, including its response to mechanical stress, viscosity variation, density and filter cake formation.

Selecting the correct bentonite concentration is essential to ensure the formation of an effective impermeable filter cake at the tunnel face. The optimal formulation must also consider the boundary condition of the ground characteristic, such as permeability and soil granulometry. An appropriate choice guarantees sufficient face support, minimizes water inflow, and ensures stable excavation performance through the entire tunnelling process.
A major issue during excavation with SS-TBM is the sudden and unforeseeable occurrence of soft and highly permeable ground, which prevents the formation of the filter cake. Under such conditions, the pressurized slurry penetrates the permeable ground and escapes without forming the proper filter cake. The resulting loss of slurry leads to a pressure drop, making it impossible to properly control the face pressure (figure 2.17). Conversely, reducing the slurry pressure would cause the collapse of the ground toward the tunnel face. Face instability can then rapidly evolve into surface subsidence, deformation, or even more severe damage.

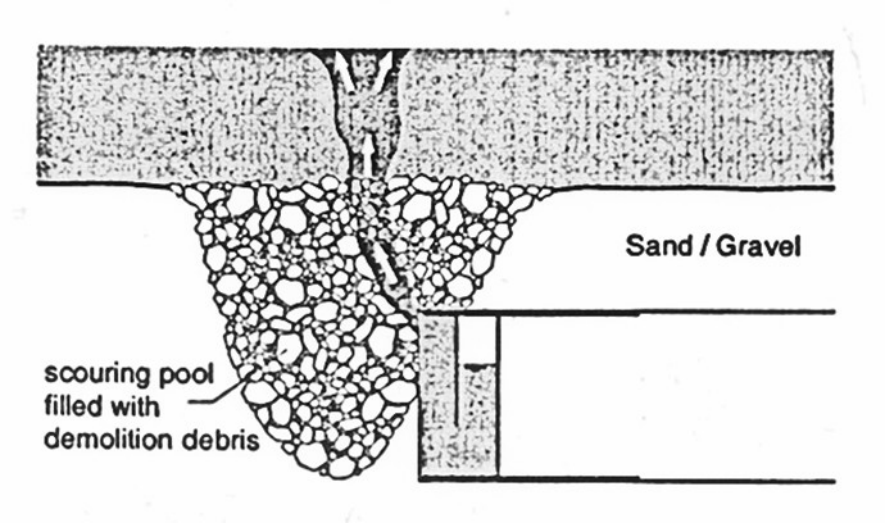

Figure 2.17 - Slurry loss during excavation in permeable ground (Peila D, 2022)

As with EPB-TBMs, another problem that may occur in SS-TBMs is clogging. The phenomena happens when the excavated soil due to its sticky behavior and low viscosity may adhere to the opening of the submerged wall, obstructing the hydraulic connection between the two chambers (figure 2.18). When this happens, the slurry feeding line continues to work but the slurry discharge line became unable to transport the excavated material, leading to the high-pressure fluctuation, and brings to a series of problems, increased cutterhead wear and decreased machine advancement rate (Zhai et al., 2022).

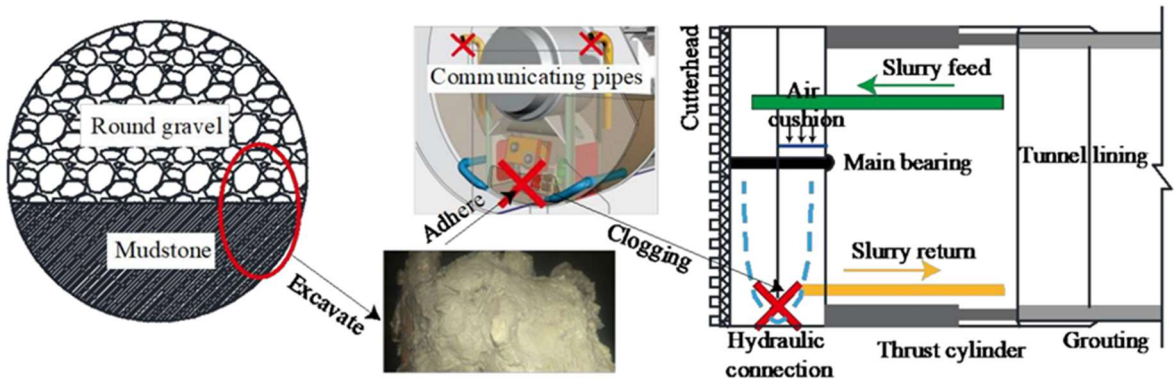

Figure 2.18 - Schematic diagram of clogging when slurry shield tunnelling in the mixed ground of round gravel and mudstone (Zhai et al. 2022)

To avoid any type problems during excavation, several fundamental parameters must be continuously controlled and monitored to perform an efficient tunnel excavation during work:

- Face support pressure: ensure that the pressure in the excavation chamber remain constant and the design value. It is controlled by means of compressed air.
- Excavation and discharge balance: ratio between excavated and discharge material.
- Grout injection volume and pressure: to detect the presence of permeable zones, soft soil or fractures in the surrounding ground.
- Cutterhead torque, stroke and rotating speed: torque reflects the cutting resistance and overall energy demand. Increasing torque indicates clogging or insufficient face pressure, whereas decreasing torque suggests potential face instability.
- Shield advancement rate: a low advancement rate can indicate clogging, high abrasion or friction between the shield and the tunnel wall, potentially meaning tunnel convergence.
- Slurry characteristics: density, yield value, viscosity, and the quality or thickness of the filter cake at the excavation face.

The slurry characteristic must be accurately controlled in laboratory and directly on site through rapid testing. Variations in slurry properties are frequent and must be closely monitored to ensure the stability and efficiency of tunnelling process. To avoid issues related to bentonite slurry during excavation, it is fundamental to carry out research that analyses its behavior related to type, composition and concentration, as was done in the research campaign presented in this thesis.

3 Bentonite

Bentonite is the common name for a series of natural clay materials widely employed in civil and geotechnical engineering due to their unique physical, chemical and rheological properties. It is a phyllosilicate mainly composed of montmorillonite, which gives bentonite the capacity to absorb water, swell and form highly viscous suspension when it comes into contact with water. Thanks to those characteristics, bentonite has a wide range of applications, including sealing, soil stabilization, and conditioning agents in different engineering fields, such as the preparation of slurry for Slurry Shield TBMs. Understanding the fundamental properties of bentonite is therefore an essential prerequisite to deeply evaluate its behavioural evolution under different conditions and study its suitability for SS-TBM tunnelling.

3.1 Origin and mineralogical composition

The name Bentonite was first proposed in 1898 by W.C. Knight, an American geologist, for a particular rock formation of swelling clay with soapy properties discovered in Wyoming, in the Fort Benton unit, from which the name derives. Some years before, around the mid-nineteenth century, a new plastic clay mineral with similar properties was discovered in Montmorillon, France, and was subsequently named montmorillonite.

Bentonite deposit typically originates from the weathering of volcanic ash or tuff. Chemical alteration may occur through interaction with seawater or when the hot water, associated with volcanic activity within the Earth's crust, flows through the porous structures of the volcanic ash beds.

During this process the obsidian (figure 3.1) present in the ashes, due to a new increase in temperature, has undergone a phenomenon known as devitrification. This process consists of the gradual transformation, of volcanic glass, such as obsidian, formed by the rapid cooling of magma that inhibits the development of a crystal lattice, into a crystalline clay. The newly formed material after the transformation is a crystal rock (figure 3.2) with a more stable structure.

Figure 3.1 - Obsidian sample (Obsidian, Encyclopedia Britannica, 2025)

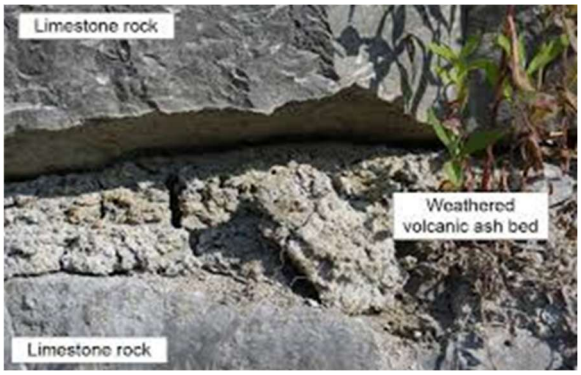

Figure 3.2 - Weathered volcanic ash bed within limestone (Ontario beneath our feet, 2025)

In the alteration process, a significant portion of amorphous silica, up to 40-50%, is subjected to dissolution and leaching, respectively the chemical breakdown of volcanic glass components into soluble species, and the transportation away by circulating fluids of the dissolved species. The residual material that remains after this process ultimately gives rise to bentonite (Bentonite, Wikipedia, 2025).

Bentonite is primarily composed of montmorillonite, a clay mineral, from the smectite group that comprises a mixture of different swelling sheet silicates bond. Montmorillonite is an aluminium phyllosilicate mineral composed of the aggregations of lamellar particles united by electrochemical forces, each with a particular crystal structure described as a TOT unit, Tetrahedra-Octahedra-Tetrahedra. Schematically each lamellar particle is composed of three layers disposed in parallel. The central octahedral part is composed of aluminium oxide (Al_2O_3) the two tetrahedral of silicate oxide (SiO_2) (figure 3.3).

Bentonite may also contain varying amounts of magnesium, calcium carbonates (MgC_3 and $CaCO_3$) and iron oxide (Fe_2O_3). This occurs because silicon and aluminium ions within the crystal lattice can be isomorphically substituted by other cations with similar ionic radii but lower valence, like magnesium or iron, without altering the crystal structure. This change in the composition generates a charge imbalance within the crystal structures, resulting in a net negative charge on the particle surface. This negative charge is compensated by the presence of exchangeable cations, primarily calcium magnesium and sodium, together with water molecules, which are held together through ion-dipole interactions. These ions cannot be accommodated in the crystal lattice and therefore reside on the external layer of the silicate structures, where they play a key role in the characteristic hydration phenomena of bentonite.

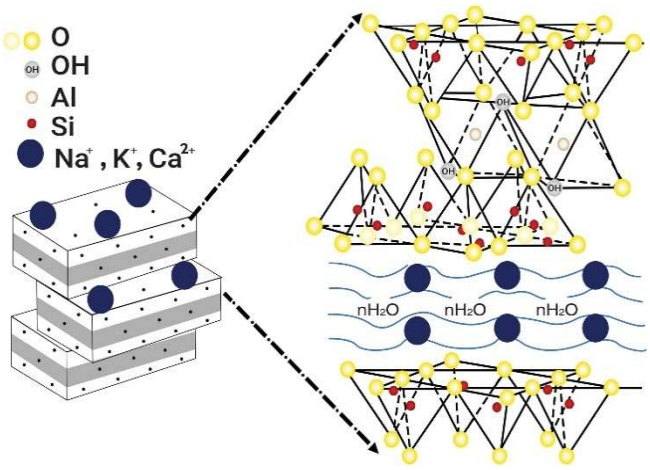

Figure 3.3 - Bentonite structure (Brown et al., 2020)

Figure 3.4 - Example of bentonite used for test

Bentonite mineralogy can vary depending on the geographic origin, it may contain, in addition to the main components, different elements like calcium, sodium and other metals and minerals. Even samples collected from the same deposit may exhibit differences in chemical composition. Some of the most common impurities include calcite, feldspar, cristobalite, quartz, mica, ferrous carbonate and pyrite. Naturally such variations in composition influence the physic-chemical properties of bentonite, making certain types more suitable for specific industrial applications. (Grim et al., 1978)

To evaluate the mineralogic and chemical composition of bentonite, the most used technique is the X-ray diffraction (XRD), a versatile non-destructive analytical technique based on the diffraction of X-rays by the crystalline structures of the mineral. When a X-ray is directed onto the sample, the rays are diffracted at specific angles characteristic of each mineral phase. By measuring the intensity of the diffracted rays as functions of the diffraction angle, it is possible to identify the type of mineral present, determine their crystal orientation, and additional aspects of the chemical composition (Thermo Fisher Scientific, 2025).

3.2 Physical-chemical properties

Bentonite has found different industrial applications thanks to its unique physical and chemical properties, which derive directly from its lamellar structures and high montmorillonite content. From a physical point of view, bentonite consists of extremely fine particles, generally smaller than 2 μm, giving it a very high specific surface area and strong

water retention capacity. These features combined with the parallel rearrangement of lamellae, result in very low permeability, which decreases exponentially with the reduction of the void ratio. Under compression, as structures became more compact, the hydraulic conductivity (k) can decrease to value as low as 10^{-11} m/s, reflecting the progressive closure of interparticle pores and the reorientation of clay platelets (Shirazi et al., 2010).

Another important property of bentonite is its high plasticity. Due to its strong affinity with water interaction, when hydrated, the lamellar clay particles separate and can easily flow over each other, forming a mouldable and viscous paste. This behavior is confirmed by the high value obtained in the Atterberg limit test.

From the chemical perspective, certain characteristics strongly influence its behavior, such as the cation exchange capacity (CEC) and the exchangeable sodium percentage (ESP). Although these two concepts are related, they are not identical.

The CEC refers to the total capacity of bentonite to retain exchangeable cations of any type. It is measured in milliequivalents for 100 grams of bentonite and represents the reserve of cations that the clay can hold. A higher CEC indicates a greater ability to absorb and exchange ions. Related to this, bentonite has also the ability to absorb molecules and ions, a property particularly valuable in the industrial field of purification and cleaning process.

The ESP, on the other hand, measures the portion of the CEC occupied by sodium (Na^+) ions, thus indicating the relative amount of sodium among the exchangeable cations. That is a peculiar characteristic that influences a lot the bentonite properties, and an indicator of the bentonite type.

3.3 Swelling capacity

Among all its properties, the most important is the swelling capacity. Due to its peculiar crystal structures, water molecules become trapped between the layers of the montmorillonite causing interlayer expansion and swelling. Bentonite can expand 10-15 times its original dry size, although the swelling power depends on several factors.

First, the type of bentonite plays a key role, sodium bentonite exhibits greater swelling than calcium bentonite because the monovalent sodium cations produce stronger repulsive force between the layers. The swelling behavior is primarily governed by the montmorillonite content, higher content leads to greater water absorption, while the presence of impurities

like quartz, feldspar mica and others, reduce the swelling capacity. This relationship is demonstrated in the study of Mishra et al. (2011), who found a strong correlation between the ESP and the free swelling index. A lower ESP, meaning lower monovalent sodium cations and higher portion of divalent cations like calcium or magnesium, corresponds to reduce swelling. When the ESP ranges from 0 to 30%, swelling increases slightly and linearly. Above 30%, the increase became more consistent, as the dissociations of sodium ions leave negatively charged montmorillonite layers that attract water molecules via electrostatic force and osmotic inflow to balance the charge, enhancing free swelling of bentonite. The same study also provided a valuable correlation between the montmorillonite content and swell index, underlining a linear relationship between the two, meaning that higher montmorillonite content led to higher swelling.

Another Important factor is the water quality. The presence of dissolved minerals and salt can significantly reduce swelling. Several studies have shown that salinity markedly affects the swelling behavior of bentonite.

Other influencing parameters on swelling capacity include temperature and pH. Bentonite generally has a near-neutral pH (around 6-7). Studies of Jeon et al. (2014), observed that at low pH (< 3), swelling tends to increase, while at high pH (11-12), swelling decreases significantly.

Additives also play a critical role in bentonite properties, with Industrial bentonites often modified with polymers to enhance performance. Depending on the additives, the swelling capacity may be improved or inhibited. When bentonite hydrates, it not only swells but also forms colloidal gel like particles, creating an impermeable mass that stops water infiltration, another properties that make bentonite effective in geotechnical and environmental applications (CMS Industries, 2025).

3.4 Types of bentonites

As previously mentioned, bentonite contains some isomorphic substitution of the base element. This capacity of exchange cations is measured by the (CEC) previously explained, this parameter is important because it varies from one bentonite to another and both the

quantity and quality of exchangeable bases represent a key criterion for distinguishing bentonites that are classified based on the predominant cations.

The most significant distinction, for industrial purposes, is between sodium and calcium bentonite, with the former being considered more valuable than the latter. The main difference between the two types lies in their water absorption capacity and the consequent swelling behavior. Sodium bentonite, dominated by Na^+ ions, is characterized by a higher tendency to absorb water molecules, for this reason it is often referred to as swelling bentonite. Calcium bentonite instead swells much less, due to the Ca^{2+} ions, attracts less water. Nurmunira and Siddiqua (2021), evaluate the swelling index by performing the free swell test on sodium and calcium bentonite. The result indicates larger swelling capacity for the sodium bentonite, almost double respect to the calcium one.

In the same study the CEC was also evaluated indicating a larger value for sodium bentonite respect to the calcium one, meaning a larger capacity of cations exchange for sodium bentonite. A greater CEC enhances the swelling ability, adsorption potential and chemical reactivity of bentonite.

4 Bentonite Slurry

While the dry form of bentonite is a relatively inert clay material, its property becomes fully active upon hydration. Bentonite is primarily employed in aqueous suspension, as nearly all industrial and geotechnical applications rely on its interaction with water.

Slurry is the general name to identify a mixture of a liquid with solid. Slurry bentonite refers to a solution composed of bentonite and mixed water (figure 4.1). When dispersed in water, bentonite particles swell, create a colloidal system with low permeability, high viscosity and gel strength.

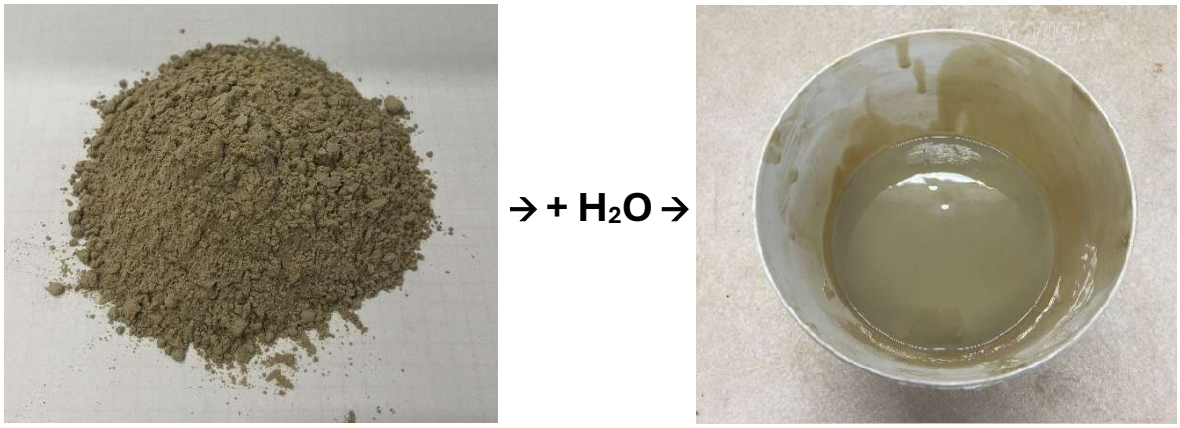

Figure 4.1 - From bentonite to bentonite slurry

The reason behind this behavior lies in the arrangement of bentonite when dispersed in water. Depending on the electrochemical conditions of the suspension three types of particle associations can occur: edge-to-face, face-to-face and edge-to-edge.

Particles generated via face-to-face association mode are larger and thicker respected to those formed by the other two modes, leading to more compact, flocculated structures with higher viscosity. The other modes lead to a card-house structure characterized by a large 3D volume, that promotes swelling and gel formation. The predominance of one configuration over the other depends on factors such as pH, ionic strength, and type of exchangeable cations present in the system.

In bentonite suspension, gel formation can occur through two main mechanisms. The first involves electrostatic attraction between the negatively charged face and the positively charged edge of the clay lamellae, leading to the development of an edge-to-face “card-house” structure. The second mechanism results from face-to-face and edge-to-edge associations, which are governed by long-range electrostatic double layer repulsion. Both mechanisms may act simultaneously, depending on the physicochemical condition of the suspension.

The long-range repulsion is explained by the formation of the electrical double layer, a structure that develops around each montmorillonite lamella when bentonite is dispersed in water. Because of isomorphic substitutions within the crystal lattice, the faces of the platelets carry a net negative charge that attracts surroundings cations, forming two distinct regions: the stern layer or inner layer, where cations are strongly bond to the particle surface, and the diffuse layer, where ions are more loosely bound, distributed in solution and their concentration decreases with increasing distance from the particle. The thickness and intensity of the double layer strongly influence particles interaction: when it is extended, particles remain dispersed and the slurry remains stable, while when it is compressed, for example due to increased electrolyte concentration, flocculation and gel formation are favoured.

It's also important to note that electrostatic interaction can cause gel formation only when the pH is below the isoelectric point (IEP), the pH value at which the net surface charge of particle's edge is zero. Remember that only the edge became positive, the overall particles remain permanently negative. Above the IEP, the particles are negatively charged and mutually repel each other, resulting in a stable, disperse system; below the IEP, the edge of the particles becomes positively charged, promoting attraction and flocculation. Experimental studies by Kelessidis et al. (2007), determine the IEP of bentonite slurries to lie between pH 5.0 and 8.0, while other investigations reported values close to pH 7. Around this range, bentonite suspension exhibits the lowest yield value and residual viscosity, indicating a less structured and more fluid system.

The rheological property of this solution makes bentonite slurry an essential material in geotechnical and civil engineering applications, particularly in slurry shield tunnelling, diaphragm wall construction and drilling fluid. In tunnelling slurry not only provide mechanical support to the excavation face but also control fluid loss thanks to the formation of a thin filter cake, while maintaining adequate flow properties for transport of the excavated particles in suspension.

4.1 Bentonite rheological behavior

The term rheology derives from the Greek verb "rheo", meaning "to flow", and refers to the study of how materials deform and flow under applied stress. This phenomenon does not concern only liquid or gas, but also solids. Different materials exhibit different mechanical responses to stress. At one extreme are elastic solids, which deform according to the Hook's law, while at the others are Newtonians fluids, which flow according to the Newtonian behavior. In between these two extremes lie suspensions, emulsions and pastes, which display intermediate viscoelastic behavior, combining characteristic of both solid and liquid and exhibiting distinctive flow properties.

In general, the flow behavior of any system is described by the relationship between shear stress (τ) and the shear rate ($\dot{\gamma}$). The shar stress represents the force per unit area acting tangentially on a surface and indicates the force required to make one layer of a fluid slide over another. The shear rate is the rate at which deformation occurs under applied stress; mathematically, it is the time derivative of the shear stress, expressed as $\dot{\gamma} = \frac{d\gamma}{dt}$. The ratio between shear stress and shear rate defines viscosity (η), which measures a fluid's resistance to flow under an applied shear stress.

$$\eta = \frac{\tau}{\dot{\gamma}}$$

By plotting the variation of shear stress versus the share rate, it's possible to obtain the so-called Flow curve. From this curve, the variation of viscosity can be determined, as it corresponds to the slope of the curve at any given point.

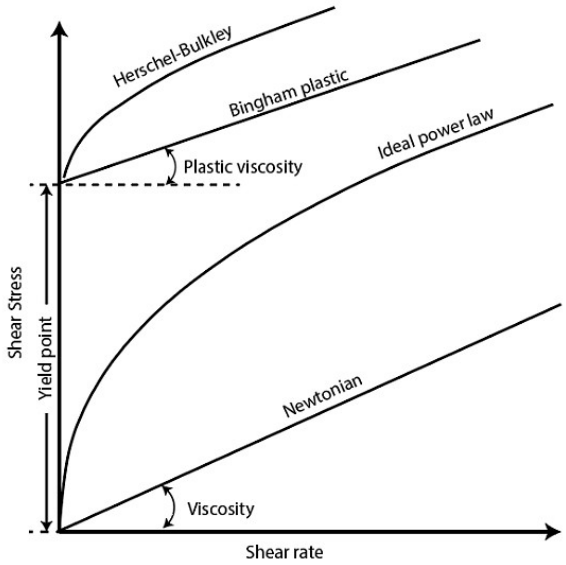

Figure 4.2 - Consistency chart for Newtonian and Bingham fluids (modified from Caenn et al., 2011).

Each material exhibits a characteristic flow curve, but in general four main flow behaviours can be distinguished: Newtonian, pseudoplastic, Bingham plastic and dilatant (fig. 4.2)
The normal behavior of fluid is Newtonian, in which the shear stress is linearly proportional to the shear rate and, consequently, the viscosity remains constant.
All the other types of flow are classified as non-Newtonian, where the viscosity varies with the shear rate. Bentonite slurries belong to this category, as their viscosity changes depending on several parameters and boundary conditions. The flow curve, also known as rheogram, is the graphical representation of shear stress versus shear rate, from which important rheological parameters can be identified.
One key parameter is the yield stress (τ_0), define as the minimum stress required to initiate flow, in a fluid at rest. Graphically, it corresponds to the intercept on the y-axis, when the shear rate is zero (yield point in the chart). Above this stress, the material behaves as a fluid, while below it, it exhibits solid-like behavior.
Bentonite slurries are typically described according to the Bingham theory of plastic flow, and in particular the Herschel-Bulkley (HB) model is the rheological model that better describes the behavior of the bentonite slurry. The constitutive equation for HB model is:

$$\tau = \tau_0 + k * \dot{\gamma}^n$$

Where τ_0 is the yield stress, k is the consistency index, $\dot{\gamma}$ is the shear rate; n is the flow index. In the HB model, the fluid's behavior depends on the flow index n.

- n = 1, the fluid behaves like Bingham plastic, with a linear relationship between shear stress and shear rate.
- n < 1, the fluid displays shear-thinning, or pseudoplastic, behavior, becoming easier to deform as the shear rate increases.
- n > 1, the fluid shows shear-thickening behavior, making it more resistant to flow as the shear rate increases.

The common bentonite behavior is shear-thinning, closely related to the internal particles' configuration. At lower shear rate, montmorillonite platelets are randomly oriented, and their electronic interactions promote a three-dimensional network. At rest this structure remains intact, meaning high viscosity and in some cases a yield stress. When the applied shear rate increases, this network progressively breaks down, and the platelets tend to align respect to the flow direction, reducing viscosity.
Another important rheological feature of bentonite slurries is thixotropy, the time dependent change of viscosity. Immediately after mixing, the suspension exhibits lower yield stress and

plastic viscosity because the applied shear disrupts the internal structures, producing a shear-thinning behavior. However, when the slurry is left to rest, viscosity and yield stress gradually recover as the network structures reform. The magnitude of this behavior can be observed from the size of the hysteresis loop that generated between the increasing and decreasing shear-rate curves.

When slurry is subjected to a constant shear rate, viscosity tends to decrease over time due to the progressive breakdown of the gel structures, until an equilibrium viscosity is reached. Several factors influence the rheological behavior of bentonite slurry. Slurry flow behavior is strongly affected by pH, storage time and bentonite concentration. With increasing hydration time, the suspension exhibits more pronounced gel-like behavior due to intensified flocculation, resulting in higher viscosity and yield stress. Similarly, increasing bentonite concentration enhances both viscosity and yield stress, and the sol-gel transition occurs at lower concentration.

4.2 Filter cake

As explained in the previous paragraph on slurry shield TBM, one of the main properties of the slurry, is its ability to form a filter cake on the excavation face. Due to its low permeability and porosity, this layer effectively seals the tunnel from water and transfers the slurry pressure onto the soil skeleton. The filter cake forms as the slurry, under chamber pressure, infiltrates inside the permeable ground at the face.

Two types of filter cake (figure 4.3) can generally be distinguished as described by Kube et al. (2019):

- External filter cake, which appears as a thin film on coarse particles and is developed when the diameter of the soil pores is smaller than the particles contained in bentonite, there is no slurry penetration and the particles deposited on each other acting as a sealing membrane.
- Inner cake, which develops when infiltration is deeper, and the pores are internally sealed within the soil matrix. The slurry penetrates the ground, the finer component passes through the pores, but the large solid particles of bentonite are unable to continue to move through the soil network, remaining stack and once deposited the particles seal the pores.

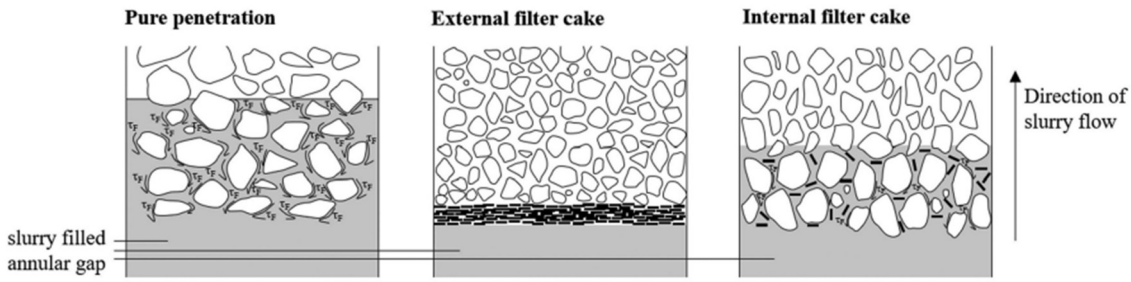

Figure 4.3 - External and inner filter cake (Kube et al., 2019)

A well developed and homogeneous filter cake is essential for stable excavation, and a critical safety aspect during maintenance and inspection activities, when workers may need to access the cutterhead chamber to replace worn tools and perform mechanical checks.

The continuous rotation of the cutterhead results in repeated cycle of cake removal and reformation, making it difficult for a fully developed filter cake to establish. From a physical point of view, bentonites with a high specific surface area and strong swelling capacity tend to produce a denser and less permeable filter cake. The formation process can be hindered by the presence of chemical contaminants such as seawater, acids or heavy metal solutions, which weaken the bentonite structures and increase its hydraulic conductivity. This occurs through flocculation, leading to a loose microstructure that allows fluid leakage. Additionally, during excavation, slurry became mixed with excavated soil, altering its composition. In particular, the presence of sand can inhibit the alignment of bentonite platelets, prevent the formation of dense and horizontally oriented structures and result in a poorly formed filter cake.

5 Experimental tests campaign

This chapter presents the laboratory test campaign carried out to investigate the rheological behavior of different bentonite slurries, at varying concentrations, hydration times and stress conditions.

The greatest part of the research aims to evaluate the rheological effect of mechanical degradation on slurry. The idea was to reproduce at laboratory scale the mechanical and hydraulic stresses that occur during slurry shield TBM excavation.

It is fundamental to underline that the mechanical stresses to which bentonite slurries are subjected during excavation can reach extremely high values that cannot be fully reproduced in laboratory using standard equipment. The rotation of the cutterhead, the hydraulic stresses generated by the pumping system, and the continuous mixing within the excavation chamber, together with the excavation soil represent complex stress conditions that cannot be replicated in laboratory.

Nevertheless, laboratory tests are extremely valuable for understanding the behavior of bentonite even under small case stress conditions, providing a reliable basis for interpreting real scale performance. If a bentonite shows a particular behavior or evidence of mechanical degradation during laboratory testing, it can be reasonably expected that such issue would be more significant under actual excavation conditions.

Furthermore, this research tries to identify the main parameters affecting the rheological behavior of bentonite and to establish an operational correlation between fast on-site measurement and detailed rheological analyses.

A significant portion of the laboratory activity focused on measuring the viscosity of slurries prepared with eight different types of bentonites through the Marsh cone test.

The eight bentonites are identified through codes composed of the prefix ID, followed by a progressive number from 1 to 8.

Limit liquid and swell index were carried out, before starting the main research campaign. These parameters are key properties because they strongly influence the rheological behavior of bentonite.

Subsequently, with each bentonite two slurries were prepared:

- A static slurry (not mechanically stressed)
- A stressed slurry, mixed at 1000 rpm for progressively longer periods

Each bentonite was tested in both static and stressed conditions at different hydration times, as summarized in Table 5.1:

Table 5.1 - Hydration time at which the tests were performed

Bentonite type	Condition	Test hydration time (h)						
ID 1 to 8	static	0	1	3	4	24	48	72
	stressed	-	-	-	4	24	48	72

For some bentonites, tests were also performed on slurry at different concentration, to evaluate the effect of concentration on the rheological behavior. Specifically, bentonite ID4, ID6 and ID7 were tested at different concentrations as shown in Table 5.2:

Table 5.2 - Bentonite slurry concentration used in experimental test

Bentonite type	Concentrations (kg/m^3)		
ID1	-	60	-
ID2	-	60	-
ID3	-	60	-
ID4	-	60	80
ID5	-	60	-
ID6	-	60	80
ID7	45	60	70
ID8	-	60	-

After this first testing phase, the campaign continues with the use of a rotational viscometer. The viscosity of three slurries, prepared each with a different concentration of bentonite ID7, was evaluated trough a rotational viscometer at varying revolutions per minute (RPM) and hydration time. The objective was to evaluate the rheological behaviours at different concentrations and possible correlation between the rapid Marsh cone result.

5.1 Materials

Only two materials were employed during the research campaign, just bentonite mixed with water.

5.1.1 Bentonite

The eight bentonites employed in the study have well-defined physical-chemical features, determined through a series of laboratory characterization tests and complemented by consulting the technical specifications provided by the manufacturers, to obtain additional information about composition and physical properties.

- **ID1** is a sodic bentonite, at high performances, perfect for the preparation of liquid suspension for slurry shield TBM excavation, horizontal drilling and microtunneling, complying with API. It is completely free of Perfluoroalkyl (PFAS), a series of chemical substances with a huge impact on health and environment. It comes from stock delivered in summer 2025, presents a brown/beige colour with a relative density of 2.6 g/cm^3.

Figure 5.1 - ID1

- **ID2** has the same commercial name and producer as bentonite ID1, but different stock, stored in laboratory since 2024. There could be some differences in the chemical composition between the two materials, maybe simply due to a different extraction point. The bentonite presents a light grey colour and a relative density of 2.6 g/cm^3.

Figure 5.2 - ID2

- **ID3** is primarily used in hole drilling with slurry, especially in applications where low bentonite concentration is needed, it is suitable for work in in gravelly and sandy soil. The material presents a light beige colour and has a relative density of 2.6 g/cm^3.

Figure 5.3 - ID3

- **ID4** is a 100% natural sodium bentonite, completely polymer free. Its usage is recommended for the preparation of drilling fluid (piles, diaphragm walls, and tunnelling) suitable for a variety of soils. The PH reported by the producer is between 7-9%. The materials come from a laboratory stock dated 2024 and present a brown coloration with a relative density of 2,6 g/cm^3.

Figure 5.4 - ID4

- **ID5** is a modified version of ID1 and ID2. It is produced by the same manufacturer but presents some differences in the composition. It comes from a different stock delivered in summer 2025. It is still a sodic bentonite, with a beige coloration and has a relative density of 2,6 g/cm^3.

Figure 5.5 - ID5

- **ID6** shares some common characteristics with ID1 and ID2, same producer and commercial name. Nevertheless, this time it is a mineral bentonite, meaning that it is fully natural, without any additives. Bentonite present a dark beige colour and relative density of 2.6 g/cm^3.

Figure 5.6 - ID6

- **ID7** shares the same name and manufactures of bentonite ID4 but different stock, dated summer 2025. It is 100% natural sodium bentonite, polymer free. The colour il light brown, and a relative density of 2,6 kg/m^3.

Figure 5.7 - ID7

- **ID8** is similar to bentonite ID3, same producer and commercial name but different stock more recent, dated 2025. As evident from the distinct colour, in this case light grey, there are some differences in the composition between the two. The relative density is 2,6 kg/m^3.

Figure 5.8 - ID8

5.2 Laboratory tests

5.2.1 Swell index test

The swell index was performed following the method in compliance with the standard ASTM D5890-18 (Standard Test Method for Swell Index of Clay Mineral Component of Geosynthetic Clay Liners).

The standard procedure describes the use of graduate cylinders with a capacity of 100 ml, which are filled with 90 ml of distilled water. Subsequently, 2 g of bentonite are added gradually to the water, in small quantities, precisely 0,1 g every 10 minutes, until the total amount of 2 g is introduced, resulting in 20 additions.

For practical reasons, and to allow simultaneous testing of different bentonites, larger graduate cylinders (250 ml capacity) were used instead. This modification slightly deviates from the standard procedure, however, as demonstrated by Todaro et al. (2021), the difference in swelling index result between the two methods is negligible, and the procedure can be considered equivalent. In addition, the larger cylinder diameter facilitates bentonite addition, reducing the risk of material adhering to the cylinder walls, which could otherwise lead to inconsistencies in the results.

The adjusted quantities of distilled water and bentonite were calculated by proportion as follows:

$$90 \text{ ml} : 100 \text{ ml} = x_1 \text{ ml} : 250 \text{ ml}$$

$$2 \text{ g} : 100 \text{ ml} = x_2 \text{ g} : 250 \text{ ml}$$

Resulting in:

- $x_1 = 225$ ml, distilled water level to be added to the cylinder
- $x_2 = 5$ g, total mass of bentonite to be added during the test

Before starting the test, standard requires approximately 100 g of bentonite to be sieved in order to have 100% passing through at 150 μm (No. 100) U.S. standard sieve and at least 65% passes through 75 μm (No. 200) sieve. All eight bentonites tested were dried and satisfied with these requirements. A small plastic beaker was tared on a precision laboratory scale and filled with 5 g of bentonite (figure 5.9), with a precision of ± 0.01g. A 250 ml graduate cylinder (±2 ml precision) was then filled with 225 ml of distilled water. After these

two preliminary operations, using a small rectangular sheet of paper, 0,25 g of bentonite, taken from the previously pre-weighted 5 g, was added to the water by gently dusting over a period of 30 seconds, avoiding contact with the cylinder walls.

This procedure, consisting of weighing 0,25 g of bentonite and adding it every 10 minutes, was repeated 20 times until all 5 g of bentonite were added to the water. After the last addition, 10 minutes were waited to allow complete settling, and then distilled water was added carefully until reaching the final volume of 250 ml. Once completed, the cylinder was sealed with plastic tape to prevent air or external materials from entering. After a minimum period of 16 hours, as prescribed by the standard, the level of the settled bentonite was measured in millilitres, and the sample temperature was recorded. The swelling index (SWI) was calculated following the same principle as in the standard method, adjusting for the bentonite mass of 5 g, to express the result in ml/2g according to the following equation:

$$SWI = \frac{V}{5} \ (ml/2g)$$

Where:

- SWI is the swell index in (ml/2g)
- V is the volume of settled bentonite after 16 hours (ml)
- 5 is the whole mass of bentonite tested (g)

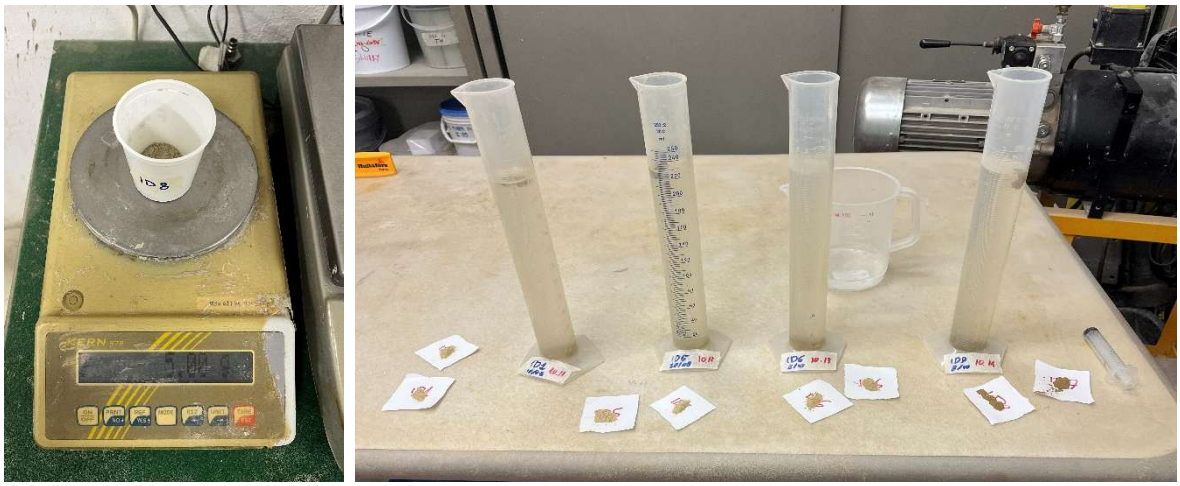

Figure 5.9 - Bentonite weighting (left) and graduate cylinder during swell index test (right)

The swelling index results are presented in table 5.3 and again in the following pages with accompanying photos of settled bentonite in the graduate cylinder.

Table 5.3 - Bentonite Swell index result

Bentonite	SWI (ml/2g)
ID1	12,2
ID2	20,4
ID3	12,4
ID4	14,0
ID5	11,2
ID6	14,0
ID7	18,0
ID8	14,8

ID1

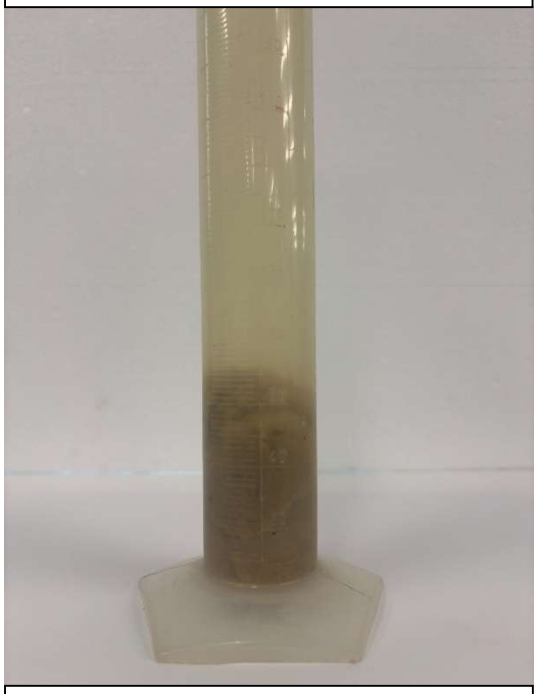

Settled bentonite volume = 61 ml

SWI = $\frac{61}{5} = 12{,}2\ ml/2g$

Figure 5.10 - Bentonite ID1swell index

ID2

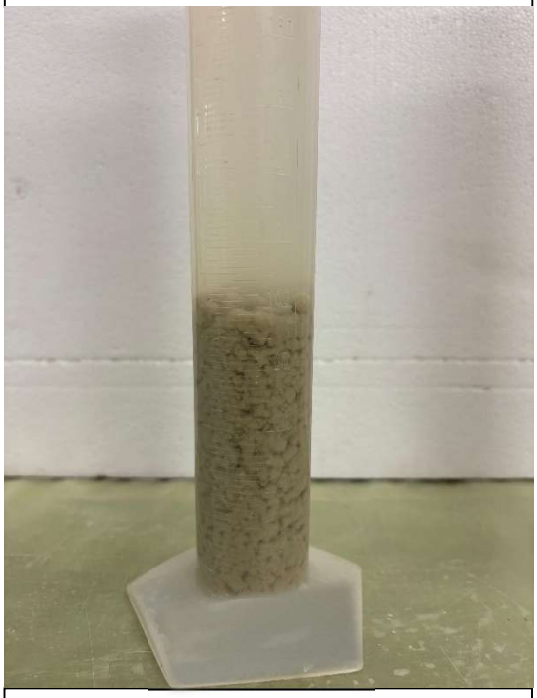

Settled bentonite volume = 102 ml

SWI = $\frac{102}{5} = 20{,}4\ ml/2g$

Figure 5.11 - Bentonite ID2 swell index

ID3
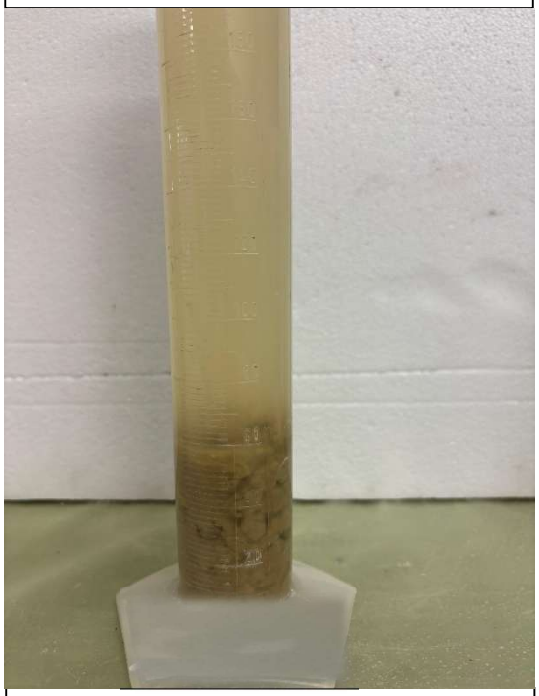
Settled bentonite volume = 62 ml
SWI = $\frac{62}{5} = 12{,}4\ ml/2g$

Figure 5.12 - Bentonite ID3 swell index

ID4
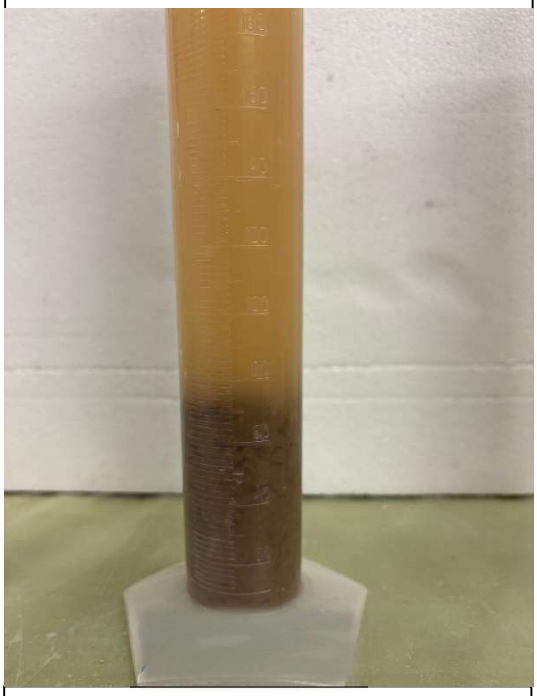
Settled bentonite volume = 70 ml
SWI = $\frac{70}{5} = 14\ ml/2g$

Figure 5.13 - Bentonite ID4 swell index

ID5

Settled bentonite volume = 56 ml
SWI = $\frac{56}{5} = 11{,}2\ ml/2g$

Figure 5.14 - Bentonite ID5 swell index

ID6

Settled bentonite volume = 70 ml
SWI = $\frac{70}{5} = 14\ ml/2g$

Figure 5.15 - Bentonite ID6 swell index

ID7

Settled bentonite volume = 90 ml
SWI = $\frac{90}{5} = 18\ ml/2g$

Figure 5.16 - Bentonite ID7 swell index

ID8
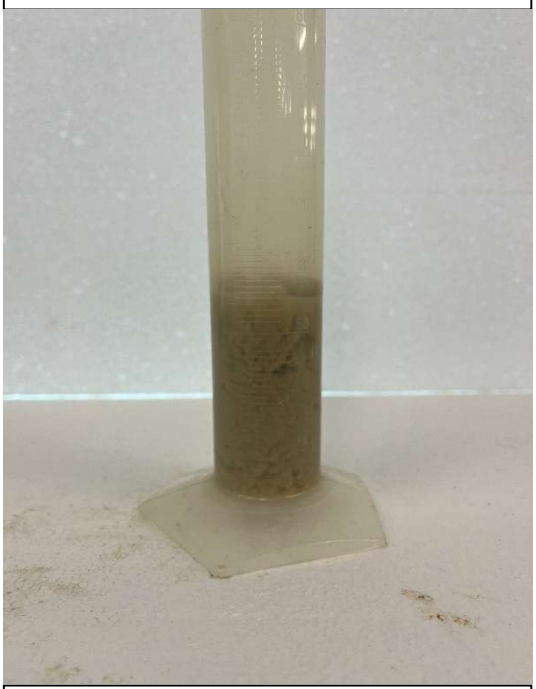
Settled bentonite volume = 74 ml
SWI = $\frac{74}{5} = 14{,}8\ ml/2g$

Figure 5.17 - Bentonite ID8 swell index

5.3 Bentonite slurry preparation

Bentonite slurries were prepared according to a well-established procedure developed by Di Giovanni et al. (2024). The main steps of the preparation process are reported in detail below. Before starting with the mixing was important to accurately determine the dosage of bentonite and water to obtain the desired concentration. For each bucket, an overall slurry volume of approximately 3 L was selected.

For the research, it was decided to test slurries with different bentonite concentrations, 45 kg/m^3, 60 kg/m^3, 70 kg/m^3 and 80 kg/m^3, expressed as mass of dry bentonite per slurry volume. To pass from concentration to masses of the two components (bentonite and water), specific calculations were carried out, considering the density of water and bentonite.

The following calculation illustrates how the masses of water and bentonite were calculated to achieve a concentration of 80 kg/m^3.

Given:

- Bentonite dry density $\gamma \approx 2{,}6$ g/cm^3
- Desire concentration C = 80 kg/m^3 = 0,08 g/cm^3
- Water density $\gamma = 1{,}0$ g/cm^3

The procedure begins with the calculation of the volumetric solid fraction:

$$\varphi_S = \frac{C}{\gamma} = \frac{0{,}08}{2{,}6} = 0{,}03076 \approx 3{,}08\,\%$$

For 3 L of slurry

- Bentonite volume = 3000 mL · 0,0308 = 92,4 mL
- Water volume = 3000 mL - 92,4 = 2907,6 mL
- Bentonite mass = 92.4 cm^3 · 2,6 g/cm^3 = 240,24 g
- Water mass = 3000 g – 92,4 g = 2907,6 g

The other concentrations were calculated in the same way, considering the same dry bentonite density and the same total slurry volume apart from the case of 45 kg/m^3 where the total suspension volume was set at 2 L. The following table 5.4 summarizes the quantities of material for the different concentrations employed in the research:

Table 5.4 - Mass of bentonite and water for slurry preparation at different concentration

Concentrations (kg/m^3)	Bentonite (g)	Water (g)
45	90,0	1965,0
60	180,0	2931,0
70	210,0	2922,2
80	240,2	2907,6

5.3.1 Material weighting

Once the dosage was established, both bentonite and water were weighed using a precision balance, with an accuracy of ± 0.01 g.

- First, a small bucket was placed on the scale, tared, and then filled with bentonite until the desired mass was reached.
- Subsequently, the water was weighed in a larger mixing bucket, where the slurry preparation would take place. The empty bucket was tared beforehand, and water was added carefully to reach the target mass as precisely as possible.

Figure 5.18 - Water weighting with the laboratory precision scale

5.3.2 Mixing

Slurry was prepared by mixing water and bentonite. After the required quantities were measured, the next phase consisted of the mixing process. The larger container filled with water was positioned under the laboratory mixer ARGO LAB AM20-D, capable of mixing at different speeds, from 50 to 2200 RPM, adjustable through a simple knob, and to work medium volume samples up to 20 L (figure 5.19).
While installing the mixing blade, some precautions were taken:

- The propeller was a sloping-blade impeller, designed to create strong turbulence in the centre of the container and promote efficient circulation of the slurry
- The propeller position was carefully adjusted to the correct high relative to the bottom of the tank, leaving a few millimetres of clearance between the blade and the base. This configuration prevents contact during rotation and ensures uniform mixing throughout the entire slurry volume.
- The selected container was a standard bucket of 5 L larger two times the propeller diameters in order to obtain proper turbulence.

Once the propeller was installed, mixing procedure began:

1) The mixing process started by stirring only water, gradually increasing the speed to 800 RPM. This preliminary step was necessary to generate a stable vortex before adding the bentonite, ensuring proper dispersion of the powder in suspension.
2) While maintaining constant speed, bentonite gradually added to the water within approximately one minute. At the end of the addition, a perforated cover was placed over the bucket to prevent bentonite splashes, which could otherwise result in a reduction of the slurry volume.
3) Once all the required bentonites had been added, the speed was increased to 2000 rpm and maintained 15 minutes to achieve complete homogenization of the slurry.

At the end of the mixing process, bentonite slurry was removed from the mixer and made ready for testing.

Table 5.5 - Slurry mixing procedure

Phases	Impeller rotation speed (RPM)	Duration (min)
Start -only water	progressively up to 800	-
Adding of the bentonite	800	Within 1 minutes
Bentonite mixing phase till end	2000	15

Figure 5.19 - Scheme of the used impeller (Todaro et al., 2019) (right) and photo of the utilized propeller (left)

5.4 Marsh cone test

Focus of the experimental campaign was the evaluation of slurries bentonite rheological properties, testing their flowability through the Marsh cone test.

The Marsh cone test is an effective method for evaluating the flowability of bentonite slurries and other mixtures like cement paste or grout. It measured the time needed by 1L of slurries to flow out of the Marsh cone, through standard nozzle, under the influence of gravity. The procedure was performed in accordance with the UNI 11152 standard. Marsh viscosity is an empirical index of the real viscosity, and between them there is a direct correlation, lower viscosity means lower Marsh viscosity but higher flowability, while higher viscosity results in higher Marsh viscosity but lower flowability. This parameter is particularly relevant in tunnelling practice, because it is an important indicator to evaluate the pumpability of a mixture and its capacity to keep excavated material in suspension.

The apparatus consists of a conical funnel made of plastic, with an overall height approximately of 350 mm and at the bottom the funnel is connected to a discharge tube of 50 mm ending with an orifice, with an internal diameter of 4.7 mm. The top funnel mouth half part is foreseen of sieving cloth 2 mm mesh (figure 5.20).

Figure 5.20 - Marsh cone apparatus and the stopwatch during test (left), checking the vertical alignment of the Marsh funnel on the metallic stand (right)

The procedure began with a manual mixing of slurry using a wooden stick. Approximately ten circular movements were performed to break the high surface tension that may otherwise lead to unreliable test results. This process was not needed for slurry tested immediately after preparation. Bentonite slurry was then carefully poured into the cone through half of the funnel's opening, where a mesh screen prevents the entry of floccules, or other coarse particles that could obstruct the flow and invalidate the measurement. During this operation, the outlet orifice at the bottom of the cone was kept closed with a finger to avoid premature slurry loss. The filling continued until the slurry level reached the mesh. The test started at the exact moment the operator removed the finger from the orifice, allowing the slurry to flow, and simultaneously activating the stopwatch. When the level of slurry in the graduate cup reached the 1 L mark, the stopwatch was stopped, and the time recorded in seconds. After each test, the remaining slurry in both the cone and the cup was poured back into the mixing bucket containing the rest of the slurry. The test was repeated three times for each condition, to obtain more accurate and reproducible results. Repetition was necessary since the rheological properties of bentonite slurries can change rapidly, even the test procedure itself induced mechanical stress that can slightly modify the viscosity and, consequently the fluidity of the mixture between consecutive runs. In some particular cases, due to the high viscosity of the slurry, the flow through the cone orifice stopped completely. When this happened, slurry inside the cone was agitated using a wooden stick trying to repristinate the flow. This procedure was adopted just in few cases only to complete the tests, and the results were considered merely as a reference, indicating the extremely high viscosity that prevented the normal execution of the test.

For each bentonite type, two slurries were prepared and tested as follows:

- **Non-stressed slurry (static):**

  The slurry was only stirred during preparation, after which it was immediately tested and then left to rest until the next measurement. Tests were performed on the same slurry after 0h, 1h, 3h, 4h, 24h, 48h, and 72 hours of resting time to assess the effect of progressive hydration.

- **Stressed slurry**:

  At different hydration time, 4h, 24h, 48h, and 72 hours, the slurry was tested under mechanical degradation. Before each test, the mixture was subjected to mechanical stress using the same laboratory mixer adopted for preparation.

5.4.1 Mechanically stressed slurry

The Marsh cone test procedure, previously explained, was adopted both for testing the non-stressed slurry and the stressed slurry. For the mechanically stressed slurry, the procedure was slightly different due to the addition of the mechanical stressing phase before the tests. At each hydration time (table 5.1), the marsh cone test was performed five times, immediately after 0 – 5' – 5' – 10' – 30' minutes of stress, applied through the same equipment used for bentonite slurry preparation, the laboratory mixer ARGO LAB AM20-D, this time at a constant speed of 1000 RPM.

The procedure was structured as follows:

- First, the marsh cone test was carried out before any mechanical stress. This initial measurement is used as a reference for evaluating the viscosity change by the subsequent stress cycles, and to evaluate the degree of microstructure recovery compared with the previous hydration stage. The test at 4 hours hydration and zero stress, allows the comparison between static the non-stressed slurry result at the same hydration time.
- Then the slurry was immediately subjected to mechanical agitation using the laboratory mixer for 5' minutes at 1000 RPM. The stress is applied using same propeller (fig. 5.19).
- Following the first 5' stress, the procedure was repeated with additional 5', then for 10' and finally for 30' of mechanical stress.
- At the end of the stressed phase, the slurry was covered with a plastic sheet and left to rest until the next schedule hydration time, when the same procedure was repeated.

Figure 5.21 - Slurry subjected to mechanical stress (left) and immediately tested (right)

5.5 Slurry unit weight and temperature measurements

Both unit weight and temperature can significantly affect the performance of bentonite slurries. Therefore, measuring these parameters was fundamental to accurately define the boundary conditions of the experimental program.

5.5.1 Unit weight

The unit weight of slurries was measured in accordance with the standard ASTM D4380-20 (standard test method for determining density of construction slurries), using a mud balance with ± 0.005 g/cm^3 resolution, designed to determine the weight of fluid suspension such as drilling muds and construction slurries (figure 5.22).
The unit weight of each bentonite slurry was measured every time the tests were performed, at all the different hydration time, for both stressed and non-stressed slurries.

Figure 5.22 - Mud balance

5.5.2 Temperature

Temperature measurements were carried out using the laboratory thermometer (Checktemp® 1 - HI98509) (figure 5.23) with an accuracy of ±0.2 °C. To carry out a precise measurement, the final metal section of the probe, which houses the thermistor sensor, was inserted into the bentonite slurry, ensuring that the entire metal portion was fully submerged. The thermometer was then left in place for a few seconds to allow temperature to stabilize, before taking the reading. The temperature control was monitored as for the density, every time the test was performed, at all the different hydration time, on both stresses and non-stressed slurries.

Figure 5.23 - Laboratory thermometer

5.6 Viscometer test

A better evaluation of bentonite slurries' rheology was also developed directly measuring the viscosity, using a rotational viscometer (Fungilab Alpha series). The instrument measures the torque of a rotating spindle in a sample at a specified velocity, measuring the viscosity in mPa·s with a precision of ± 1%. Different spindles are provided with the instrument to cover a wide range of viscosity measurements.

The viscometer test was performed on slurries prepared using only bentonite ID7.

The test was carried out on different slurries at varying concentration and only few hydration times. The choice was made because the results of the Marsh cone test showed a marked increase in viscosity after 24h of hydration, making slurry became too viscous to provide meaningful results, difficult to measure through the viscometer. In table 5.6 the slurry concentrations and hydration time at which the viscometer tests were performed are indicated.

Table 5.6 - Concentration and hydration time adopted for the Viscometer tests

Bentonite	Concentrations (kg/m^3)	Test hydration time (h)				
ID7	45	0	1	3	4	24
	60	0	1	3	4	24
	80	0	1	-	-	24

Before performing the test, some preliminary procedures were completed to prepare the viscometer for testing:

- A small bucket was filled with slurry bentonite until reaching a line that runs all the bucket wall, near the top.
- The viscometer, positioned on a laboratory bench, was levelled by adjusting its three support feet to ensure proper horizontal alignment, checking the built-in bubble level. When the bubble level was centred within the marked circle, the test could begin.
- The spindle was then screwed onto a preinstalled support, making sure to select the right one. Four different cylindrical shape spindles are provided with the instrument, for increasing mixture viscosity L1, L2, L3 and L4. Starting from L1, which presents the biggest dimensions in diameter and height, used for very low viscosity mixture, to L4, in which the spindle dimension became millimetric, used for very high viscosity. To select the correct spindle, the display during measurement apart from the viscosity, gives also a percentage of the full-scale range. This value represents

the torque applied to the spring, relative to its maximum deflection, and must be comprised between 15% up to 100%, for an optimal operational range, otherwise the measurement cannot be considered valid.

- A metallic U-shaped metal frame, called spindle protector, completes the viscometer configuration. It is a fundamental element that defines the influence area of spindle rotation.
- The bucket with the bentonite slurry was positioned under the spindle, and by rotating the adjustment wheel, the entire viscometer head was lowered until the spindle was submerged by the slurry to the halfway mark in the axle.
- Before starting the measurements, both the spindle type and the wanted rotational speed in rpm had to be selected on the display.

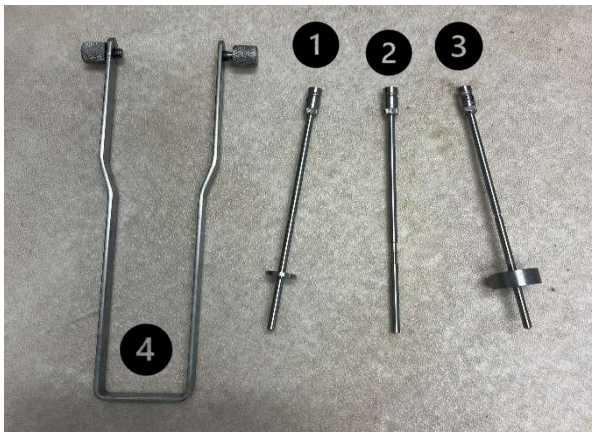

Figure 5.24 - Spindle types and spindle protector

1) Spindle type L2
2) Spindle type L4
3) Spindle type L3
4) Spindle protector
5) Viscometer head
6) Viscometer adjustable support feet

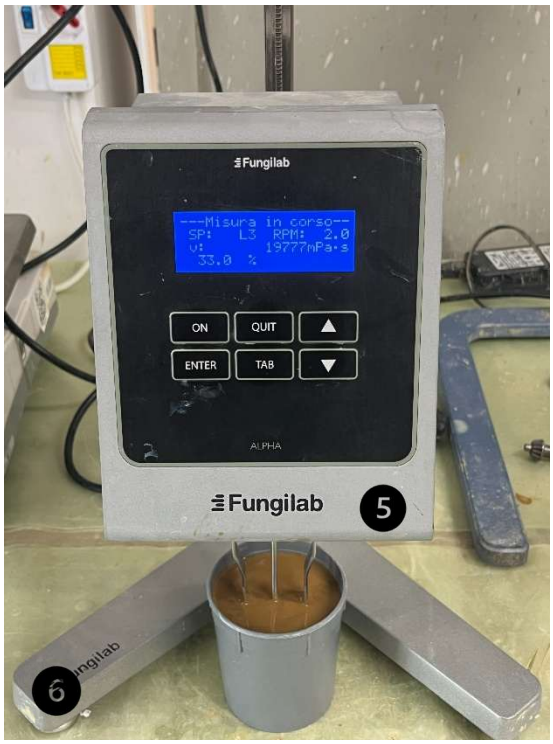

Figure 5.25 - Viscometer and bentonite slurry

The test procedure was established after some trial tests were done before starting the effective research campaign. Due to the thixotropy of bentonite slurry, the viscosity will vary when subjected to different shear stresses applied by the rotating spindle during tests. In addition, the instrument does not provide a specific viscosity value immediately, but changes rapidly in the first second of tests, until reaching an almost constant value or the variation remains under a certain threshold.

The viscometer measurements were performed by applying a sequence of decreasing and increasing rotational speed selecting it before starting the measurement. Starting from the

maximum shear rate that the viscometer can generate (100 rpm), the spindle rotational speed was progressively reduced to the minimum value (1 rpm), passing through some of the intermediate speeds, supported by the viscometer. Two full down-up cycles were completed for each slurry at each selected hydration time, every time using a fresh sample taken from the main container where the slurry had been prepared.

Table 5.7 - Up and down cycle during viscometer measurements

Cycle	Test sequence	Rotational speed range (RPM)
1	Decreasing	100 to 1
	Increasing	1 to 100
2	Decreasing	100 to 1
	Increasing	1 to 100

For each rotational speed, measurement duration was adjusted accordingly, due to the continuous viscosity variation through the entire test (figure 5.8). The viscosimeter manufacturer suggests, to wait at least five rotations, corresponding to five measurements, before considering valid the measurement. For this reason, it was decided to record the display of the instrument, using a mobile phone video, to capture the viscosity reading, instead of manually writing the results. The recording started when the first value of viscosity appeared on the display, typically few seconds or minutes from the beginning of the measurements, depending on the time that the instrument needs to stabilize, which varied with the chosen rotational speed. Based on the selected rotational speed, the video recording was set to a precise number of seconds, trying to capture all the main viscosity variation and deciding during the post-processing result analysis, which value to use.

In case of very low rotational speed, such as 1, 2 rpm, instead of a video, a photo of the display showing the first viscosity measurement was taken, instead of waiting for the five measurements as indicated by the producer. This decision was supported by previous tests, which showed very low differences, around 1%, between the first viscosity value and the one obtained after five complete rotations. In addition, as previously mentioned, the instrument needs sometimes before showing the first measurement, at low speed, such as 1 rpm, needs up to 1-1.5 minutes, meaning that the first recorded value could be already considerably stable.

Table 5.8 - Viscosity measurement duration for each selected RPM

Rotational speed (RPM)	Measurement/recording duration (s)
100	40
60	40
50	40
30	40
20	40
10	40
6	30
5	30
4	20
3	20
2	photo only
1	photo only

All the video recordings from each measurement campaign were reviewed during the post processing phase of the data analysis. From each video the viscosity value was extracted every 5 seconds. Consequently, based on the measurement duration, corresponding to each rotational speed, a varying number of viscosity values was obtained and noted into an Excel spreadsheet.

5.7 Filter cake formation test

To evaluate the capacity of bentonite to produce a filter cake and its quality in terms of pressure seal and thickness, a filter cake formation test was performed.

The investigation on the filter cake formation is important to understand how the slurry interacts with the soil, because as previously explained, the formation, thickness, permeability and hydraulic behavior of the filter cake also depend on slurry rheological properties. The test was caried out using slurry prepared with bentonite ID7, having also available both the Marsh cone and viscometer measurement, the results were useful to evaluate the correlation between the rheological properties and the bentonite filter cake quality and to assess its effectiveness in real word tunnelling applications, in avoiding fluid infiltration and maintain face excavation integrity.

The cake formation test was evaluated by applying a pressure of 2 bars for 10 minutes. The procedure utilized a laboratory set-up composed of a compressed air system and specimen holding cells (figure 5.26).

1) The compressed air system produces constant and controlled pressure ensuring precise and stable testing conditions. The apparatus is composed of galvanized steel pipes and fittings, with a nominal diameter of 1-2 inches (=12.7 mm), to which vertical branches are connected, to allow the attachment of the specimen holding cells. For pressure control the system presents a manometer to monitor the applied pressure, a ball valve, and a vent valve.
2) The specimen holding cells are Plexiglas tubes, which contain during tests both the soil sample and the bentonite slurry. The tube dimensions are 50 mm internal diameter, a thickness of 5 mm and a length of 380 mm. The cell is securely screwed to the vertical branch, with the gasket at the top that ensures the cell pressurization. At the bottom of the cells, before being filled with the sample are inserted in order, a porous stone blocking the sand grain while letting the water flow, and a filter cloth to prevent clogging of the porous stone. The base is fitted with a Plexiglas disc, with a threaded aperture in the center that accommodates a valve positioned at the bottom.

1) Specimen holding cell
2) Galvanized steel pipes
3) Gasket
4) Manometer
5) Cell bottom vale
6) Bentonite slurry
7) Test specimen

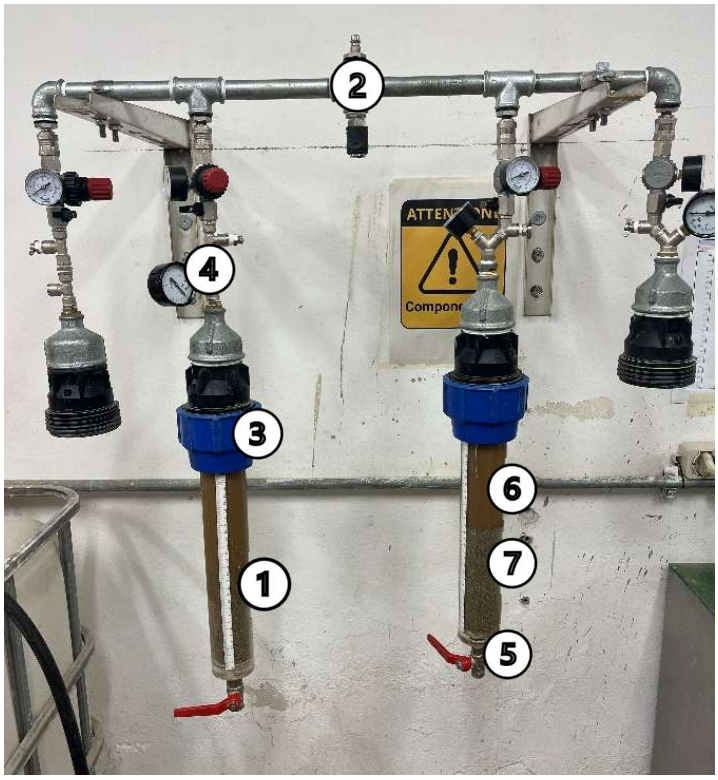

Figure 5.26 - Filter cake test apparatus

The test was carried out filling the specimen holding cells with a different type of soil and slurry, at varying concentrations 45 kg/m^3, 60 kg/m^3, 80 kg/m^3, to evaluate concentration influence.

Two types of soil were prepared using different grain size fractions:

- T1: soil composed of 50 % soil with a grain size of 0.5 mm and 50% with a grain size of 1 mm. Soil with this grain distribution is generally classified as coarse sand with very fine gravel, a granular medium with high permeability
- T2: soil composed of 50 % soil with a grain size of 0.25 and 50 % with a grain size of 0.5mm. This less-coarse soil can be considered representative of a medium to coarse sand with low fines, with lower permeability.

Each grain size material was taken from a bucket containing soil previously separated by sieving. The different grain size fractions were then mixed in another container, adding water, to make the sample saturated.

The specimen holding cells, after inserting the porous stone and filter cloth, were filled with the loose pre-saturated terrain in different steps. Each 5 cm layer of material was compacted by dropping a weight of 2 kg from a height of 5 cm from the soil free surface 5 times, each layer. The process is repeated until the sample reaches a thickness of 15-17 cm, checking the millimetre strips placed on the outer cylindrical surface of the cell. After the last layer of material was compacted, the bentonite slurry was added, making sure to fill the cell all the way up, to avoid air infiltration. Then the specimen was sealed and screwed to the compressed air system. The system valve, already pressurized at 2 bars, was opened to pressurize the specimen holding cell. During the 10 minutes waiting period, for some interval of time, the valve at the bottom of the cell was opened to allow the water in excess to flow out, driven by the applied pressure.

After 10 minutes the valve at the top and the bottom were closed and the specimen cells unscrewed from compressed air system. After discharging the excess slurry and cleaning the cell as much as possible, the soil sample was carefully removed, gently spraying compressed air through an air pressure gun, without breaking the filter cake formed on top of the specimen, allowing further measurement of its thickness and quality.

6 Results

In the following section will be presented the results obtained during the research campaign developed in the Tunnelling & Underground Research Center of Politecnico di Torino. The tests aim to evaluate the rheological behavior of slurries prepared with 8 different bentonites, analysing their response under varying bentonite concentration, hydration time and mechanical stress.

6.1 Marsh cone tests results

The Marsh cone test results provide a direct measure of bentonite slurry fluidity and an empirical indication of its viscosity, commonly referred to as Marsh viscosity.
In the following paragraph, Marsh cone results for each bentonite type and concentration are presented, both in static condition, without applying mechanical stress, and after being stressed. For each Bentonite, a result table and corresponding graph are provided, showing for each hydration time, the following parameters in addition to the Marsh viscosity result:

- Mean marsh viscosity value ($\mu_{\text{Marsh viscosity}}$), calculated from at least three Marsh viscosity measurements (Mv) carried out at each (i) hydration time.

$$\mu_{iMarsh\ viscosity} = \frac{Mv_1 + Mv_2 + Mv_3}{3}$$

- Relative variation (Δ_i), which expresses, in percentage, the Marsh viscosity variation between two consecutive hydration periods or, in case of stressed slurry, between two consecutive stress cycles at the same hydration stage:

$$\Delta_i = \frac{\mu_i - \mu_{i-1}}{\mu_{i-1}} \cdot 100$$

- Standard deviation ($\sigma_{\text{Marsh viscosity}}$), used to evaluate the variability, between repeated test, and to assess the reliability of the measurements and the suspension stability

For the Marsh cone result obtained on stressed slurry, additional parameter are provided to evaluate the rheological behavior and resistance to stress:

- Stress Resistance Index (SRI), which expresses, in percentage, the mechanical resistance of the slurry, evaluating the original portion of viscosity retained after each stress time, compared to the initial viscosity measured before stress.

$$SRI = \frac{\mu_{i_{after\ stress}}}{\mu_{before\ stress}} \cdot 100$$

- As will be presented in the following paragraph, the Marsh viscosity of the stressed slurries exhibits a plateau-like trend. To analyse this behavior, an exponential interpolation model was applied to the experimental data. The main objective was to evaluate the plateau viscosity value and the time needed at each hydration stage to reach these conditions.

The exponential interpolation equation is defined as follows:

$$\mathrm{Mv}\,(\mathrm{t}) = \mathrm{Mv_{fin}} + (\mathrm{Mv_{in}} - \mathrm{Mv_{fin}}) \cdot e^{\frac{t}{\tau}}$$

Where:

- Mv (t) is the interpolated Marsh viscosity at the stress time t
- Mv_{fin} = mean Marsh viscosity result after the last 30 minutes of stress
- Mv_{in} = mean Marsh viscosity value at 0 minutes of stress
- t = stress time (min)
- τ = characteristic time to reach the plateau conditions (min)

The interpolations were performed using the Excel Solver tool, fixing the value of Mv_{in} and varying τ, Mv_{fin}, to minimize the residual, Root Mean Square Error (RMSE), and maximize the coefficient of determination (R^2), which quantifies the variability between the experimental data respect the interpolation value of the interpolation model. To complete the result for both static and mechanically stressed slurry, the assessments of density and temperature are given to define the boundary conditions of the test measurement and complete the framework for an exhaustive analysis.

6.1.1 ID1 - 60 kg/m^3 static

The static test aimed to assess the natural viscosity evolution over hydration time, without mechanical agitation. In table 6.1 and graphically in figure 6.1, are presented the results of the Marsh cone test on slurry prepared with bentonite ID1 at a concentration of 60 kg/m^3.

Table 6.1 - ID1 static Marsh cone test results

Hydration time (h)	$\mu_{Marsh\ viscosity}$ (s)	Relative variation (%)	$\sigma_{Marsh\ viscosity}$ (s)	γ (L/m^3)	T (°C)
0	67,26	0%	0,6	1,04	28,0
1	78,47	16,67%	2,3	-	27,3
3	88,76	13,11%	1,3	-	26,8
4	97,75	10,13%	11,3	-	25,5
24	164,75	68,55%	34,2	1,04	24,9
48	175,20	6,34%	25,5	1,04	25,1
72	171,45	-2,14%	14,7	1,04	25,0

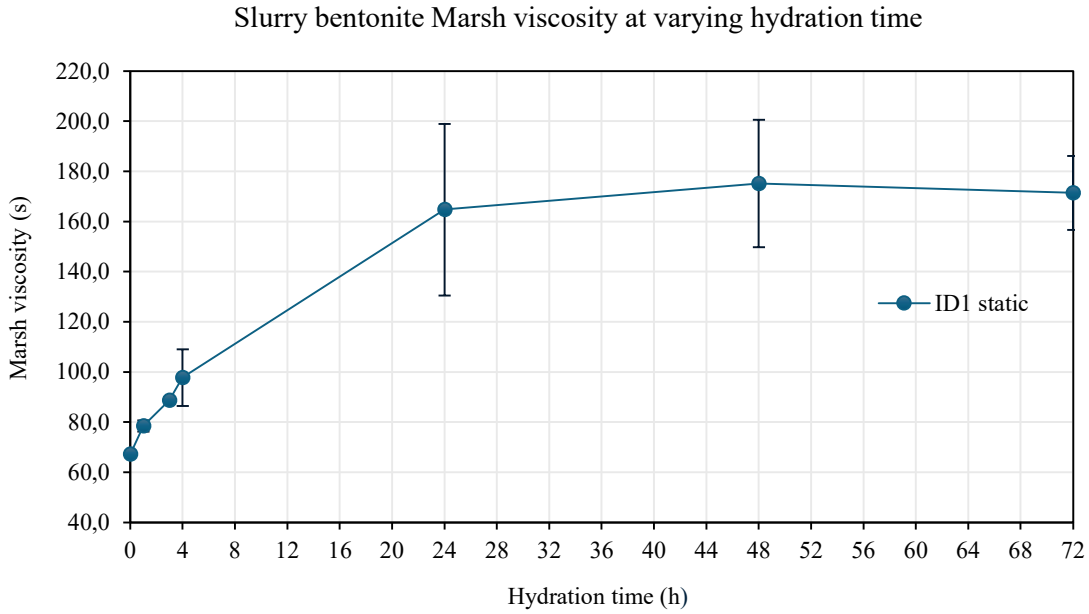

Figure 6.1 - ID1 Graphical representation of the Marsh viscosity variation at each hydration time

The obtained values provide interesting results, showing the variation of viscosity, at different hydration times. ID1 shows almost constant increment during the first 4 hours of hydration, adding 10 s at the Marsh viscosity time, during each hydration phase. Between 4 and 24 hours the increment became more relevant passing from 98 s to 165 s, subsequently the variation tends to stabilize around a constant value. The standard deviation demonstrates good precision and stable suspension until 4 hours of hydration, while at 24 hours the suspension became less stable, more susceptible to the low agitation which was subjected during test.

6.1.2 ID1 - 60 kg/m^3 mechanically stressed

This section presents the Marsh cost test results, for slurry prepared with bentonite ID1, subjected to multiple stress cycle, each consisting of a defined mixing time, applied using a laboratory mixer, at a constant speed of 1000 rpm. After each stressing phase, a Marsh cone test was performed to measure the corresponding change in slurry viscosity.

Table 6.2 - ID1 stressed Marsh cone test results

Hydration time (h)	stress time (min)	$\mu_{Marsh\ viscosity}$ (s)	relative variation (%)	$\sigma_{Marsh\ viscosity}$ (s)	SRI	γ (kg/L)	T (°C)
4	0	97,80	0,00%	11,3	100,0%	1,04	25
	5'	57,91	-40,79%	2,1	59,2%		
	5'+5'	57,27	-1,09%	2,6	58,6%		
	5'+5'+10'	53,83	-6,01%	1,0	55,0%		
	5'+5'+10'+30'	52,74	-2,02%	0,2	53,9%		
24	0	138,22	0,00%	13,0	100,0%	1,04	27
	5'	57,59	-58,33%	2,1	41,7%		
	5'+5'	54,79	-4,87%	1,6	39,6%		
	5'+5'+10'	53,38	-2,58%	1,0	38,6%		
	5'+5'+10'+30'	52,82	-1,04%	1,3	38,2%		
48	0	119,05	0,00%	28,7	100,0%	1,04	25
	5'	56,87	-52,23%	1,2	47,8%		
	5'+5'	54,97	-3,34%	1,4	46,2%		
	5'+5'+10'	54,87	-0,18%	0,8	46,1%		
	5'+5'+10'+30'	54,40	-0,86%	1,2	45,7%		
72	0	148,02	0,00%	31,0	100,0%	1,04	27
	5'	56,20	-62,03%	1,7	38,0%		
	5'+5'	53,60	-4,63%	1,1	36,2%		
	5'+5'+10'	53,43	-0,31%	0,4	36,1%		
	5'+5'+10'+30'	53,53	0,18%	0,2	36,2%		

In table 6.2 the viscosity decreases after mechanical stress is evident. The marsh viscosity drops down to a mean value of 52 s after the first 5 minutes of stress at all hydration times. The additional stress cycles imply slightly additional loss in viscosity, in the order of -1/2%.

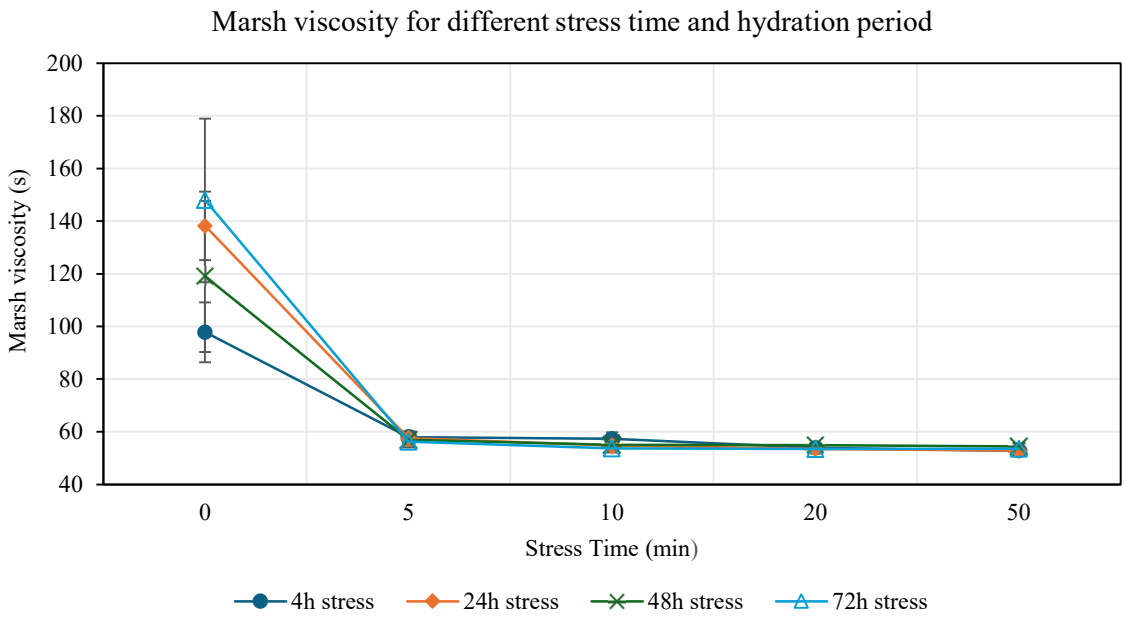

Figure 6.2 - ID1 Graphical representation of Marsh viscosity variation after mechanical stress cycles

Graphically, the Marsh viscosity reduction after the first 5 minutes of stress is immediately visible. It's also possible to visualize constant behavior after being subjected to additional stress cycles. It is also evident the decrease of the standard deviation, which became almost null after the stress cycle.

6.1.3 ID1 result analysis, stress vs static behavior

The Marsh cone test result for bentonite ID1 presents interesting rheological behavior in both static and stressed conditions. In static conditions, the effect of hydration is clearly visible. Marsh viscosity undergoes a significant increase during the first 4 hours, with the highest relative growth occurring within the first hour. This demonstrates the good water absorption capacity of bentonite and the rapid development of three-dimensional flocculated structures of montmorillonite particles that increase viscosity.

Viscosity increases till the 48h, where the maximum value is reached, with value similar to those obtained at 24 h, and the subsequent variation at 72 h remains limited. This indicates that bentonite ID1 is essentially fully hydrated after approximately 24 hours, value, that represents the stabilization time, the time after which no important viscosity variations are visible, and the relative variation remains under 10%.

The high standard deviation observed at 24 h suggests that the slurry structure is not yet completely uniform at this stage, likely due to localized flocculation or regions not fully

hydrated. As a result, slight movements or disturbances during testing may still have influenced the measurements, reflecting a microstructure that is not fully stable, highly sensitive to mechanical effects.

The susceptibility to mechanical effect became more evident after the stress cycle. Stress results show an important decrease in viscosity after the first 5' minute of applied stress. This indicates that bentonite ID1 structure easily deteriorates if subjected to mechanical stress. The hydrated particles that have formed a three-dimensional structure with electrostatic attraction between the clay platelets, are almost destroyed under shear. But the result demonstrates also an important thixotropic recovery behavior. Analysing the viscosity value at 0 stress time after 4 hours of hydration, the viscosity passes to a value of approximately 52 s to 138 seconds at 24 hours, this represents an almost complete recovery of the original structures, creating again a viscous gel.

In figure 6.3, the whole results of the March cone measurements are reported to easily visualize the viscosity variation at varying hydration time and stress condition, focusing on the viscosity drop and recovery after being stressed.

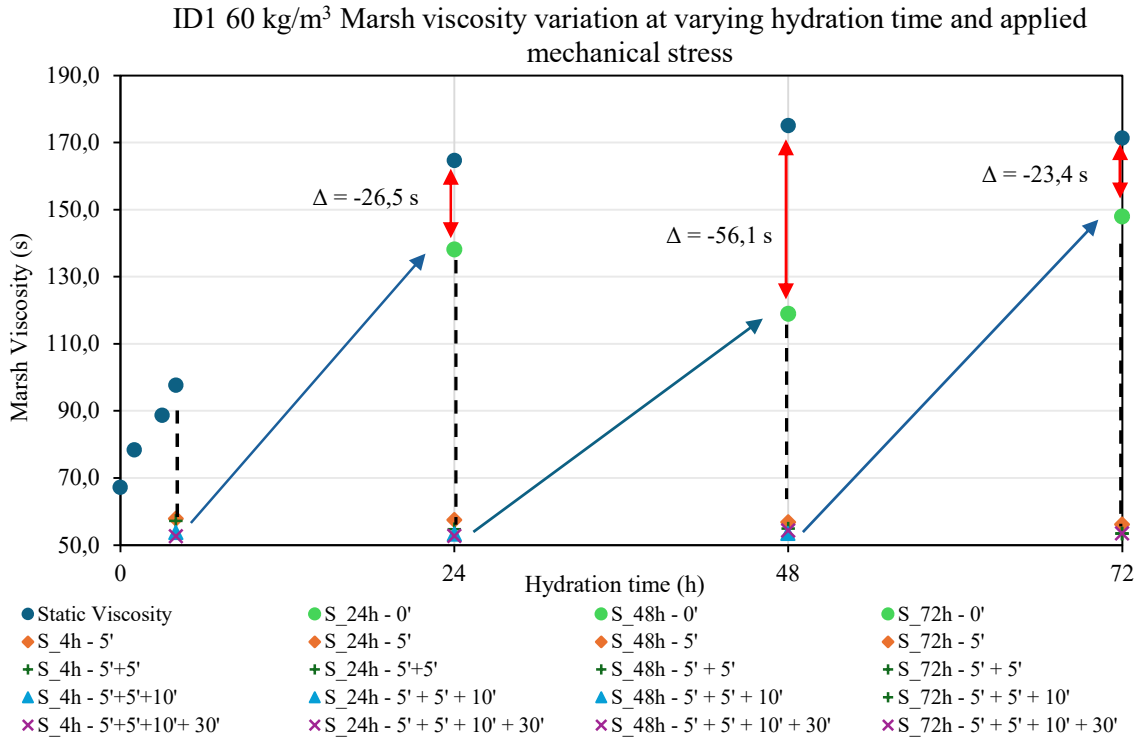

Figure 6.3 - Graphical visualization of the viscosity result of bentonite ID1 in static and stressed condition

The dash line arrows and blue arrows highlighted the strong thixotropic behavior of bentonite ID1. Under mechanical stress the viscosity loss is marked (dash black line) but after rest bentonite shows significant capacity of rebuilding particles interaction and partially

recovers the original structures, leading to a viscosity recovery (blue arrows) near the static value at each hydration time.

The graph highlights an interesting behavior at 48 h, where the slurry exhibits the highest static viscosity, but the lowest viscosity recovery after stress, with a difference in Marsh viscosity between the static value and prestress condition of approximately 56 s (red arrow). That important differences can be related to a well-developed flocculated structure, that once fully hydrated show a form of rheological hysteresis, meaning that the structure rebuilding after stress breakdown, need more resting time to reach similar prestress value to those observed at 24 or 72 hours.

The exponential interpolation of the experimental result (table 6.3) clearly shows the immediate stress impact on the slurry viscosity.

Table 6.3 - Bentonite ID1 interpolation value and relative error

Hydration time (h)	τ (min)	$Mv_{,in}$ (s)	$Mv_{,inf}$ (s)	(RMSE)	Δ Marsh (%)	R^2
4h	2,1	97,80	54,34	1,9151	-44,44	0,99
24h	1,7	138,22	53,56	0,3287	-61,25	1,00
48h	1,5	119,05	54,72	0,0313	-54,04	1,00
72h	1,4	148,02	53,49	0,0012	-63,86	1,00

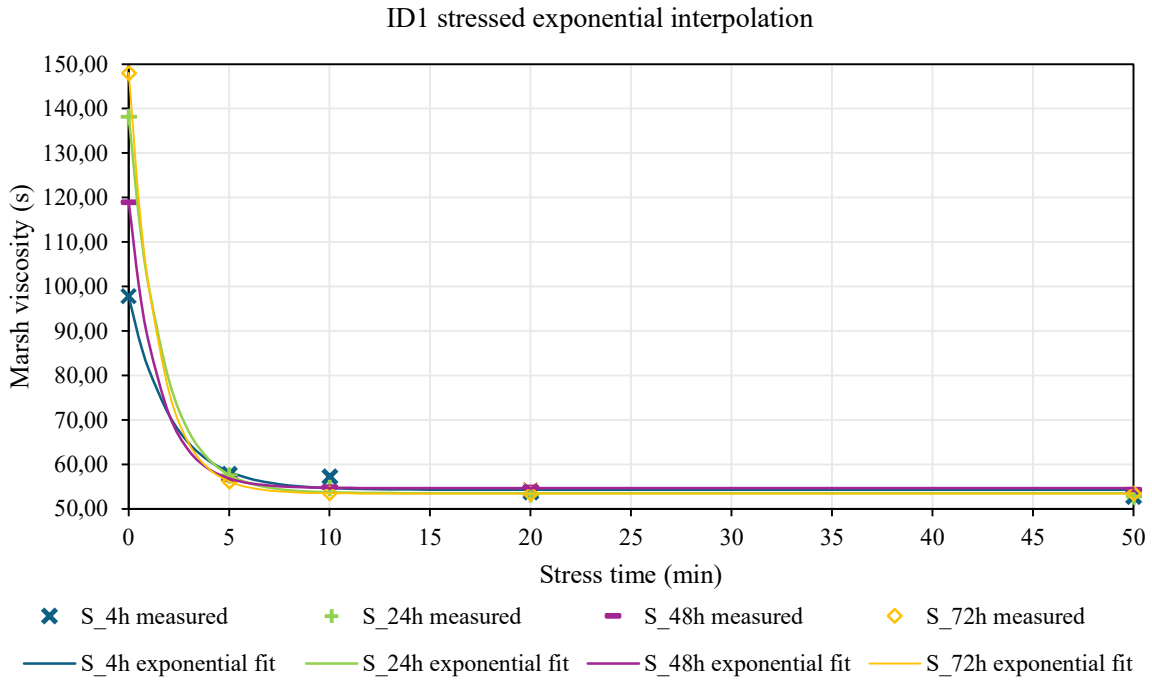

Figure 6.4 - ID1 graphical interpolation of the experimental result

The interpolation fits quite well the experimental result, with the correlation value (R^2) all around 1, meaning very limited differences between the interpolated value and the experimental result.

The approximative time at which the viscosity reaches the plateau is around 2 minutes for all hydration time. This result is compliance with the Marsh cone test results, that shows the mechanical degradation immediately during the first minutes of stress. This describes deeply the rheological behavior of bentonite ID1, showing that the viscosity decreases also under small mechanical intensity stress and most important, the drop is not affected by the stress duration, but happens quickly.

6.1.4 ID2 - 60 kg/m^3 static

In table 6.4 and graphically in figure 6.5, are presented the results of the Marsh cone test carried out on slurry prepared with bentonite ID2 at a concentration of 60 kg/m^3.

Table 6.4 - ID2 static Marsh cone test results

Hydration time (h)	$\mu_{Marsh\ viscosity}$ (s)	Relative variation (%)	$\sigma_{Marsh\ viscosity}$ (s)	γ (kg/L)	T (°C)
0	40,64	0,00%	0,7	1,04	27,2
1	41,85	2,96%	0,3	-	26,6
3	43,90	4,91%	0,1	-	27,0
4	45,10	2,73%	0,6	-	27,0
24	48,85	8,32%	0,7	1,04	25,0
48	52,24	6,93%	0,7	1,04	25,2
72	47,82	-8,46%	0,4	1,04	25,0

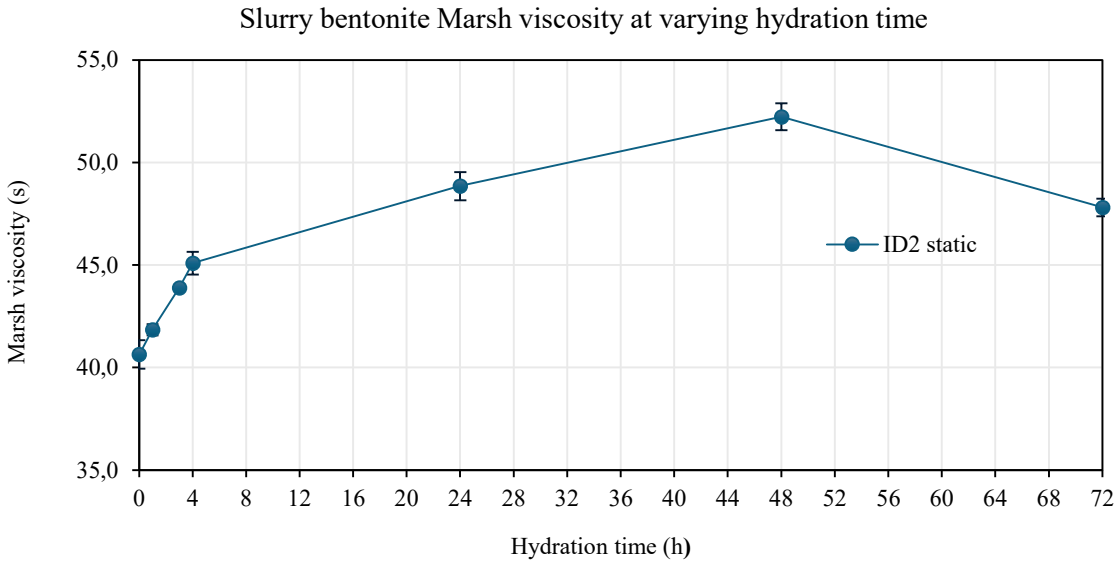

Figure 6.5 - ID2 Graphical representation of the Marsh viscosity variation at each hydration time

The slurry prepared with bentonite ID2 presents Marsh viscosity values ranging from 40 s, measured immediately after preparation, to a maximum of 52 s after 48 hours of hydration. The standard deviation is very low, reaching the maximum value of 0,7 s. In figure 6.4, the Marsh viscosity trend is presented, highlighting also a small reduction of viscosity, after 48 hours.

6.1.5 ID2 - 60 kg/m^3 mechanically stressed

This paragraph presents the Marsh cost test results for the slurry prepared with bentonite ID2, subjected to mechanical stress using a laboratory mixer, at a constant speed of 1000 rpm with progressively increasing stress duration. After each stressing phase, a Marsh cone test was performed to measure the corresponding change in slurry viscosity.

Table 6.5 - ID2 stressed Marsh cone test results

Hydration time (h)	stress time (min)	$\mu_{Marsh\ viscosity}$ (s)	relative variation (%)	$\sigma_{Marsh\ viscosity}$ (s)	SRI	γ (kg/L)	T (°C)
4	0	41,49	0,00%	0,5	100,0%	1,04	26,2
	5'	39,94	-3,73%	0,4	96,3%		
	5'+5'	39,89	-0,13%	0,5	96,2%		
	5'+5'+10'	39,91	0,05%	0,0	96,2%		
	5'+5'+10'+30'	39,99	0,18%	0,2	96,4%		
24	0	44,98	0,00%	0,5	100,0%	1,04	24,9
	5'	41,24	-8,31%	0,3	91,7%		
	5'+5'	40,98	-0,64%	0,4	91,1%		
	5'+5'+10'	41,03	0,12%	0,3	91,2%		
	5'+5'+10'+30'	41,01	-0,04%	0,3	91,2%		
48	0	45,69	0,00%	0,5	100,0%	1,04	25,0
	5'	42,43	-7,12%	0,3	92,9%		
	5'+5'	41,04	-3,29%	0,6	89,8%		
	5'+5'+10'	41,46	1,04%	0,2	90,8%		
	5'+5'+10'+30'	41,94	1,15%	0,1	91,8%		
72	0	45,72	0,00%	1,0	100,0%	1,04	24,7
	5'	42,49	-7,06%	0,0	92,9%		
	5'+5'	41,65	-1,98%	0,2	91,1%		
	5'+5'+10'	42,12	1,13%	0,5	92,1%		
	5'+5'+10'+30'	41,83	-0,67%	0,1	91,5%		

Slurry prepared with bentonite ID2 shows a stable behavior after each stress cycle, with viscosity that remains almost constant, with very low decrease respect to the not stressed

results (table 6.5). The very low relative viscosity variation confirms the stability of the suspension. Viscosity passes from a value of 41 s, before stress, to 39 s after all the stress cycles, resulting in a drop of just 2 s and a relative variation of less than 7%, after 50 minutes of stress.

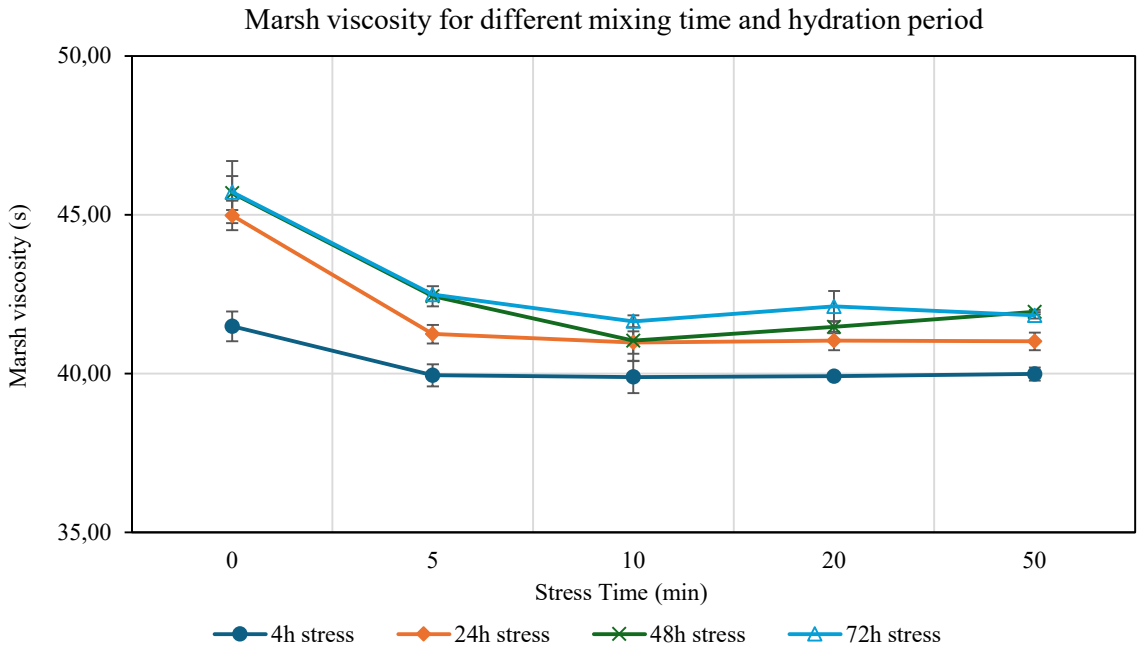

Figure 6.6 - ID2 Graphical representation of Marsh viscosity variation after mechanical stress cycles

Figure 6.6 shows the marked viscosity drop after the first 5-minute stress but highlights also that the viscosity remains nearly constant also increasing the stress time.

6.1.6 ID2 result analysis, stress vs static behavior

The results obtained from the Marsh cone test for bentonite ID2 exhibit a distinct behavior related to the hydration phenomena and stress applied.

The result shows that the rheological behavior in static conditions remains almost the same for all hydration times. Although a slight increase in Marsh viscosity is observed, it is not as pronounced as for bentonite ID1. The overall trend is similar, with a peak in viscosity reached at 48 h followed by a small reduction at 72 h. However, the magnitude of the increase is limited, approximately just 12 seconds, which indicates a bentonite with low hydration capacity. Although this result seems in contrast with the high measured value of the swell index, this is likely due to the highly sodic nature of bentonite with ESP over 30%. This composition led to a strong electrostatic repulsion and the expansion of the diffuse

double layer that promoted a disperse particle arrangement with few edges to face interaction. The result is a slurry where particles swell significantly, but that retains low viscosity and the lower mechanical degradation stress, due to the low amount of bond that can break under shear.

For this reason, the suspension appears also more stable with respect to the ID1, as the viscosity of the stressed slurry remains nearly constant after each stress cycle. The SRI shows value above 96 % for all hydration time after each stress time, indicating low susceptibility to mechanical degradation. Nevertheless, a small shear thinning behavior can also be identified in this bentonite. Figure 6.6 highlights a drop in marsh viscosity during the first 5-minute stress, indicating a little breakdown of the particles network.

The stability of the slurry is also underlined by the standard deviation, which tends to zero for every measurement, meaning less susceptibility to the agitation applied during the static testing procedure, differently from what was shown by bentonite ID1.

In figure 6.7 the whole result of the March cone tests for bentonite ID2 are presented to easily understand the particular stable behavior of this type of bentonite.

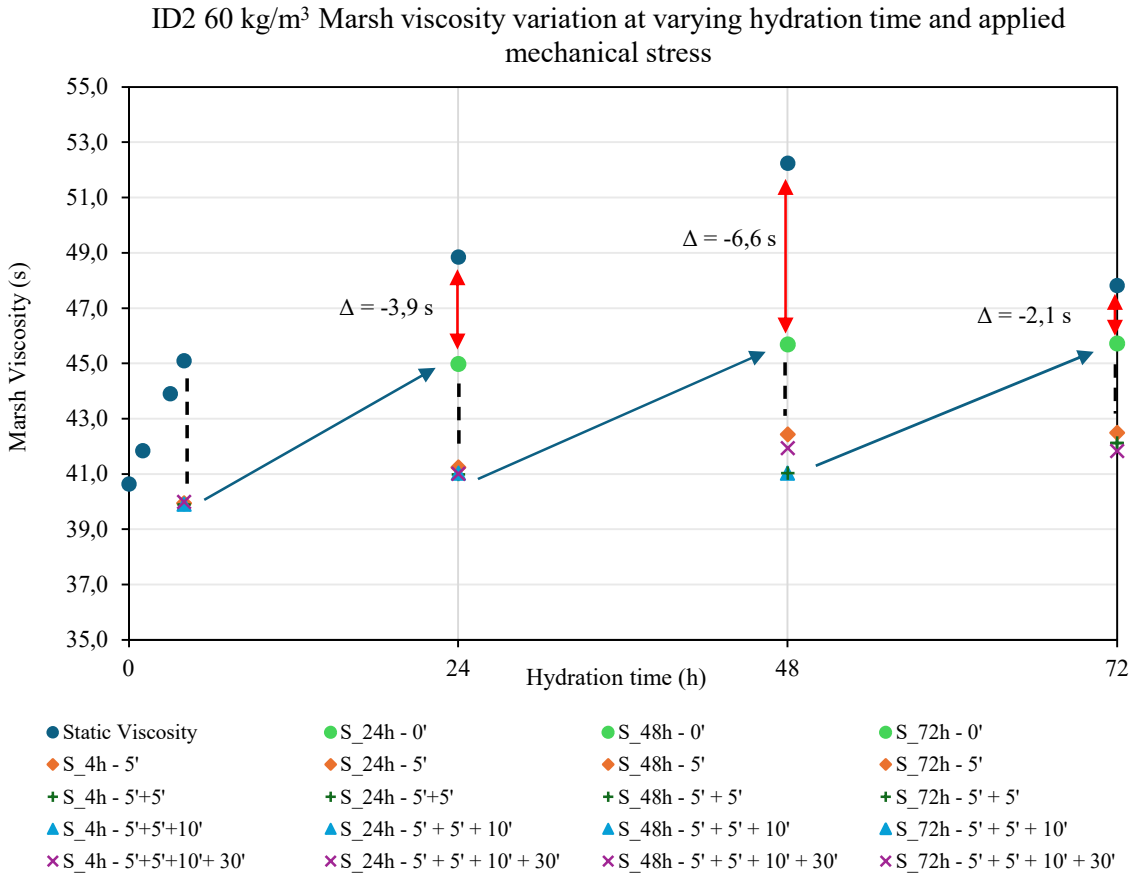

Figure 6.7 - Graphical visualization of the viscosity result of bentonite ID2 in static and stressed condition

With respect to ID1, the blue arrows indicating the viscosity recovery after stress, have almost the same inclination, highlighting that the thixotropic behavior is constant at each hydration time, so the structure rapidly recovers part of the original structures. Viscosity does not reach the previous value obtained in static conditions, meaning that the flocculated network tends to rebuild, but not fully recover the original configuration. This incomplete recovery can be due to irreversible bond breakage. The exponential interpolation of the experimental result, also for ID2, shows total independence from stress duration, because the major drop in Marsh viscosity is obtained immediately after some minutes of mechanical stress.

Table 6.6 - Bentonite ID2 interpolation value and relative error

Hydration time (h)	τ (min)	$Mv_{,in}$ (s)	$Mv_{,inf}$ (s)	(RMSE)	Δ Marsh (%)	R^2
4h	0,8	41,49	39,94	0,0010	-3,74	1,00
24h	1,8	44,98	41,00	0,0004	-8,84	1,00
48h	2,9	45,69	41,50	0,1171	-9,17	0,96
72h	2,6	45,72	41,86	0,0314	-8,43	0,99

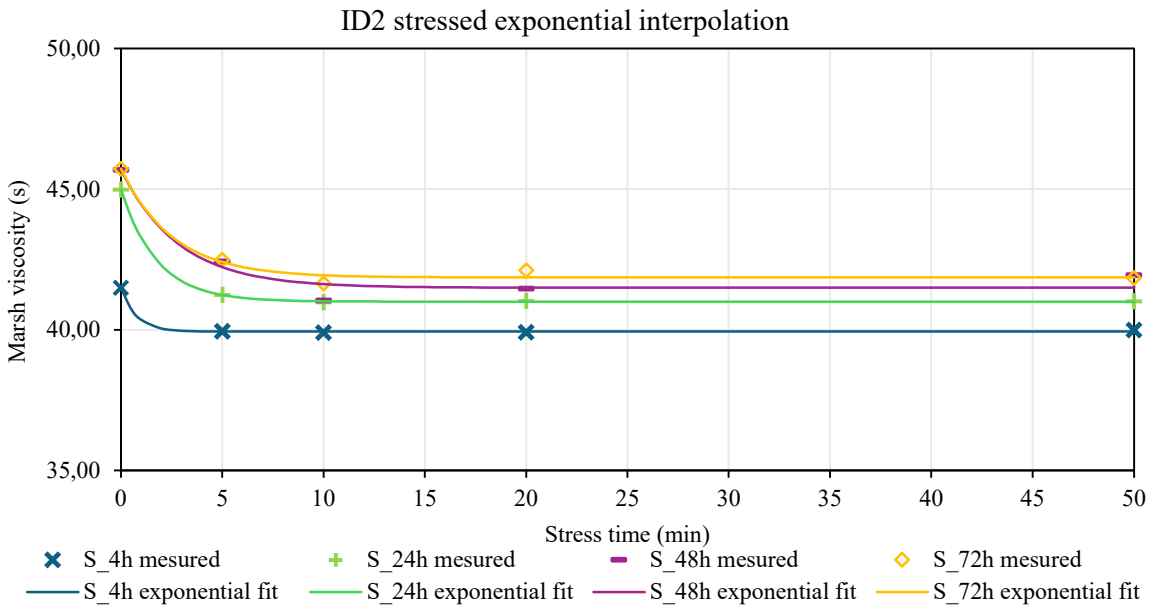

Figure 6.8 - ID2 graphical interpolation of the experimental result

The interpolation fits quite well the experimental result, and the value of R^2 is practically one for each hydration time (table 6.6). At 4 hours, the drop in viscosity is so limited that the plateau value is reached in less than a minute, just 50 seconds. This result represents a less developed structure that immediately breaks after some seconds of stress. The similar τ value obtained at 48 and 72 hours of hydration represents that bentonite is fully hydrated, and a solid structure already developed, which resists more to the stress applied. The slight

decrease in time needed to reach the plateau after 48 hours represents a saturation in water absorption capacity.

6.1.7 ID3 - 60 kg/m^3 static

In table 6.7 and graphically in figure 6.9, are presented the results of the Marsh cone test carried out on slurry prepared with bentonite ID3 at a concentration of 60 kg/m^3.

Table 6.7 - ID3 static Marsh cone test results

Hydration time (h)	$\mu_{Marsh\ viscosity}$ (s)	Relative variation (%)	$\sigma_{Marsh\ viscosity}$ (s)	γ (kg/L)	T (°C)
0	71,25	0,00%	3,3	1,05	25,3
1	94,97	33,28%	7,2	-	25,6
3	113,73	19,76%	12,6	-	26,1
4	121,25	6,61%	9,9	1,05	26,6
24	185,17	52,71%	13,5	1,04	25,5
48	278,18	50,23%	35,0	1,04	24,9
72	253,03	-9,04%	16,3	1,04	25,1

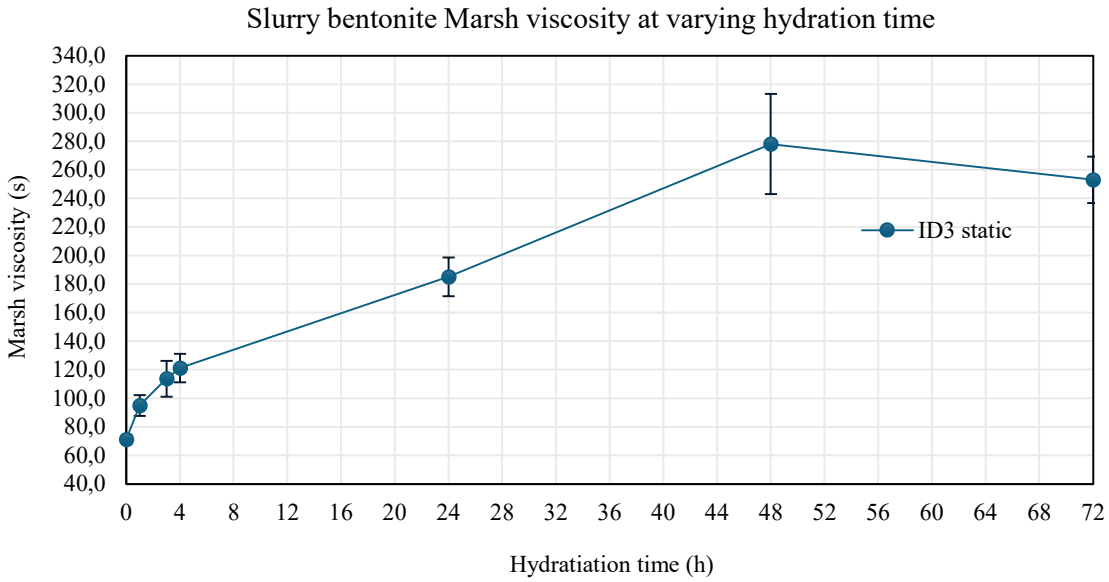

Figure 6.9 - ID3 Graphical representation of the Marsh viscosity variation at each hydration time

The slurry prepared with bentonite ID3 exhibits higher Marsh viscosity compared to the previous bentonites. The maximum value reached after 48 hours of hydration is 278 s, starting from an initial value of 71 s immediately after preparation.

6.1.8 ID3 - 60 kg/m^3 mechanically stressed

This section presents the Marsh cost test results for the slurry prepared with bentonite ID3, subjected to mechanical stress using a laboratory mixer, at a constant speed of 1000 rpm with progressively increasing stress duration. After each stress phase, a Marsh cone test was performed to measure the corresponding change in slurry viscosity (table 6.8).

Table 6.8 - ID3 stressed Marsh cone test results

Hydration time (h)	stress time (min)	$\mu_{Marsh\ viscosity}$ (s)	relative variation (%)	$\sigma_{Marsh\ viscosity}$ (s)	SRI	γ (kg/L)	T (°C)
4	0	71,25	0,00%	0,5	100,0%	1,04	25,5
	5'	57,01	-19,98%	0,4	80,0%		
	5'+5'	54,25	-4,85%	0,5	76,1%		
	5'+5'+10'	52,55	-3,13%	0,0	73,8%		
	5'+5'+10'+30'	50,93	-3,09%	0,2	71,5%		
24	0	121,81	0,00%	0,5	100,0%	1,04	26,6
	5'	57,03	-53,19%	0,3	46,8%		
	5'+5'	53,74	-5,76%	0,4	44,1%		
	5'+5'+10'	52,09	-3,08%	0,3	42,8%		
	5'+5'+10'+30'	50,68	-2,71%	0,3	41,6%		
48	0	102,77	0,00%	0,5	100,0%	1,04	26,0
	5'	54,36	-47,11%	0,3	52,9%		
	5'+5'	52,44	-3,52%	0,6	51,0%		
	5'+5'+10'	50,96	-2,83%	0,2	49,6%		
	5'+5'+10'+30'	50,15	-1,58%	0,1	48,8%		
72	0	93,04	0,00%	1,0	100,0%	1,04	26,7
	5'	53,61	-42,37%	0,0	57,6%		
	5'+5'	52,33	-2,39%	0,2	56,2%		
	5'+5'+10'	52,51	0,34%	0,5	56,4%		
	5'+5'+10'+30'	50,61	-3,62%	0,1	54,4%		

The slurry prepared with bentonite ID3 shows a significant drop in viscosity during the first 5 minutes of stress. The viscosity loss became more pronounced after 24 hours of hydration, the reduction after 5 minutes of stress is approximately -19% at 4 hours, while -53% after 24 hours. As hydration increases the viscosity loss became lower with a relative variation of approximately -45%. A slight decrease continues also under additional stress cycles at each hydration period but limited to few seconds.

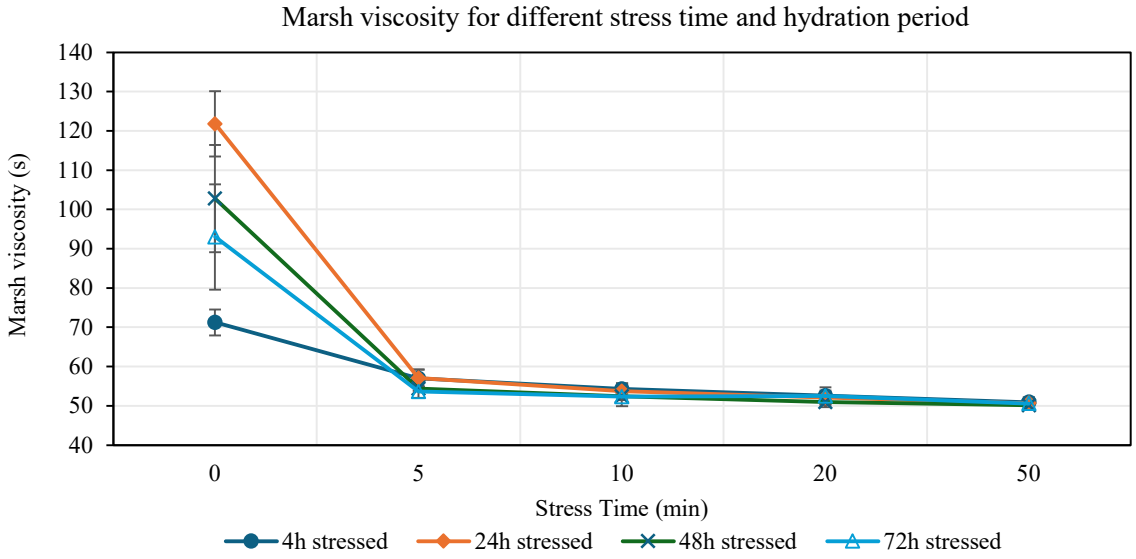

Figure 6.10 - ID3 Graphical representation of Marsh viscosity variation after mechanical stress cycles

The slurry behavior shown in figure 6.10, is more like ID1. Bentonite shows a significant amount of viscosity decrease during the first 5 stress. The drop is more marked at 24 hours, time at which viscosity before stress reaches its maximum value, indicating the biggest recovery among the different hydration times. Another important data is the linear decrease of viscosity in the following stress cycles.

6.1.9 ID3 result analysis, stress vs static behavior

The hydration phenomenon is clearly visible in this bentonite, with the Marsh viscosity increasing from an initial value of 70 s to a maximum of approximately 278 s after 48 hours. The hydration trend is similar to those observed for the previous bentonite, again an increase till 48 hours followed by a small decrease, indicating that the hydration process reaches a saturation point. The important difference is the magnitude and rate of hydration.

The test under static conditions underlines the great water absorption capacity of this bentonite, especially within the first 4 hours, during which the viscosity almost doubled with an increase of 70%. Viscosity continues to rise, reaching an overall increase of 290 % at 48h, corresponding to the hydration peak and its final disperse structures. This behavior is likely explained by a well-organized open bentonite structure where the negative surface charge of the particles attracts positive sodium ions and promotes stable dispersion. This led to the development of an extended diffuse double layer, where a lot of water particles remain

trapped in the interlayer spaces. Unlikely ID2, the double layer does not expand excessively, resulting in more cohesive but still well-dispersed microstructures.

The small decrease observed at 72 hours suggest that once the full hydration is reached, a secondary flocculation is promoted leading to a structure reorganization and viscosity reductions. The increase in standard deviation at longer hydration times highlights the higher heterogeneity of the slurry, suggesting that the system becomes more sensitive to local variation in structure and agitation during the test procedure.

ID3 exhibits strong shear-thinning and thixotropic behavior with an evident viscosity drop within the first 5 of stress. Differently from the previous bentonite, the breakdown of the structures continues during the following stress cycles. The viscosity reduction continues linearly, during the following stress times applied, at a variable rate between -5% to -3%. This behavior underlines that for this bentonite, stress duration is an influencing factor, leading to bigger viscosity loss if the stress time increases.

An interesting behavior of the bentonite is visible looking at the value of the SRI, that shows an important decrease before the 24 h of hydration, meaning that bentonite ID3 is more sensible to stress during the hydration phase when the structure as not reached a stable flocculated configuration. Once the equilibrium has been reached at 48 h, a slight increase of mechanical resistance is visible, sign of a more well-organized structure.

In figure 6.11 the whole result of the March cone tests for bentonite ID3 are presented, to easily visualize the shear thinning and thixotropic behavior.

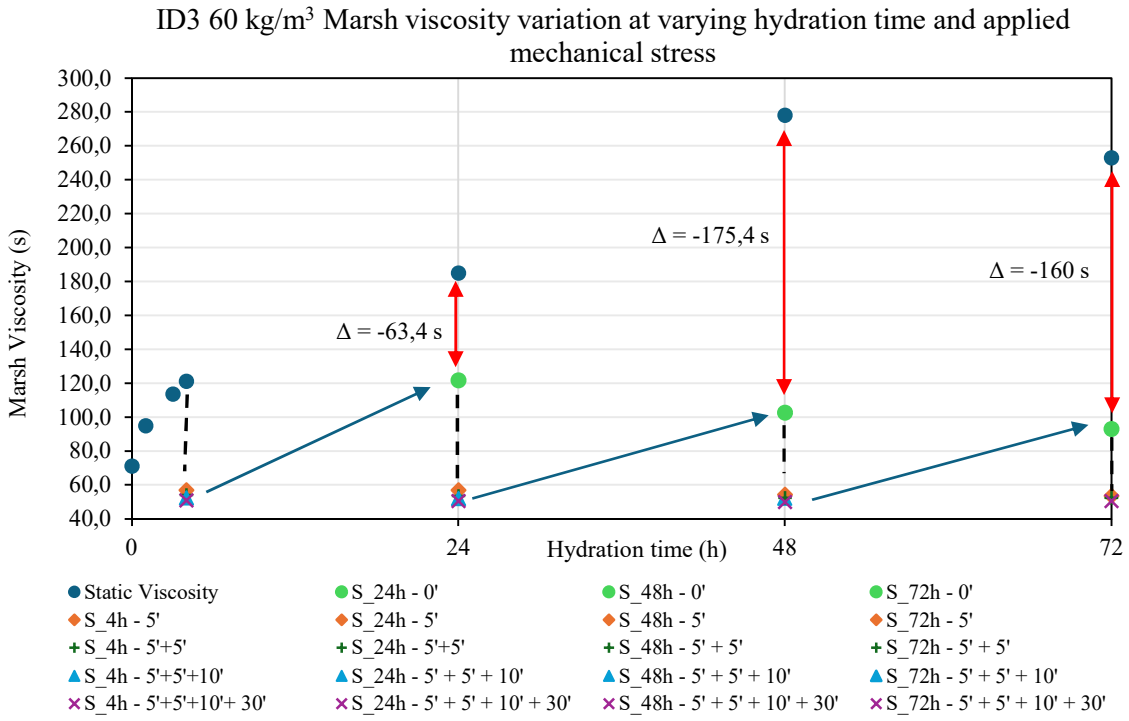

Figure 6.11 - Graphical visualization of the viscosity result of bentonite ID3 in static and stressed condition

The bentonite slurry shows an important thixotropic behavior with marked viscosity decrease during stress and recovery at rest. The suspension is able to partially rebuild its internal structure over time, increasing its viscosity from an average of 50 s after stress, to approximately 110 s after rest. The red arrow highlights important differences between the static value and the prestress value at each hydration time. In addition, the viscosity recovery capacity decreases after 24 hours, likely due to the irreversible structural damage induced by shear after the first stress campaign at 4 hours. Another possible reason for these phenomena is that once reached full hydrations at 48 hours, the reorganization of the structure and excessive flocculation influences the capacity to rebuild the structures.

The interpolation fits well with the experimental result, the value of R^2 is one for each hydration time, showing the usual drop within the first minute of stress.

Table 6.9 - Bentonite ID3 interpolation value and relative error

Hydration time (h)	τ (min)	$Mv_{,in}$ (s)	$Mv_{,inf}$ (s)	(RMSE)	Δ Marsh (%)	R^2
4h	4,1	71,25	51,84	0,3940	-27,25	0,99
24h	1,9	121,81	51,97	0,7249	-57,34	1,00
48h	1,8	102,77	51,06	0,4372	-50,32	1,00
72h	1,6	93,04	51,77	0,4244	-44,35	1,00

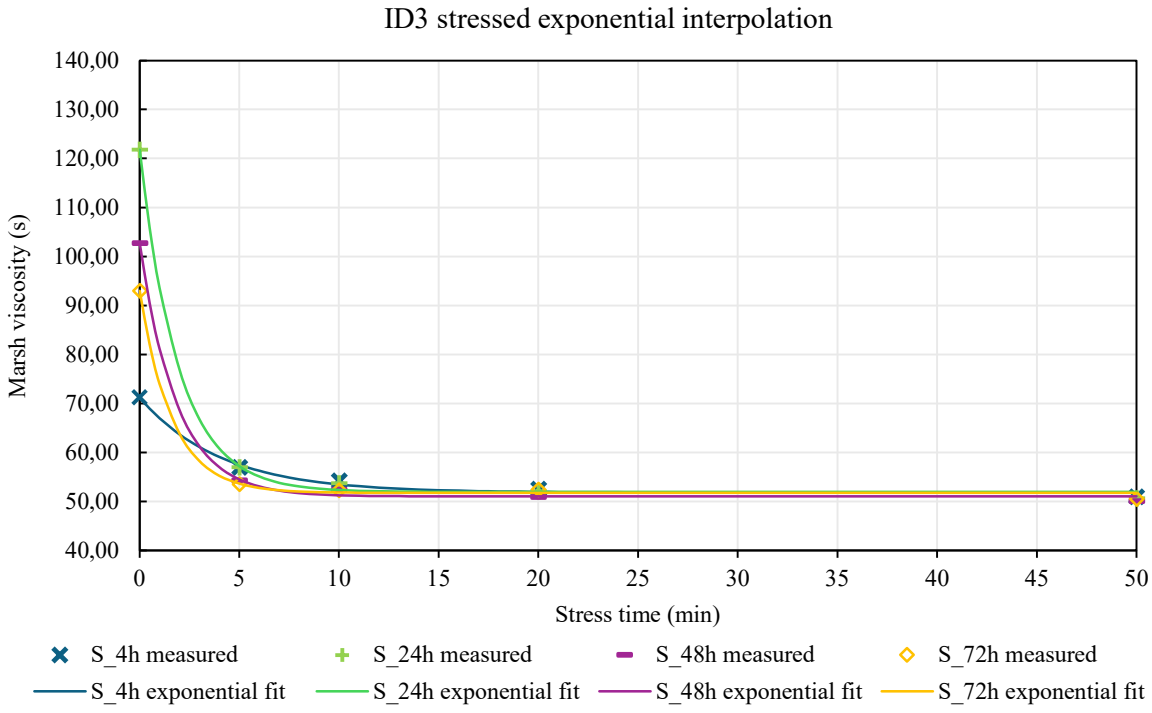

Figure 6.12 - ID3 graphical interpolation of the experimental result

Interpolation results highlight the slight dependency of the stress time on the mechanical degradation, mainly at the first hydration stage, where structure is not fully developed, underlining progressive viscosity decrease with increasing stress time.

6.1.10 ID4 - 60 kg/m^3 static

In table 6.10 and graphically in figure 6.13, are presented the results of the marsh cone test carried out on slurry prepared with bentonite ID4 at a concentration of 60 kg/m^3.

Table 6.10 - ID4 static Marsh cone test results

Hydration time (h)	$\mu_{Marsh\ viscosity}$ (s)	Relative variation (%)	$\sigma_{Marsh\ viscosity}$ (s)	γ (kg/L)	T (°C)
0	37,77	0%	0,3	1,04	25,9
1	39,55	4,71%	0,3	-	25,9
3	41,39	4,65%	0,1	-	25,9
4	42,20	1,96%	0,4	-	26,6
24	44,84	6,26%	0,4	1,04	25,4
48	46,49	3,68%	0,1	1,04	24,9
72	49,41	6,27%	1,0	1,04	24,7

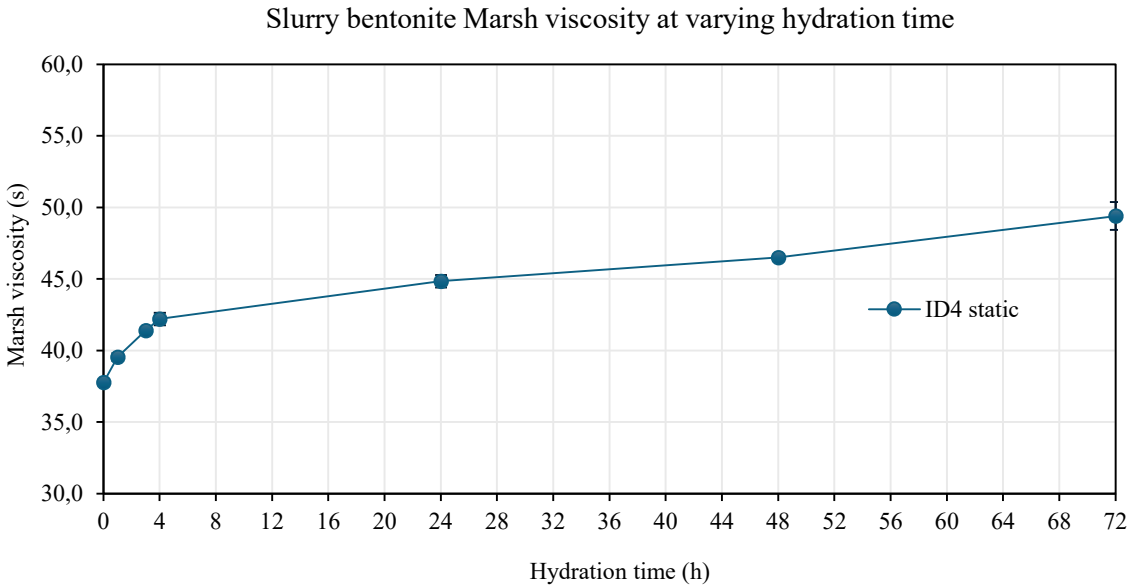

Figure 6.13 - ID4 Graphical representation of the Marsh viscosity variation at each hydration time

Slurry prepared with bentonite ID4 shows very low viscosity value ranging from 37 s to a maximum value of 49 s, reached at 72 hours of hydration. The overall variation is limited, with relative viscosity variation below 7 % respect to following hydration time.

6.1.11 ID4 - 60 kg/m^3 mechanically stressed

This section presents the Marsh cost test results for the slurry prepared with bentonite ID4, subjected to mechanical stress using a laboratory mixer, at a constant speed of 1000 rpm with progressively increasing stress duration. After each stressing phase, a Marsh cone test was performed to measure the corresponding change in slurry viscosity (table 6.11).

Table 6.11 - ID4 stressed Marsh cone test results

Hydration time (h)	stress time (min)	$\mu_{Marsh\ viscosity}$ (s)	relative variation (%)	$\sigma_{Marsh\ viscosity}$ (s)	SRI	γ (kg/L)	T (°C)
4	0	41,80	0,00%	0,4	100,0%	1,04	26,2
	5'	40,36	-3,44%	0,3	96,6%		
	5'+5'	39,96	-1,00%	0,5	95,6%		
	5'+5'+10'	40,05	0,23%	0,1	95,8%		
	5'+5'+10'+30'	40,03	-0,03%	0,3	95,8%		
24	0	45,98	0,00%	1,0	100,0%	1,04	25,2
	5'	42,70	-7,13%	0,3	92,9%		
	5'+5'	42,11	-1,38%	0,4	91,6%		
	5'+5'+10'	41,83	-0,68%	0,2	91,0%		
	5'+5'+10'+30'	41,69	-0,33%	0,2	90,7%		
48	0	46,59	0,00%	1,4	100,0%	1,04	25,2
	5'	43,71	-6,19%	0,2	93,8%		
	5'+5'	43,36	-0,79%	0,3	93,1%		
	5'+5'+10'	42,76	-1,38%	0,2	91,8%		
	5'+5'+10'+30'	43,38	1,44%	0,7	93,1%		
72	0	48,31	0,00%	2,4	100,0%	1,04	25
	5'	44,12	-8,66%	0,4	91,3%		
	5'+5'	43,45	-1,53%	0,3	89,9%		
	5'+5'+10'	43,57	0,29%	0,8	90,2%		
	5'+5'+10'+30'	43,40	-0,41%	0,7	89,8%		

The result shows how bentonite behavior is almost not affected by mechanical degradation. At each hydration time after 5 minutes of stress, the viscosity reduces by less than 4 seconds. The standard deviation, both in static and in stressed condition, is almost null, the maximum value is ± 2 s.

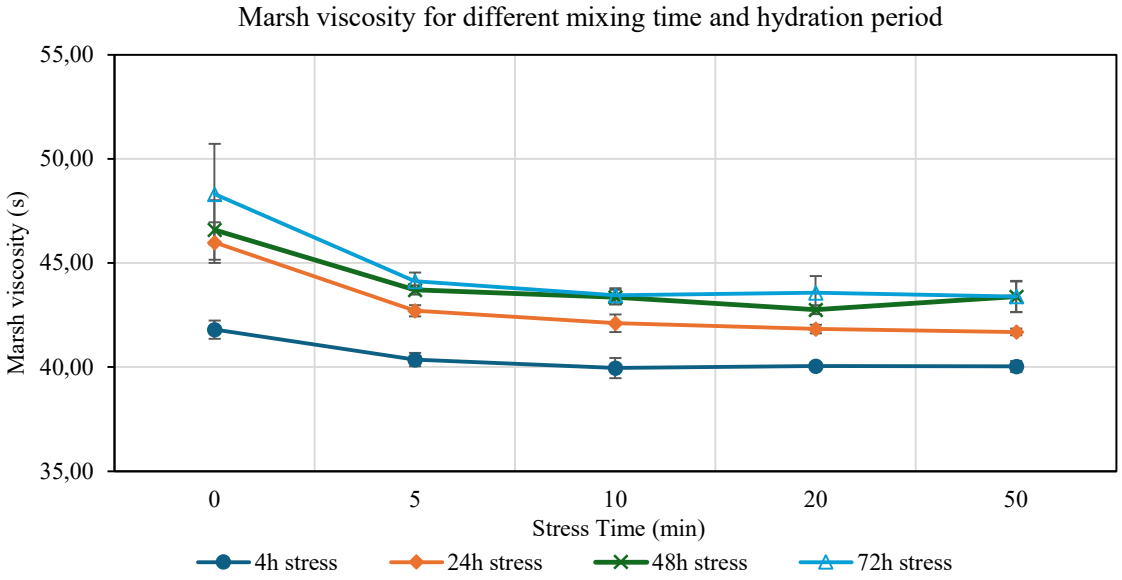

Figure 6.14 - ID4 Graphical representation of Marsh viscosity variation after mechanical stress cycles

The figure 6.14 shows that, for all hydration periods, the viscosity undergoes a limited decrease during the first five minutes, then stabilizes reaching a nearly constant value

6.1.12 ID4 result analysis, stress vs static behavior

Different from the previously tested bentonite, the trend observed for bentonite ID4 is quite unique. The curve in figure 6.13 shows a gradual and continuous hydration process, without a clear stabilization point within the first 72 h. The small viscosity values are sign of a bentonite with low water absorption capacity, likely due, to a low ESP value or low content of montmorillonite that reduces the hydration capacity as confirmed by the low value of the measured swell index. The almost null standard deviation confirms the homogeneity and stability of the slurry suspension, with no significant structural or rheological evolution over time. This behavior is also confirmed by the Marsh cone result on stressed slurry. Although figure 6.14 highlights a reduction in viscosity, the difference is limited to about 5 seconds. This demonstrates the great stability of the slurry, which presents a highly flocculated structure, not subjected to mechanical degradation. The strong face-to-face particles interaction between montmorillonite platelets promotes a highly flocculated structure that prevents the system from trapping additional water molecules, but at the same time allows the structure to resist under high shear stress.

In figure 6.15 the whole result of the March cone tests for bentonite ID4 are presented, showing the stability of the suspension over time, and the structure recovery after stress.

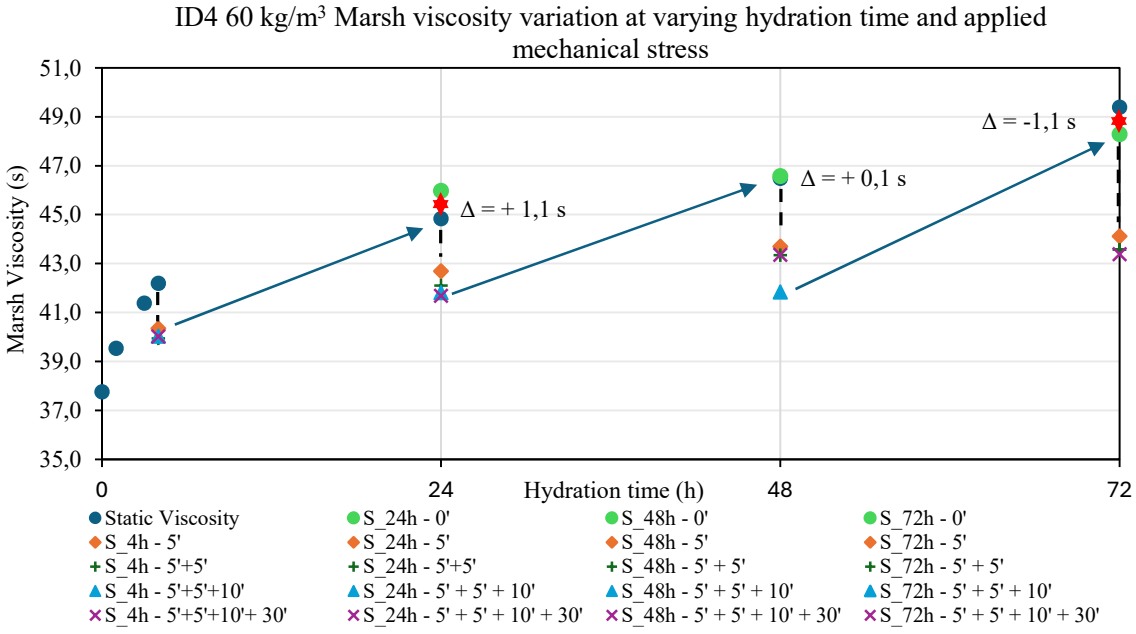

Figure 6.15 - Graphical visualization of the viscosity result of bentonite ID4 in static and stressed condition

The thixotropic behavior of bentonite ID4 allows the complete recovery of its structures during the resting phase. At certain hydration times, like 24 and 48 hours, the structure not only recovers but also continues to hydrate with respect to the static condition, leading to a small increase of viscosity. Although this difference is within the range of experimental uncertainty, a possible explanation is that the applied shear stress disrupts the high flocculation, resulting in spatial redistribution of particles into a more homogeneous and dispersed configuration, allowing more water molecules between particles, enhancing the slurry hydration.

The experimental data of bentonite ID4 under mechanical stress are well fitted by the exponential model, with a coefficient of determination always near 1, confirming the reliability of the interpolation.

Table 6.12 - Bentonite ID4 interpolation value and relative error

Hydration time (h)	τ (min)	$Mv_{,in}$ (s)	$Mv_{,inf}$ (s)	(RMSE)	Δ Marsh (%)	R^2
4h	2,9	41,80	40,00	0,0029	-4,30	0,99
24h	3,4	45,98	41,78	0,0047	-9,13	1,00
48h	1,8	46,59	43,38	0,0789	-6,90	1,00
72h	1,6	48,31	43,40	0,0570	-10,16	0,99

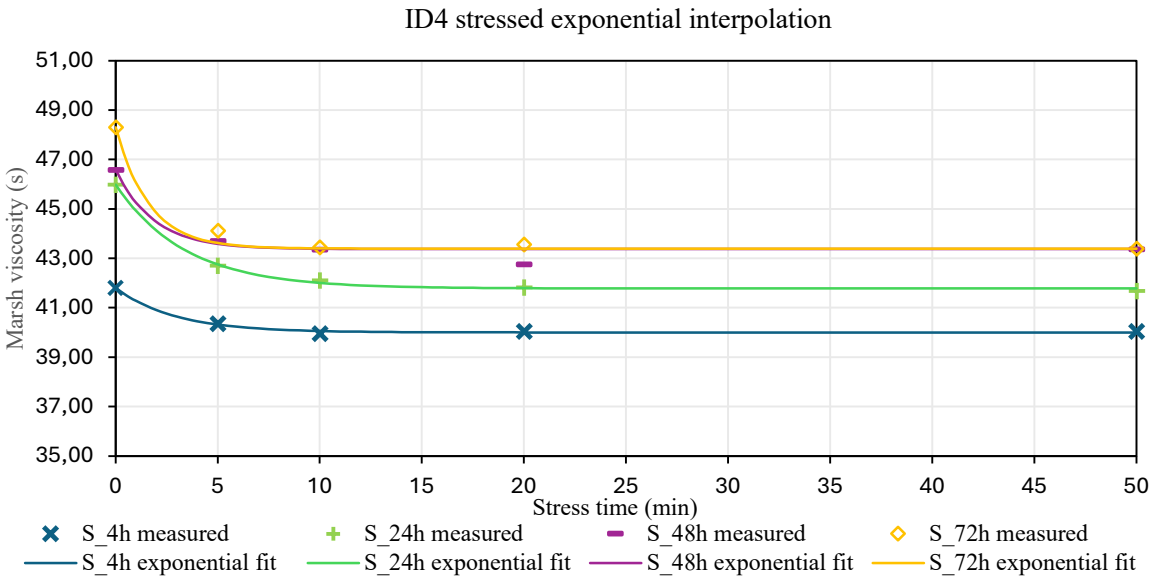

Figure 6.16 - ID4 graphical interpolation of the experimental result

The time to reach the plateau ranges between 1.6 and 3.4 minutes, highlighting that at 4 and 24 hours of hydration the stabilization process requires more time. This behavior is also reflected in a small but perceptible reduction in viscosity also after the first 5 minutes of stress. In addition, Figure 6.16 shows that minimum viscosity value is reached after stress at 4 hours of hydration, while at longer hydration times 24, 48, 72 h, the recovery and

reorganization of the structure during resting phase led to higher viscosity value both before and after the stress.

6.1.13 ID4 - 80 kg/m^3 static

In table 6.13 and graphically in figure 6.17, are presented the Marsh cone results carried out on slurry prepared with the ID4, this time at a concentration of 80 kg/m^3.

Table 6.13 - ID4 80 kg/m^3 static Marsh cone test results

Hydration time (h)	$\mu_{Marsh\ viscosity}$ (s)	Relative variation (%)	$\sigma_{Marsh\ viscosity}$ (s)	γ (L/m^3)	T (°C)
0	55,57	0%	0,9	1,04	25,5
1	66,22	19,15%	0,9	-	25,8
3	81,67	23,33%	0,8	-	25,8
4	83,39	2,11%	1,3	-	25,8
24	122,43	46,82%	6,4	1,04	25,4
48	154,52	26,20%	14,5	1,04	25,2
72	202,95	31,35%	18,8	1,04	25,4

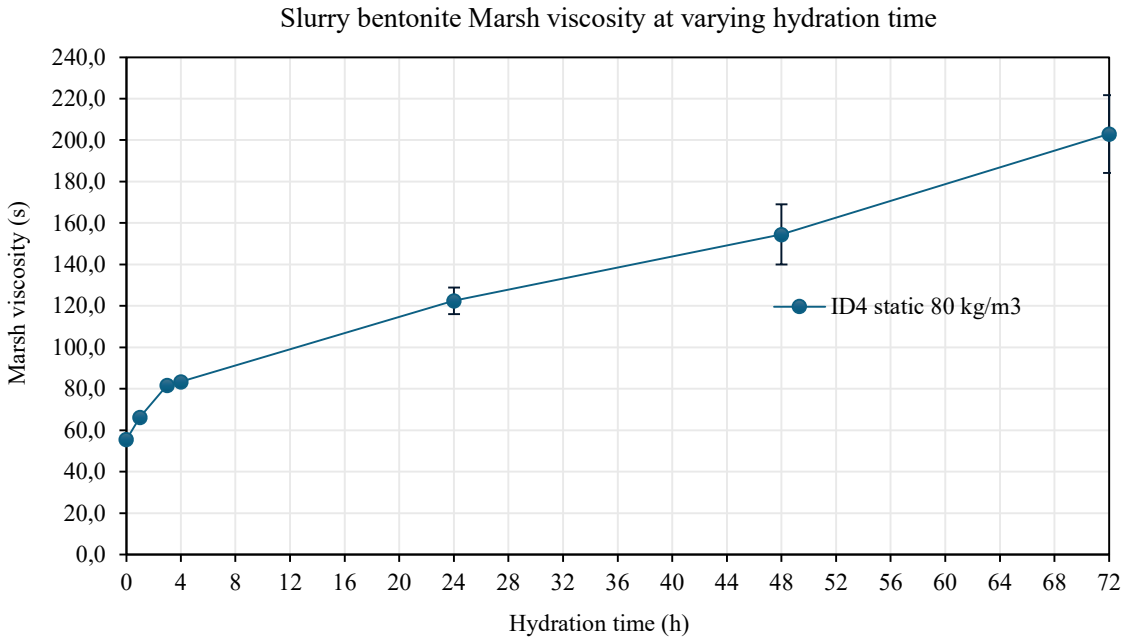

Figure 6.17 - ID4 80 kg/m^3 Graphical representation of the Marsh viscosity variation at each hydration time

Marsh viscosity increases with longer hydration times from a value of 55 s reaching a maximum of 203 s. Completely different result with respect to the slurry with concentration 60 kg/m^3, although the overall trend remains similar between the two. The standard deviation stays low until 4 hours hydration, then increases, reaching higher value with longer hydration times.

6.1.14 ID4 - 80 kg/m^3 mechanically stressed

This section presents the Marsh cost test results for the slurry prepared with bentonite ID4 at a concentration of 80 kg/m^3, subjected to mechanical stress using a laboratory mixer, at a constant speed of 1000 rpm with progressively increasing stress duration. After each stressing phase, a Marsh cone test was performed to measure the corresponding change in slurry viscosity (table 6.14).

Table 6.14 - ID4 80 kg/m^3 stressed Marsh cone test results

Hydration time (h)	stress time (min)	$\mu_{Marsh\ viscosity}$ (s)	relative variation (%)	$\sigma_{Marsh\ viscosity}$ (s)	SRI	γ (kg/L)	T (°C)
4	0	73,38	0,00%	1,0	100,00%	1,04	26,2
	5'	66,00	-10,06%	1,0	89,94%		
	5'+5'	68,14	3,25%	4,3	92,86%		
	5'+5'+10'	65,98	-3,17%	1,9	89,92%		
	5'+5'+10'+30'	68,28	3,48%	2,0	93,04%		
24	0	92,84	0,00%	1,9	100,00%	1,04	25,2
	5'	76,59	-17,50%	1,8	82,50%		
	5'+5'	73,61	-3,90%	2,6	79,28%		
	5'+5'+10'	73,12	-0,66%	3,6	78,76%		
	5'+5'+10'+30'	74,25	1,55%	1,7	79,98%		
48	0	119,61	0,00%	11,9	100,00%	1,04	25,2
	5'	91,62	-23,40%	3,1	76,60%		
	5'+5'	89,53	-2,28%	2,9	74,85%		
	5'+5'+10'	85,00	-5,06%	3,1	71,07%		
	5'+5'+10'+30'	79,61	-6,34%	3,9	66,56%		
72	0	137,02	0,00%	10,6	100,00%	1,04	25,4
	5'	98,45	-28,15%	4,8	71,85%		
	5'+5'	99,67	1,25%	3,6	72,74%		
	5'+5'+10'	99,37	-0,30%	4,3	72,52%		
	5'+5'+10'+30'	92,07	-7,35%	3,4	67,20%		

As always, the first 5 minutes of stress are crucial, showing an important variation in bentonite rheological properties. Viscosity shows an important drop after stress at each hydration time, with reductions ranging between 10 to 30 %. The standard deviation shows limited variation during test repetition, almost always ± 4 seconds.

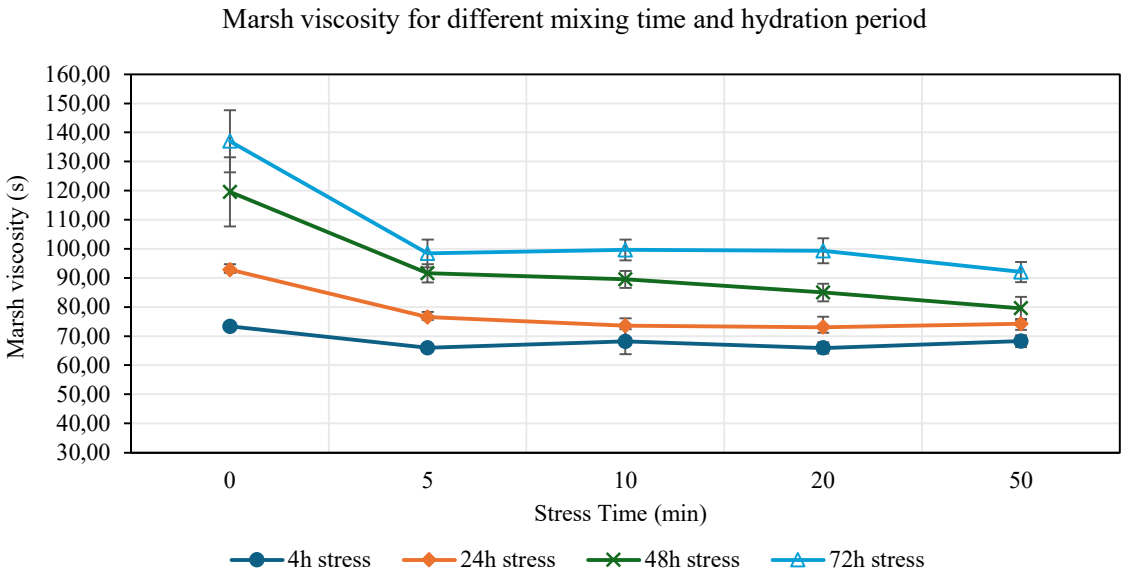

Figure 6.18 - ID4 80 kg/m³ Graphical representation of Marsh viscosity variation after mechanical stress cycles

Figure 6.18 shows, for each hydration time, the trend of viscosity variation during mechanical stress cycles. A marked decrease occurred immediately after the application of stress, after which the slurry progressively approach a constant viscosity value for the subsequent stress cycles.

6.1.15 ID4 - 80 kg/m^3 result analysis, stress vs static behavior

Slurry prepared with bentonite ID4 shows a continuous viscosity increase at all hydration time. The growth rate is higher within the first 3 hours, and becomes more gradual, although still positive in the following hydration stages. The viscosity keeps increasing till 72 hours, indicating a structural development over time. The total viscosity increment reaches approximately 265 % in relation to the viscosity value after preparation.

The mechanical degradation has a moderate effect on bentonite. The structure breakdown is evident, with the Marsh viscosity dropping after applying the stress. It is interesting to note that viscosity loss is not so evident respect to the previously analyzed bentonite. The SRI is always over 70% highlighting a good resistance to mechanical stress, meaning that a large portion of bentonite structure remains intact even after applying various stress cycles. This behavior confirms that bentonite ID4 is characterized by a stable compacted structure and strong interconnection between particles. The reduction in SRI with hydration times indicates that the internal structures, while strong, become more susceptible to irreversible arrangement when subjected to stress. However, slurry thixotropic response is quite

important, capable of partially rebuilding the network during rest periods, bringing again viscosity to higher value.

In figure 6.19 the thixotropic behavior is clearly visible, showing a higher viscosity recovery, with longer hydration times. This phenomenon can be explained by the strongly flocculated structure that characterizes this type of bentonite, which allows a slight increase in hydration.

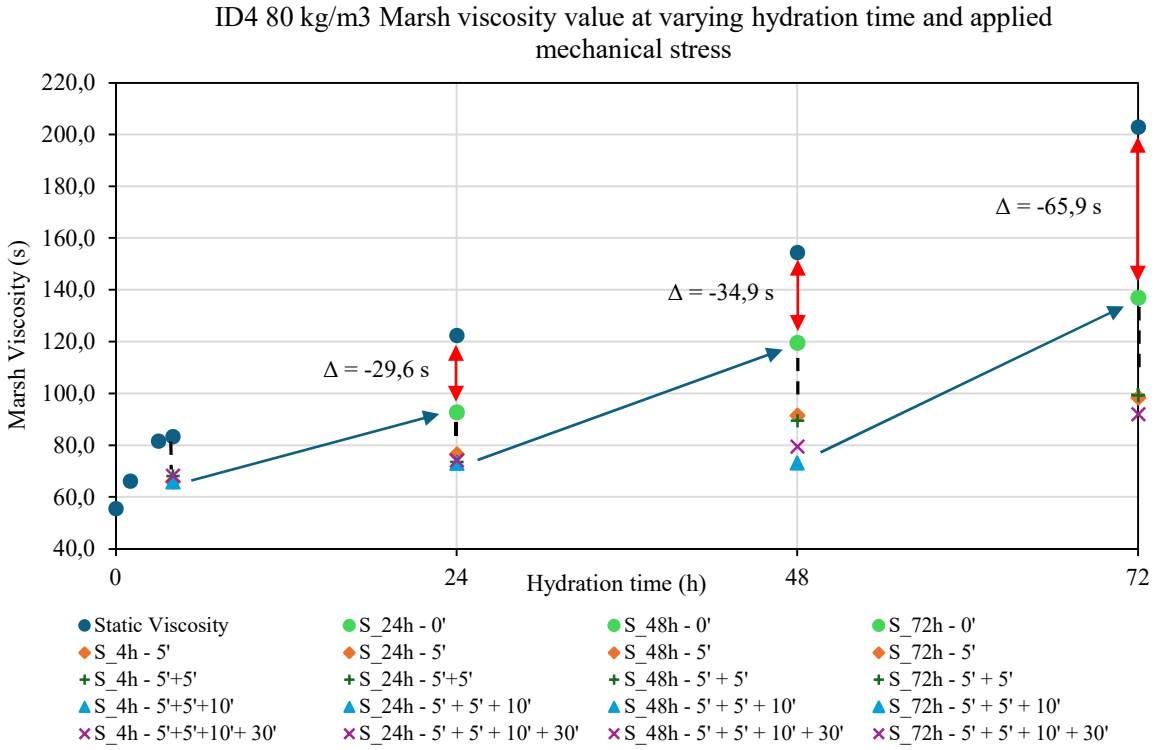

Figure 6.19 - Graphical visualization of the viscosity result of bentonite ID4 80 kg/m³ in static and stressed condition

Although some parts of the internal structure are inevitably destroyed under mechanical stress, the slurry is able to partially rebuild its structure during the resting phase. This mechanism is mainly governed by the reorganization of the structures that enhance particle dispersion and promotes the reformation of a solid three-dimensional network composed of edge-to-face interaction, leading to higher viscosity value after resting phase.

The experimental data of ID4 under mechanical stress are quite well fitted by the exponential model, with good correlation values, apart from the interpolation of the data related to the 4-hours hydration.

Table 6.15 - Bentonite ID4 80 kg/m³ interpolation value and relative error

Hydration time (h)	τ (min)	$Mv_{,in}$ (s)	$Mv_{,inf}$ (s)	(RMSE)	Δ Marsh (%)	R^2
4h	0,3	73,38	67,10	0,9860	-8,56	0,86
24h	2,6	92,84	73,55	0,1698	-20,78	1,00
48h	4,1	119,61	82,93	6,0800	-30,67	0,97
72h	1,6	137,02	96,94	7,3446	-29,25	0,97

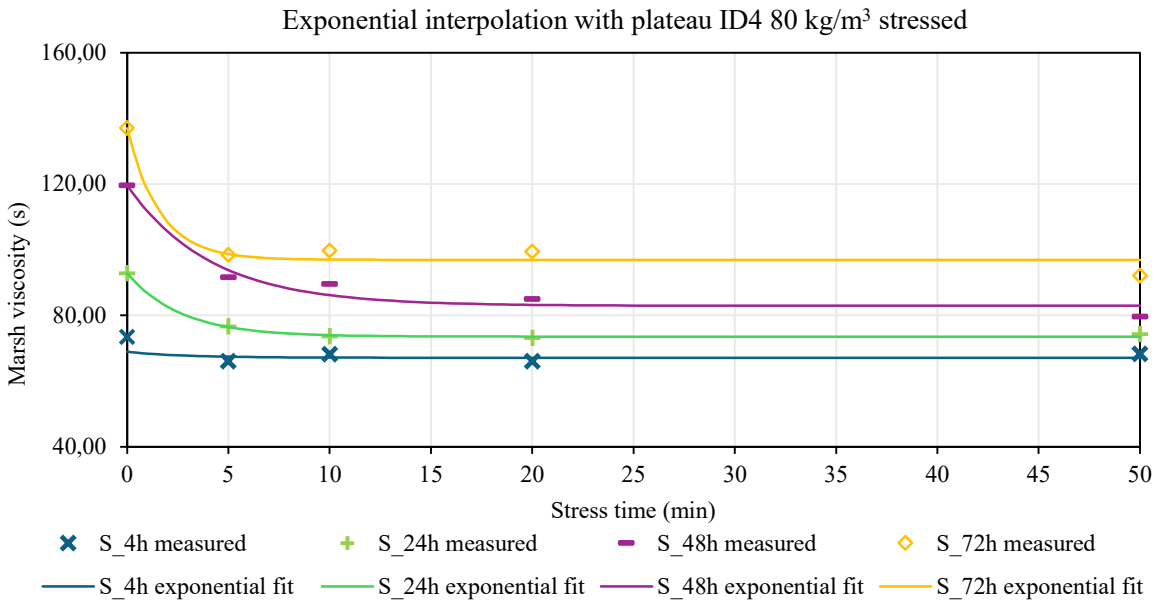

Figure 6.20 - ID4 80 kg/m³ Graphical interpolation of the experimental result

The time to reach the plateau ranges between 0.3 and 4.1 minutes, showing different trends to reach the plateau. The figure 6.20 also highlights that minimum viscosity value is reached after stress at 4 hours of hydration, then at longer hydration times, 24, 48, and 72 h. The recovery and reorganization of the structure during resting led to higher viscosity value both before and after stress.

6.1.16 Bentonite ID4 concentration effect

Bentonite slurry prepared with ID4, presents important differences due to the concentration variation. As visible in figure 6.21, the overall trend is similar, both concentrations present a continuous viscosity increase, with a higher rate before the 4 hours and lower rate for longer hydration hours.

The increase in viscosity with higher bentonite concentration is not directly result of a greater hydration capacity. The higher hydration capacity is a collateral effect of the increased number of contact points present, due to the increased number of bentonite particles in suspension, but the overall hydration capacity remains low, as evidenced in the tests on bentonite at lower concentration. This explanation is also supported by the medium value of swell index, that underline a not so marked hydration capacity.

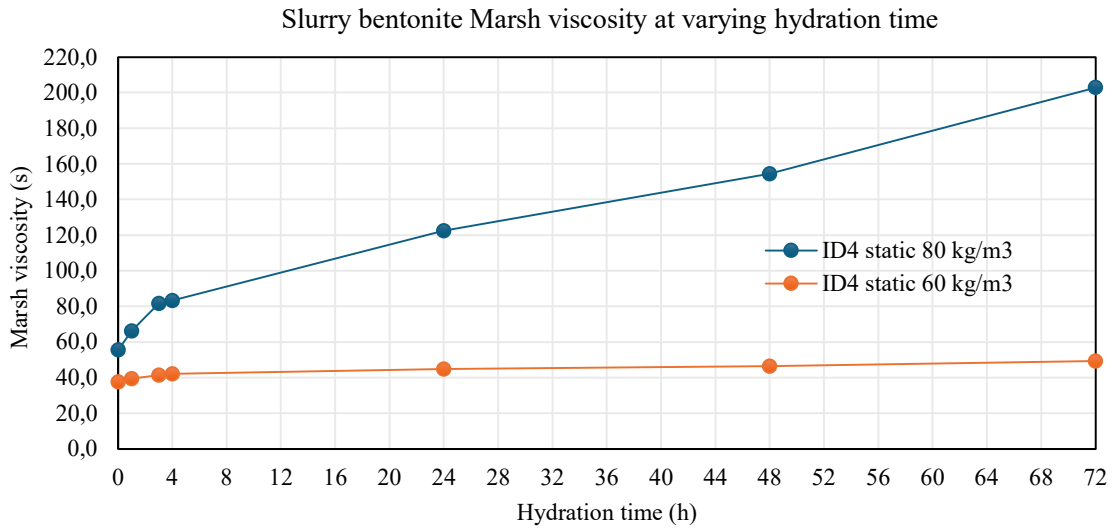

Figure 6.21 - Viscosity variation at increasing hydration time for Bentonite ID4 at lower and higher concentrations.

Higher concentration likely means more edge to face or face to face interconnection between particles, that develop a well three-dimensional compact structure, leading to higher viscosity.

Although the viscosity value differs in magnitude, the structural stability of the slurry remains very high and slightly affected by mechanical degradation.

At both concentrations, a reduction in viscosity due to mechanical stress is observed, but the resistance to stress remains excellent, with an SRI value over 90% for the lower concentrations and above 70% for the higher one (figure 6.22). This behavior confirms the previously discussed interpretation, the bentonite is probably not completely sodic but contains a significant amount of calcium or magnesium cations, which reduce the interparticle repulsion promoting a compact flocculation. As result, the slurry forms a dense and mechanically resistant structure that keeps its integrity even under prolonged stress.

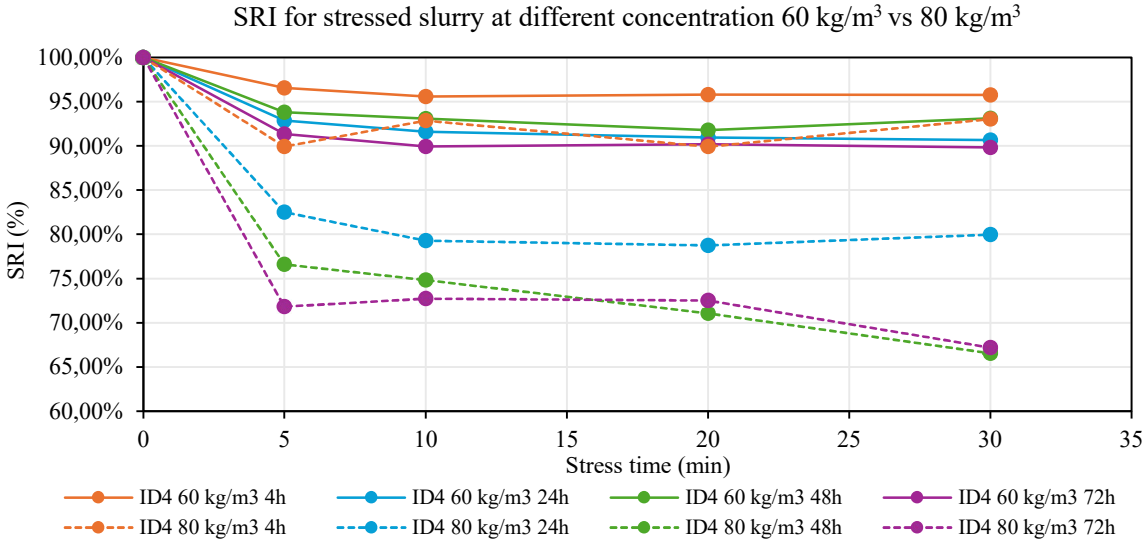

Figure 6.22 - Stress resistance Index variation for bentonite ID4 at different concentrations

6.1.17 ID5 - 60 kg/m^3 static

In table 6.16 are presented the results of the Marsh cone test carried out on slurry prepared with bentonite ID5 at a concentration of 60 kg/m^3.

Table 6.16 - ID5 static Marsh cone test results

Hydration time (h)	$\mu_{Marsh\ viscosity}$ (s)	Relative variation (%)	$\sigma_{Marsh\ viscosity}$ (s)	γ (kg/L)	T (°C)
0	47,8	0%	0,8	1,04	25,4
1	55,4	15,90%	1,5	1,04	25,3
3	67,6	21,98%	6,2	1,03	24,9
4	69,1	2,25%	4,6	1,03	24,9
24	107,6	55,67%	17,8	1,04	24,8
48	122,0	13,40%	18,7	1,04	24,8
72	141,6	16,10%	20,0	1,4	25,0

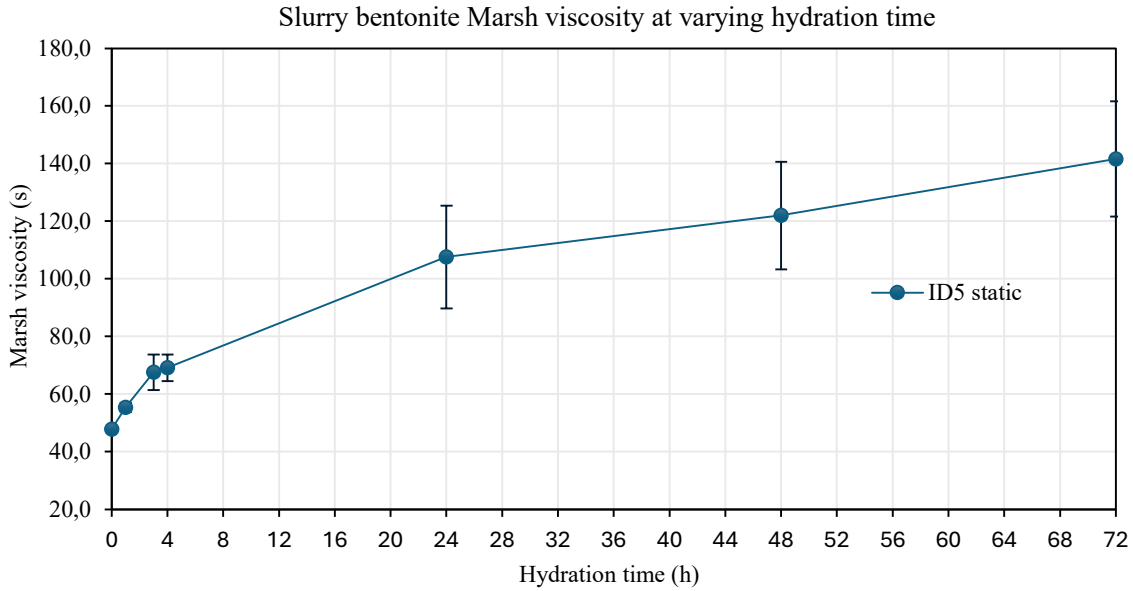

Figure 6.23 - ID5 graphical representation of the Marsh viscosity variation at each hydration time

Viscosity increases with progressive hydration times, passing from 49 to 141 s, continuously till 72 hours. This trend is common to the standard deviation, which increase reaching a value of ± 20 s at 72 h of hydration.

6.1.18 ID5 - 60 kg/m^3 mechanically stressed

This section presents the Marsh cone test results for the slurry prepared with bentonite ID5, subjected to mechanical stress using a laboratory mixer, at a constant speed of 1000 rpm with progressively increasing stress duration. After each stressing phase, a Marsh cone test was performed to measure the corresponding change in slurry viscosity (table 6.17).

Table 6.17 - ID5 stressed Marsh cone test results

Hydration time (h)	stress time (min)	$\mu_{Marsh\ viscosity}$ (s)	relative variation (%)	$\sigma_{Marsh\ viscosity}$ (s)	SRI	γ (kg/L)	T (°C)
4	0	65,40	0,00%	5,1	100,00%	1,04	25,4
	5'	45,82	-29,93%	1,0	70,07%		
	5'+5'	43,44	-5,19%	0,7	66,43%		
	5'+5'+10'	43,01	-1,00%	0,3	65,76%		
	5'+5'+10'+30'	43,14	0,29%	0,7	65,96%		
24	0	80,47	0,00%	7,9	100,00%	1,04	24,9
	5'	46,38	-42,37%	0,7	57,63%		
	5'+5'	45,50	-1,89%	0,9	56,54%		
	5'+5'+10'	43,27	-4,90%	0,6	53,77%		
	5'+5'+10'+30'	44,61	3,09%	0,5	55,43%		
48	0	100,95	0,00%	20,3	100,00%	1,04	25,0
	5'	45,81	-54,62%	0,9	45,38%		
	5'+5'	44,86	-2,08%	0,6	44,44%		
	5'+5'+10'	44,42	-0,98%	0,4	44,00%		
	5'+5'+10'+30'	42,69	-3,90%	0,5	42,28%		
72	0	97,95	0,00%	21,8	100,00%	1,04	25,0
	5'	48,51	-50,48%	0,5	49,52%		
	5'+5'	45,51	-6,19%	0,5	46,46%		
	5'+5'+10'	45,19	-0,70%	0,5	46,13%		
	5'+5'+10'+30'	44,75	-0,97%	0,5	45,69%		

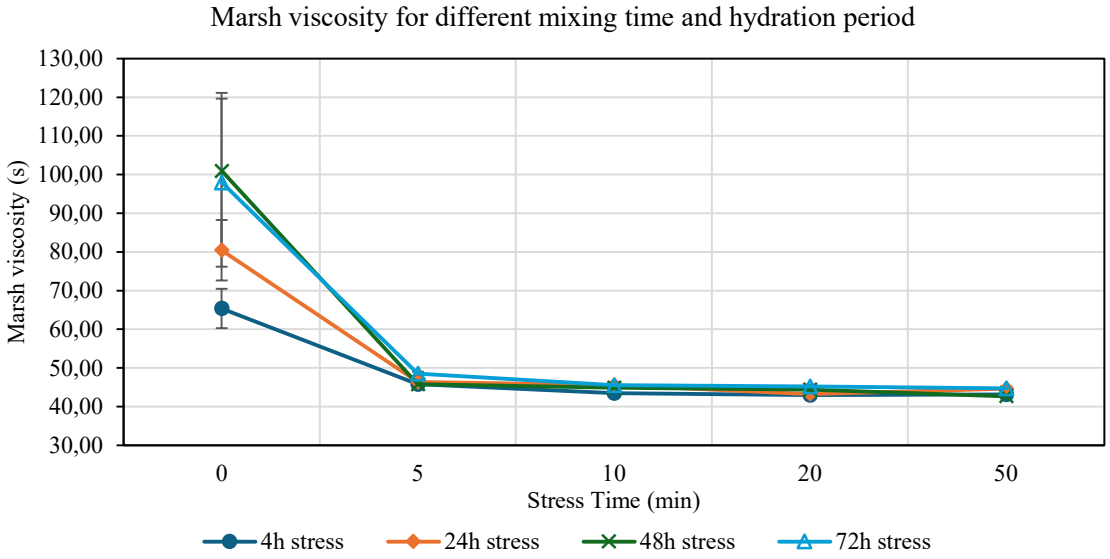

Figure 6.24 - ID5 Graphical representation of Marsh viscosity variation after mechanical stress cycles

Figure 6.24 shows viscosity variation with increasing stress time and hydration. A further decrease can also be observed after the second 5 minutes stress cycle, although extremely limited, in the order of approximately 2 seconds.

6.1.19 ID5 result analysis, stress vs static behavior

ID5 develops relatively high viscosity values, indicating a good hydration capacity. The viscosity trend increases over time, without a clear stabilization point. Excluding the small viscosity variation between 3 and 4 hours of hydration, the percentage is always high, above 15%. This hydration behavior is likely due to the great amount of exchangeable sodium ions, which promote a diffuse double layer that allows of trapping a lot of water molecules. Both the diffuse layer and the interparticle space need time to expand, increasing the hydration time. This phenomenon is not constant in time and depending on the bentonite requires more or less time.

Slurry viscosity is subject to an important decrease after the first minute of stress, and for all hydration time it reaches a constant value of approximately 45 s, after which the successive stress cycles are responsible only for minor changes.

The SRI value reflects this behavior, showing the higher resistance of slurry at shorter hydration time, whereas resistance progressively decreases at 24 h, 48h and 72h. This trend is consistent with the hydration mechanism previously supposed. To reach its final three-dimensional configuration, bentonite requires time, to fully expand the interlayer between spaces and the diffuse double layer. This means that initially the structure is still compact, with limited separation and less hydrated, leading to lower viscosity and higher resistance to mechanical stress. As hydration progresses, bentonite dispersion increases, trapping more water, resulting in a higher viscosity but more susceptible to degradation under shear. This behavior is not in contrast with the low value of the swell index measured for this bentonite. It is likely that if the swelling test was performed at 48 hours instead of 24 hours, it would have resulted in much higher value.

In figure 6.25 presentes all the Marsh cone results for both static and stressed slurry, highlighting the higher resistance to mechanical stress at lower hydration time.

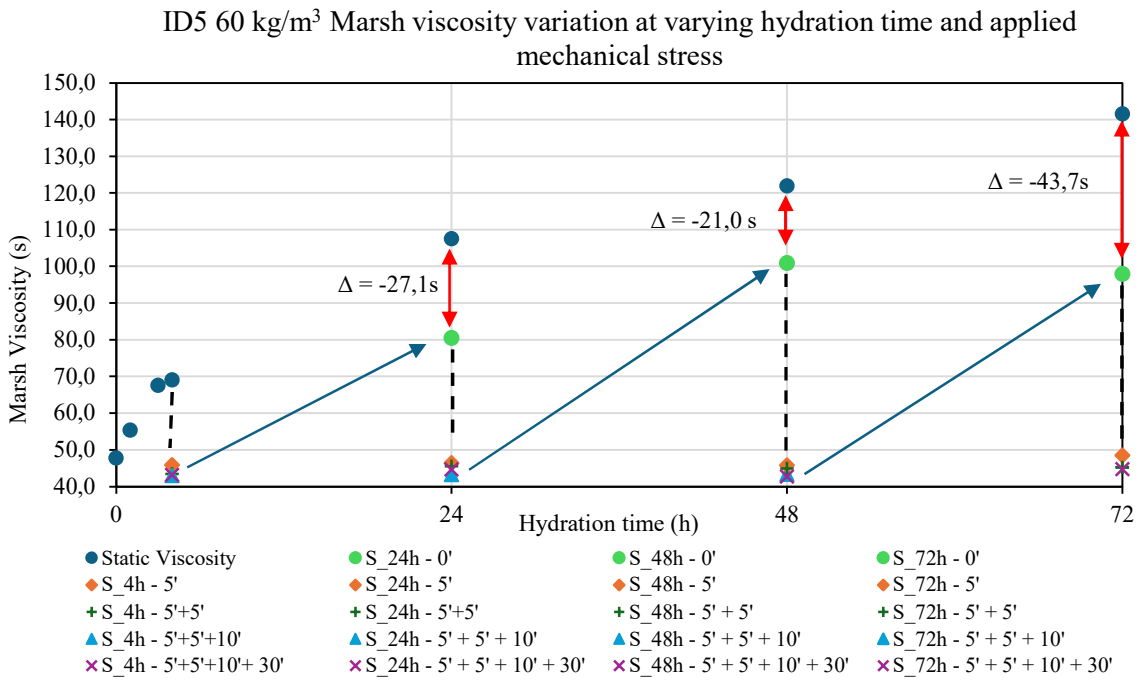

Figure 6.25 - Graphical visualization of the viscosity result of bentonite ID5 in static and stressed condition

Bentonite ID5 shows high thixotropic behavior, demonstrating a marked viscosity decrease during stress but also good ability to rebuild its internal structures after breakdown. The red arrow indicates the small difference between the static Marsh viscosity and prestress value, confirming the strong structural recovery. At 72 hours difference became larger, suggesting that once the structure is almost fully hydrated and reaches its most expanded configuration, mechanical degradation destroys irreversibly part of the interparticle network leading to an inevitably lower recovery during rest.

The experimental results of bentonite ID5 under mechanical stress are quite well fitted by the exponential model, as the high correlation values demonstrates (table 6.18).

Table 6.18 - Bentonite ID5 interpolation value and relative error

Hydration time (h)	τ (min)	$Mv_{,in}$ (s)	$Mv_{,inf}$ (s)	(RMSE)	Δ Marsh (%)	R^2
4h	2,4	65,40	43,08	0,0019	-34,13	1,00
24h	1,8	80,47	44,38	0,4581	-44,85	1,00
48h	1,4	119,61	43,96	70,1265	-63,25	1,00
72h	1,8	97,95	45,06	0,0322	-54,00	1,00

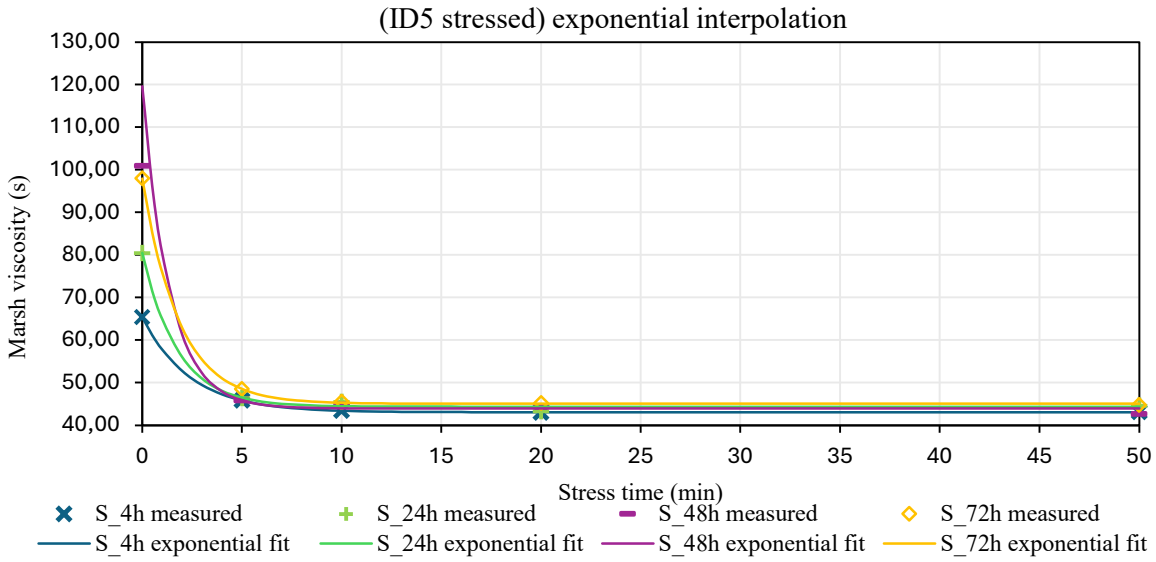

Figure 6.26 - ID5 Graphical interpolation of the experimental result

Time to reach the plateau viscosity value increases progressively with hydration time, representing again the increasing structural fragility for higher hydration time. The final plateau value is common for all the hydration times, independently from the initial viscosity.

6.1.20 ID6 - 60 kg/m^3 static

In table 6.19 and graphically in figure 6.27, are presented the results of the Marsh cone test carried out on slurry prepared with bentonite ID6 with concentration of 60 kg/m^3.

Table 6.19 - ID6 static Marsh cone test results

Hydration time (h)	$\mu_{Marsh\ viscosity}$ (s)	Relative variation (%)	$\sigma_{Marsh\ viscosity}$ (s)	γ (kg/L)	T (°C)
0	38,9	0,00%	0,5	1,04	25,5
1	47,1	21,00%	0,6	-	-
3	82,5	75,14%	3,3	-	-
4	92,3	11,82%	4,5	-	-
24	91,6	-0,68%	5,6	1,04	25,2
48	97,8	6,67%	9,2	1,04	24,7
72	100,3	2,62%	7,2	1,04	25,6

Bentonite ID6 shows a rapid viscosity increase in the first 4 hours and then tends to stabilize. Viscosity increases from a value of 38 seconds, right after preparation, to 92 s after 4 hours of hydration. The standard deviation increases with hydration time, but remains always at small values, ranging from 0,5 s to approximately 9 s.

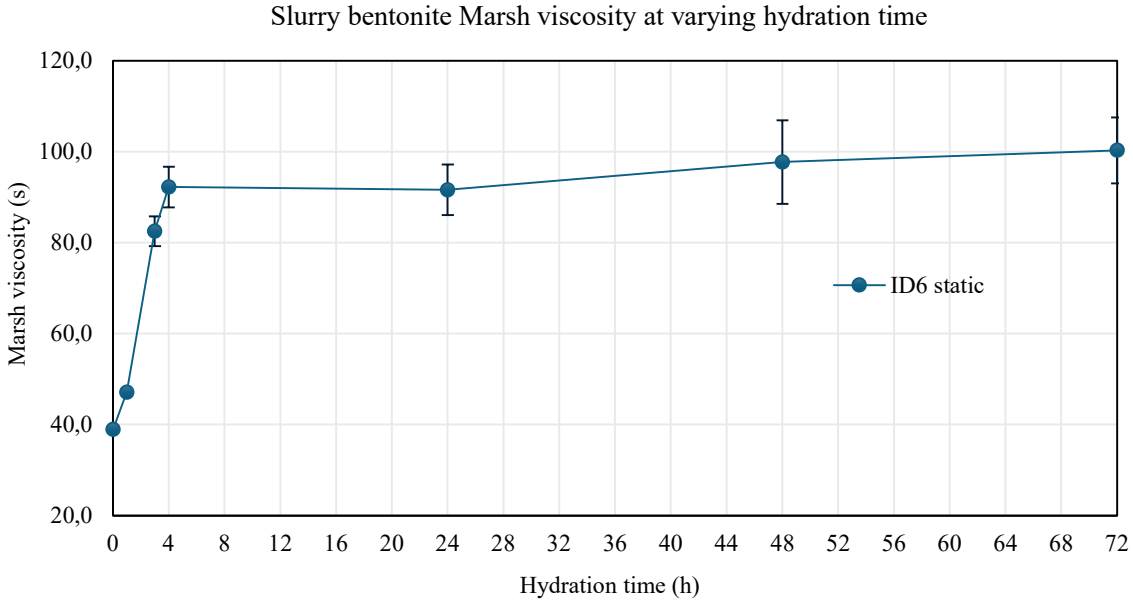

Figure 6.27 - ID6 Graphical representation of the Marsh viscosity variation at each hydration time

Figure 6.27 clearly illustrates the viscosity evolution with increasing hydration time. The steep line between the first points highlights an important growing rate in the first hours. As hydration progresses, the line became more horizontal, indicating a lower growth rate and the viscosity stabilized around a constant value.

6.1.21 ID6 - 60 kg/m^3 mechanically stressed

This section presents the Marsh cost test results for the slurry prepared with bentonite ID6 at a concentration of 60 kg/m^3, subjected to mechanical stress using a laboratory mixer, at a constant speed of 1000 rpm with progressively increasing stress duration (table 6.20).

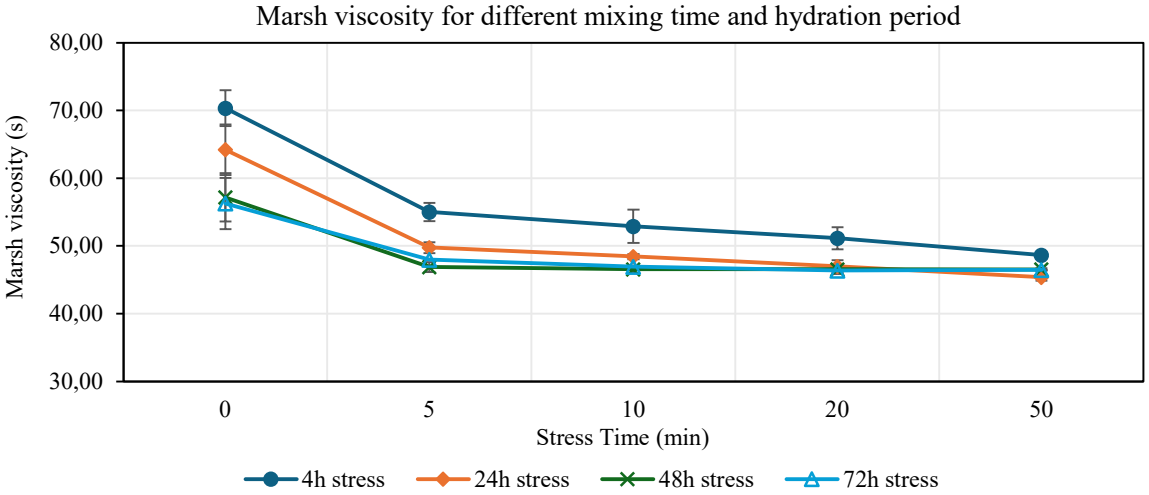

Figure 6.28 - ID6 Graphical representation of Marsh viscosity variation after mechanical stress cycles

Table 6.20 - ID6 stressed Marsh cone test results

Hydration time (h)	stress time (min)	$\mu_{Marsh\ viscosity}$ (s)	relative variation (%)	$\sigma_{Marsh\ viscosity}$ (s)	SRI	γ (kg/L)	T (°C)
4	0	70,35	0,00%	2,6	100,00%	1,04	25,0
	5'	55,03	-21,77%	1,3	78,23%		
	5'+5'	52,90	-3,86%	2,4	75,20%		
	5'+5'+10'	51,16	-3,30%	1,6	72,72%		
	5'+5'+10'+30'	48,64	-4,92%	0,3	69,14%		
24	0	64,21	0,00%	3,7	100,00%	1,04	24,9
	5'	49,76	-22,50%	0,8	77,50%		
	5'+5'	48,43	-2,69%	0,4	75,42%		
	5'+5'+10'	46,98	-2,98%	0,9	73,17%		
	5'+5'+10'+30'	45,39	-3,38%	0,5	70,70%		
48	0	57,18	0,00%	3,6	100,00%	1,04	24,4
	5'	46,88	-18,01%	0,7	81,99%		
	5'+5'	46,57	-0,67%	0,6	81,44%		
	5'+5'+10'	46,55	-0,04%	0,7	81,40%		
	5'+5'+10'+30'	46,54	-0,01%	0,2	81,39%		
72	0	56,27	0,00%	3,8	100,00%	1,04	25,6
	5'	47,96	-14,77%	0,0	85,23%		
	5'+5'	46,95	-2,11%	0,1	83,44%		
	5'+5'+10'	46,38	-1,21%	0,2	82,43%		
	5'+5'+10'+30'	46,47	0,19%	0,0	82,58%		

Figure 6.28 show viscosity variation with increasing stress time and hydration. Viscosity strongly decreases during the first 5 minutes of stress. At 4 and 24 hours of hydration a slight viscosity decrease at subsequent stress cycles can be observed.

6.1.22 ID6 result analysis, stress vs static behavior

ID6 demonstrates a huge increase in viscosity within the first hydration phase, with relative variation that reaches 75% at 4 hours. Viscosity does not reach high value; the maximum result is achieved at 72 hours with a value approximately of 100 s. The interesting fact is that the slurry viscosity is fully developed in the first 4 hours of hydration, representing the stabilization point. At higher hydration time, viscosity remains nearly constant with some minor changes. This behavior indicates a moderate hydration capacity, which develops very quickly, reaching full hydration within the first hours. This means that bentonite is able to rapidly create a well-disperse three-dimensional structure, which respect to what was

discussed for ID5, rapidly expands without requiring long hydration times to establish an effective diffuse double layer and trapping water in the interlayer. This behavior could be the result of highly treated bentonite during the production process, characterized by a high concentration of sodium cations.

ID6 suffered moderate mechanical degradation. The largest viscosity reduction is observed during the first stress cycle, with a decrease between -15% and -22%. At 4 and 24 hours of hydration, the viscosity continues to decrease slightly linearly during the subsequent stress cycle, indicating that the structure is not fully stabilized and remains partially susceptible to breakdown. This result suggests that the final stable bentonite structure is reached at 24 hours of hydration. Although the static viscosity increase appears to level off 4 hours, the resting phase until the 24 hours, likely promotes a rearrangement of the particle structures, improving mechanical resistance. This reflects that at 48 and 72 hours, the SRI is higher and the viscosity after a slight decrease after the first minute of stress, remains stable even as the stress duration increases.

In figure 6.29 are shown all the Marsh cone results for both static and stressed slurry.

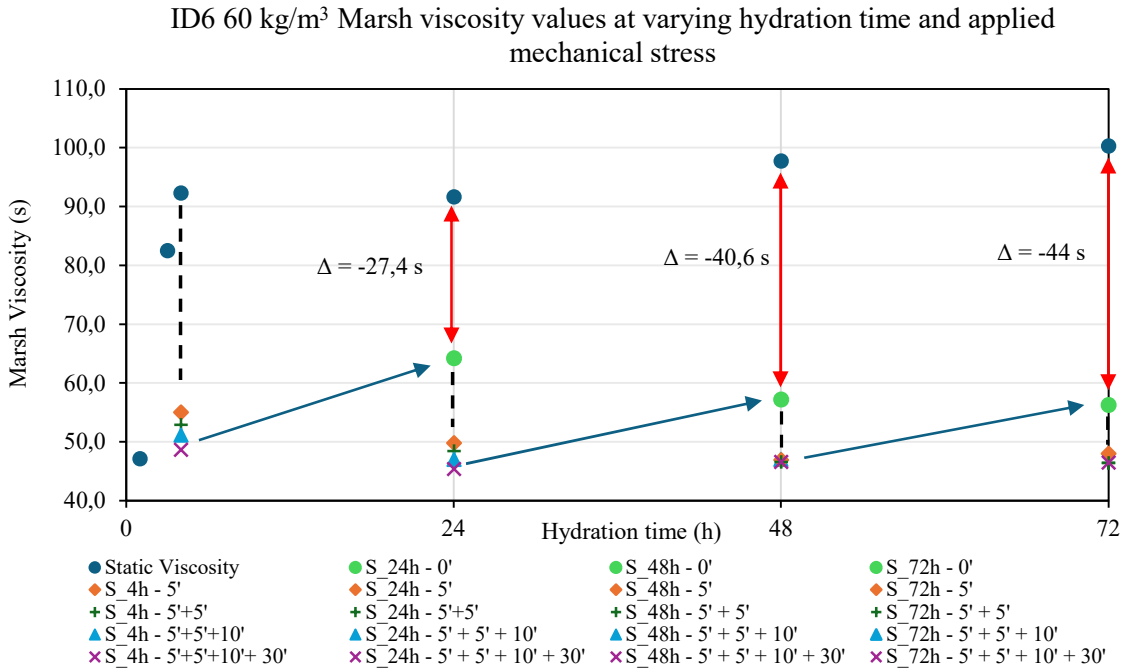

Figure 6.29 - Graphical visualization of the viscosity result of bentonite ID6 in static and stressed condition

Bentonite ID6 exhibits important thixotropy behavior, but limited ability to rebuild its internal structure after mechanical breakdown. Figure 6.29 clearly demonstrates that the differences between static and prestress viscosity are significant, and the viscosity recovers very low.

This behavior matches perfectly with the hydration trend previously discussed. Bentonite becomes fully hydrated at 24 hours, after that point the microstructure is already fully developed and stable. When mechanical stress is applied, some parts of the structure are inevitably destroyed, and bentonite is no longer able to reconstruct it.

The experimental data of ID6 under mechanical stress are quite well fitted by the exponential model, as demonstrated by the good correlation values.

Table 6.21 - Bentonite ID6 interpolation value and relative error

Hydration time (h)	τ (min)	$Mv_{,in}$ (s)	$Mv_{,inf}$ (s)	(RMSE)	Δ Marsh (%)	R^2
4h	3,9	70,35	50,12	1,0050	-28,76	0,98
24h	3,2	64,21	46,51	0,5889	-27,56	0,99
48h	1,4	57,18	46,55	0,0000	-18,59	1,00
72h	2,7	56,27	46,50	0,0130	-17,36	1,00

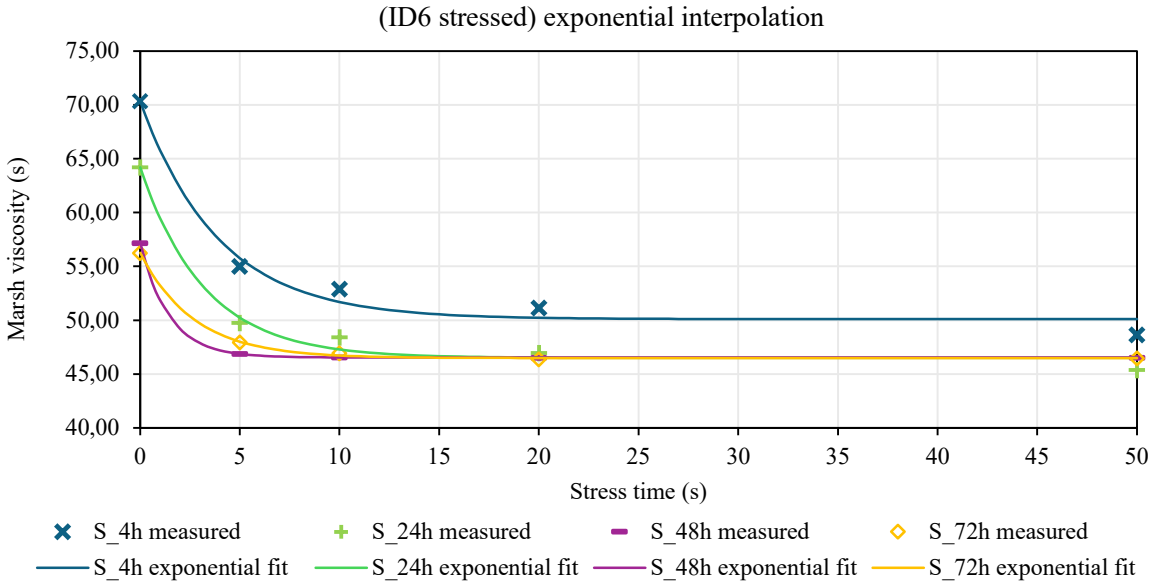

Figure 6.30 - ID6 graphical interpolation of the experimental result

The figure 6.30 shows that the time to reach the plateau is longer at 4 and 24 hours of hydration. It also highlights that at 4 hours a different plateau value is reached respect to the following hydration time. This suggests that maybe if the stress were extended beyond 50 minutes, the viscosity would likely continue to decrease reaching that lower equilibrium value.

6.1.23 ID6 - 80 kg/m^3 static

In table 6.22 are presented the Marsh cone test results, carried out on slurry prepared with bentonite ID6 at concentration of 80 kg/m^3.

Table 6.22 - ID6 80 Kg/m^3 static Marsh cone test results

Hydration time (h)	$\mu_{Marsh\ viscosity}$ (s)	Relative variation (%)	$\sigma_{Marsh\ viscosity}$ (s)	γ (kg/L)	T (°C)
0	50,3	0%	1,7	1,05	26,0
1	406,5	708,37%	183,7	1,05	26,0
3	Slurry too viscous cannot pass in Marsh cone mesh				
4					
24					
48					
72					

With increasing bentonite ID6 concentration, viscosity evaluation became more difficult due to the high value reached after just 3 hours of hydration, beyond which it was no longer possible to perform the test. Since only two data points were available the graphical representation of the Marsh result is not reported.

6.1.24 ID6 - 80 kg/m^3 mechanically stressed

This section presents the Marsh cost test results for the slurry prepared with bentonite ID6 at a concentration of 80 kg/m^3, subjected to mechanical stress using a laboratory mixer, at a constant speed of 1000 rpm with progressively increasing stress duration. After each stressing phase, a Marsh cone test was performed to measure the corresponding change in slurry viscosity (table 6.23).

Table 6.23 - ID6 80 kg/m^3 stressed Marsh cone test results

Hydration time (h)	stress time (min)	$\mu_{Marsh\ viscosity}$ (s)	relative variation (%)	$\sigma_{Marsh\ viscosity}$ (s)	SRI	γ (kg/L)	T (°C)
4	0	too viscous				1,05	26,0
	5'	After 6 minutes, only 350 mL of slurry had flowed out, and the cone was no longer dripping					
	5'+5'	> 12'					
	5'+5'+10'	> 12'					
	5'+5'+10'+30'	163,22	-	-	-		

24	0	too viscous				1,05	25,2
	5'	157,99	-	25,6	-		
	5'+5'	138,70	-	30,6	-		
	5'+5'+10'	110,67	-12,21%	16,5	-		
	5'+5'+10'+30'	103,77	-20,21%	11,6	-		
48	0	246,14	-6,23%	26,8	100,00%	1,05	25,4
	5'	104,75	-57,44%	15,7	42,56%		
	5'+5'	106,78	1,93%	14,3	43,38%		
	5'+5'+10'	104,37	-2,26%	12,3	42,40%		
	5'+5'+10'+30'	111,39	6,73%	18,3	45,25%		
72	0	514,80	0,00%	54,2	100,00%	1,05	25,4
	5'	148,89	-71,08%	33,2	28,92%		
	5'+5'	162,65	9,24%	38,1	31,59%		
	5'+5'+10'	141,43	-13,05%	27,4	27,47%		
	5'+5'+10'+30'	148,68	5,12%	23,2	28,88%		

At 4 hours of hydration the viscosity is so high that the slurry does not flow through the orifice of the Marsh cone making it impossible to perform the test. Even after applying the mechanical stress, slurry confirms the incredibly high viscosity values. At longer hydration time it was possible to develop some measurements, and the slurry presents a more fragile structure.

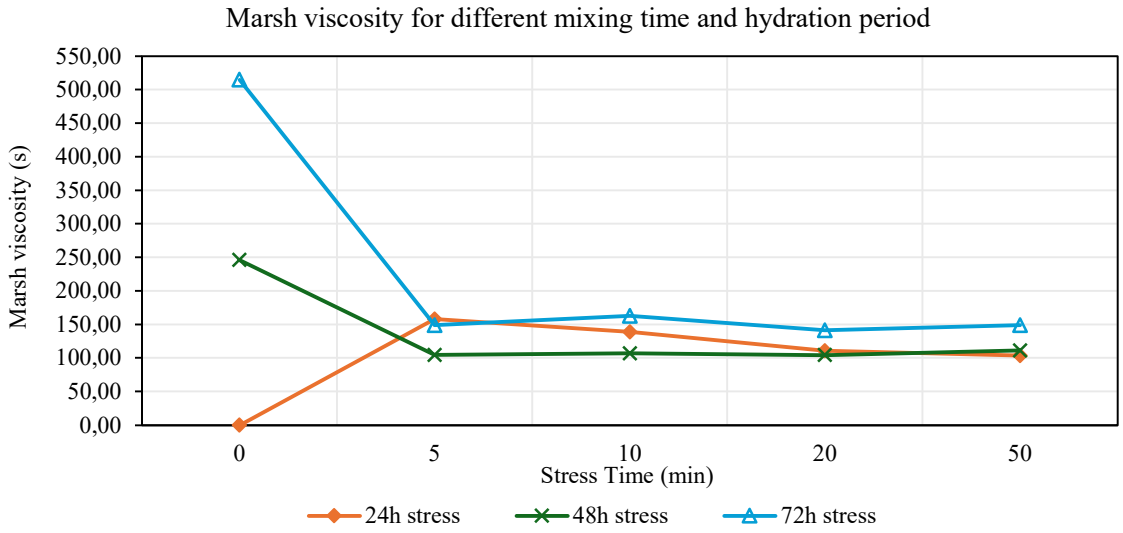

Figure 6.31 - ID6 80 kg/m3 Graphical representation of Marsh viscosity variation after mechanical stress cycles

Figure 6.31 shows an important viscosity decrease during the first 5 minutes of applied stress, with value dropping from approximately 500s to 150s. After this initial breakdown, the slurry reaches an almost constant viscosity value.

6.1.25 ID6 result analysis, stress vs static behavior

Increasing bentonite concentration, the static behavior still demonstrates a huge hydration capacity within the first hour of hydration. Viscosity increases by 708% in just one hour, passing from 50 s to 406 s. At longer hydration hours it was no longer possible to perform the Marsh cone test, due to the incredible viscosity reached by the suspension, which was no longer able to pass through the cone mesh. This result demonstrates an important hydration capacity, and the additional number bentonite particles promotes higher hydration leading to higher viscosity values.

During the evaluation of the stressed bentonite, in some cases it was not possible to evaluate the viscosity. Slurry showed a good mechanical resistance at 4 hours hydration, with Marsh cone viscosity greater than 12 minutes after 20 minutes of applied stress. At longer hydration time it was possible to record all the viscosity values, including the prestress measurement, indicating a lower thixotropic behavior. At 48 and 72 hours, the first 5 minutes of stress showed an important viscosity decrease of approximately -70%. This result presents the high susceptibility of this bentonite to mechanical degradation, with fragility that increases as hydration time progresses.

In figure 6.32 are shown all the available Marsh cone results for both static and mechanically agitated slurry.

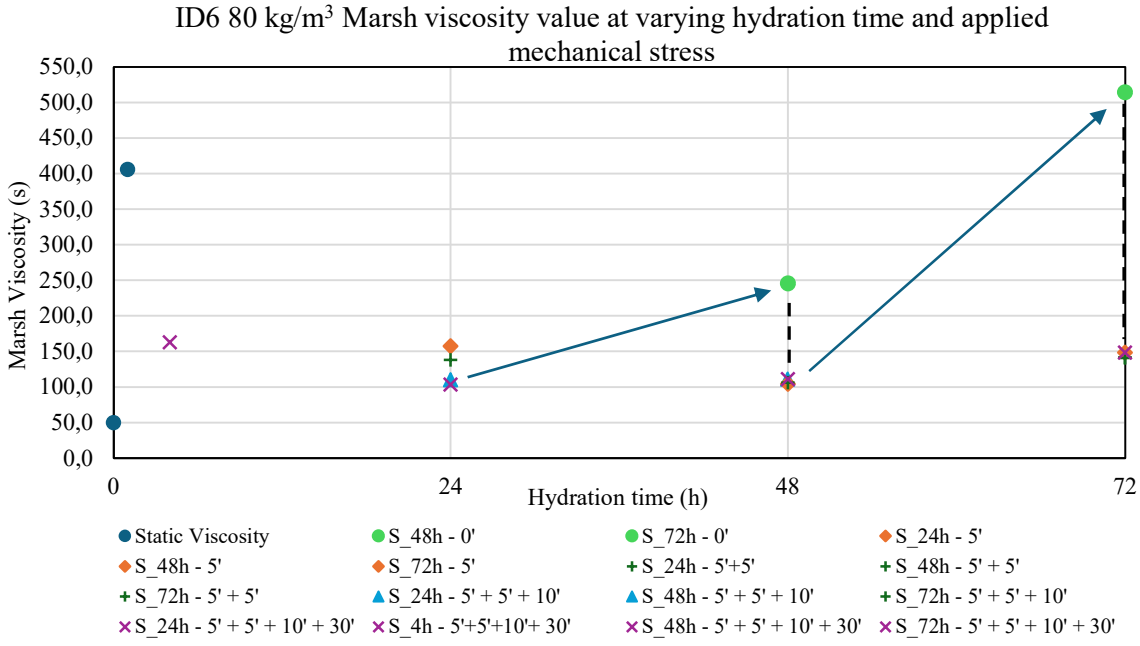

Figure 6.32 - ID6 80 kg/m³ Graphical representation of Marsh viscosity variation after mechanical stress cycles

From the few results in figure 6.32, it is possible to evaluate how the structure recovery increases with hydration, especially after 48 hours, meaning that the abundance of fully hydrated bentonite platelets allow slurry to partially recreate part of the original bonds destroyed during stress. Although the recovery is limited, the behavior suggests that a greater number disperse particles, allows the reconstruction after stress.

6.1.26 Bentonite ID6 concentration effect

The results obtained from tests performed on slurry prepared at two different concentrations show similar trend and overall behavior. Fast hydration is an important characteristic of bentonite ID6. At both concentrations, the slurry reaches high viscosity value within the first hours, confirming a fast water absorption capacity of this material. The concentration effect is clearly observed in the higher viscosity reached by the slurry prepared at 80 kg/m^3. The greater number of hydrated particles creates a well dispersed microstructure, characterized by edge-to-face interaction, leading to a substantial increase in viscosity. Higher concentration also influences post-stress behavior. Although both slurries suffer from structural breakdown under stress, the suspension at a higher concentration is able to recover at a higher viscosity after rest. However, the relative viscosity loss is more significant at 80 kg/m^3, indicating not necessarily a more fragile structure but a larger number of bonds disrupted during mechanical stress. However, unlike the lower concentration slurry, this breakdown does not lead to low final viscosity value but maintains high viscosity value more adapt for tunnelling with SS-TBM.

6.1.27 ID7 - 70 kg/m^3 static

In table 6.24 and graphically in figure 6.33, are presented the results of the Marsh cone test carried out on slurry prepared with bentonite ID7 with a concentration of 70 kg/m^3.

Table 6.24 - ID7 70 kg/m^3 static Marsh cone test results

Hydration time (h)	$\mu_{Marsh\ viscosity}$ (s)	Relative variation (%)	$\sigma_{Marsh\ viscosity}$ (s)	γ (kg/L)	T (°C)
0	77,4	97,61%	4,6	1,04	26,3
1	153,0	170,83%	7,4	-	-
24	414,3	14,48%	-	-	-
48	474,3	4,57%	-	-	-
72	496,0	97,61%	-	-	-

Slurry with bentonite ID7 shows an increasing viscosity during hydration. The viscosity increases from a value of 77 s, immediately after preparation, to 496 s after 72 hours. The increments are quite big, the variation between the viscosity result after preparation and the first hour of hydration reaches a value of 170%. Starting from the 24 hours of hydration, just one measurement was carried out, due to the too high level of viscosity reached in the first test's repetition. For this reason, the standard deviations after 1 hour are not available. Beyond 24 hours of hydration, the Marsh viscosity became so high that slurry no longer flowed naturally through the cone. The material completely blocked the orifice or started to drip, increasing the test time to useless and meaningless value. For this reason, a little deviation from the test standard procedure was adopted. Through the use of a small wooden stick, the slurry inside the cone was stirred during the measurement.

Different from bentonite ID6, for which even this procedure did not allow to complete the measurements, it was necessary in some cases to obtain at least an approximate estimation of the viscosity at such elevated values, although this system may introduce some measurement uncertainty. This measurement must be interpreted with caution, just as an indication of slurry rheological behavior.

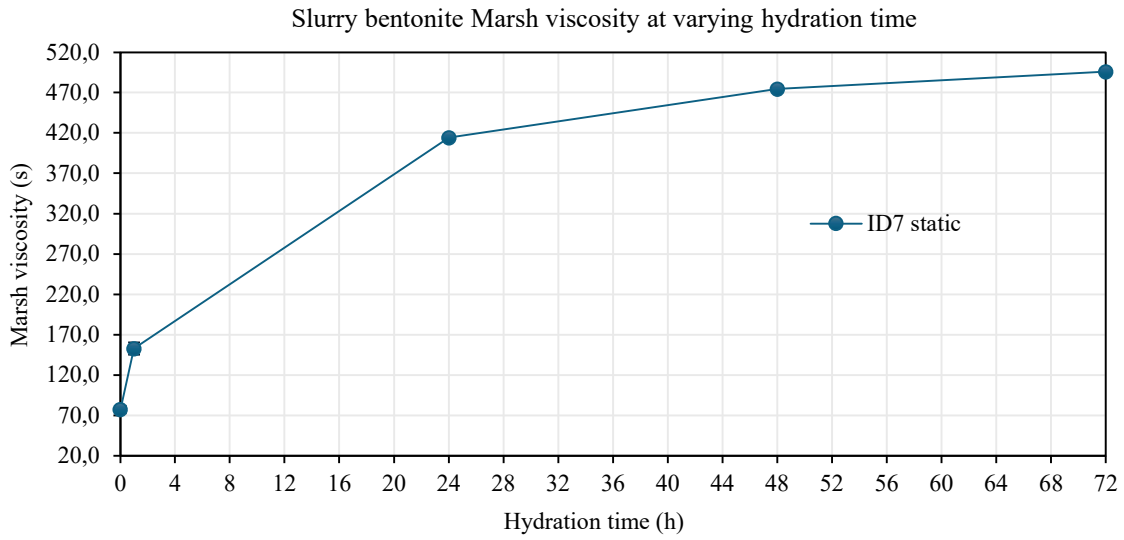

Figure 6.33 - ID7 70 kg/m³ Graphical representation of the Marsh viscosity variation at each hydration time

The Graph clearly highlights the viscosity increase with hydration time. The steep line connecting the first two points shows the rapid increment in the first hour. Subsequently, the viscosity continues to increase, reaching remarkably high values.

6.1.28 ID7 - 70 kg/m^3 mechanically stressed

This section presents the Marsh cost test results for the slurry prepared with bentonite ID7 at a concentration of 70 kg/m^3, subjected to mechanical stress using the laboratory mixer, at a constant speed of 1000 rpm with progressively increasing stress duration. After each stressing phase, a Marsh cone test was performed to measure the corresponding change in slurry viscosity (table 6.25).

Table 6.25 - ID7 70 kg/m^3 stressed Marsh cone test results

Hydration time (h)	stress time (min)	$\mu_{Marsh\ viscosity}$ (s)	relative variation (%)	$\sigma_{Marsh\ viscosity}$ (s)	SRI	γ (kg/L)	T (°C)
4	0	330,00	0,00%	-	100,00%	1,04	26.3
	5'	204,58	-21,77%	44,3	61,99%		
	5'+5'	189,52	-3,86%	41,0	57,43%		
	5'+5'+10'	186,52	-3,30%	44,0	56,52%		
	5'+5'+10'+30'	212,14	-4,92%	54,8	64,28%		
24	0	485,36	0,00%	-	100,00%	1,04	25
	5'	297,72	-22,50%	72,0	61,34%		
	5'+5'	265,99	-2,69%	56,0	54,80%		
	5'+5'+10'	264,20	-2,98%	52,5	54,43%		
	5'+5'+10'+30'	255,32	-3,38%	62,1	52,60%		
48	0	637,00	0,00%	-	100,00%	1,04	24,8
	5'	422,46	-18,01%	76,3	66,32%		
	5'+5'	358,33	-0,67%	35,5	56,25%		
	5'+5'+10'	335,67	-0,04%	49,7	52,69%		
	5'+5'+10'+30'	311,33	-0,01%	39,7	48,87%		
72	0	720,00	0,00%	-	100,00%	1,04	25,0
	5'	Too long time, slurry does not flow					
	5'+5'						
	5'+5'+10'						
	5'+5'+10'+30'	375,00	0,19%	-	52,08%		

Bentonite ID7 presents important viscosity reduction after stress, but also marked thixotropic behavior that did not allow to perform the Marsh test at 72 hours, due to the high viscosity value reached even after the first 5 minutes of stress.

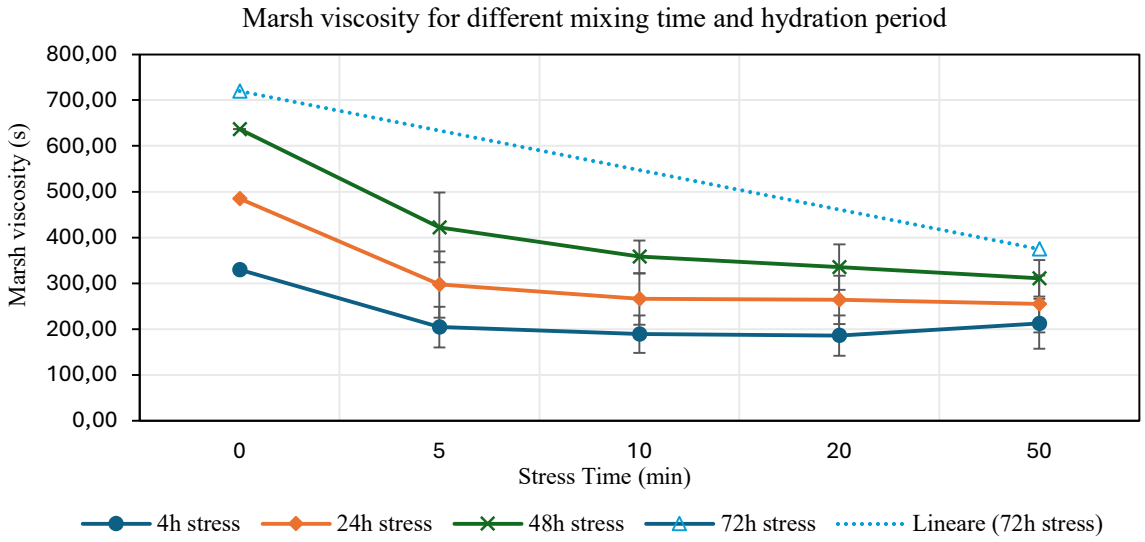

Figure 6.34 - ID7 70 kg/m³ Graphical representation of Marsh viscosity variation after mechanical stress cycles

Figure 6.34 shows viscosity decrease, along with stress cycles. During the first five minutes stress is evident the high viscosity loss, almost 200 s at each hydration time. After the following stress cycles, viscosity continues to decrease until 10 minutes of stress, after which there are only some slight variations.

6.1.29 ID7 result analysis, stress vs static behavior

Bentonite ID7 shows an extremely rapid and intense hydration capacity, with an increase of viscosity superior to the largest part of bentonite tested. The increment within the first hour is approximately 97%, and at 24 hours, the total increment respect to the initial values reaches 435%, indicating a fast hydration, compatible with a highly sodic bentonite, as confirmed by the huge swell index measured. For this reason, to complete almost every measurement, the slurry was stirred directly inside the cone during test. Although this activity inevitably altered the real Marsh viscosity value, it still provides a useful indication of the slurry behavior, observing the continuous viscosity increase despite the manual agitation provided, indicating a strong thixotropic behavior and a particularly strong three-dimensional structure. The viscosity growth continues over time without reaching any stabilization point, indicating the hydration continues, although at a reduced rate, and the structure continues to create a well-dispersed three-dimensional structure. Under stressed condition bentonite ID7 demonstrates a fragile behavior if subjected to mechanical degradation. During the first 5 minutes of stress, viscosity decreases by almost 50% at each hydration time, except at 72 hours, where this value is reached only after 30 minutes of

stress. Apart from the test at 4 hours, for all later hydration hours to complete the Marsh cone test, in addition to the applied stress, was applied also a manual agitation during the tests directly in the cone, typically after reaching 200 second of flow time. Nevertheless, the behavior of stressed slurry shows a clear dependency on the stress duration. The final viscosity is always about half of the initial, in some cases reached after more stress cycle. This result indicates that the bentonite structure suffers of a moderate breakdown during stress but remains on good viscosity value suitable for tunnelling applications with SS-TBM. The standard deviation values further highlight the important thixotropic recovery of this bentonite. The deviations are consistently over 40 seconds, mainly due to slurry's ability to rapidly rebuild its internal structure, between tests repetitions of Marsh cone measurement after stress.

The great thixotropic capacity can be seen also in figure 6.35 where all the Marsh cone results, both for static and stressed slurry are reported.

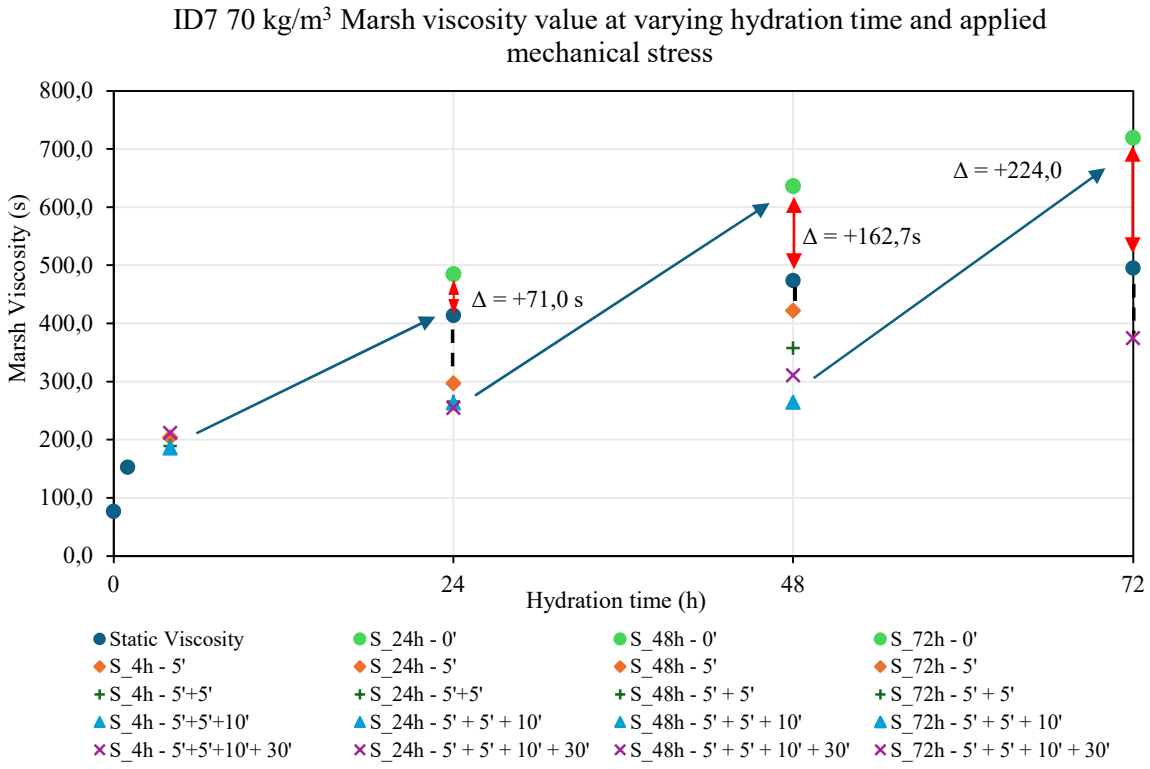

Figure 6.35 - Graphical visualization of the viscosity result of bentonite ID7 70 kg/m³ in static and stressed condition

The green points, which correspond to viscosities measured after resting phase following the previous stress cycle, represent the thixotropic recovery capacity. These points are constantly above the blue markers, which represent the static viscosities, indicating that the slurry is not only able to rebuild its internal structure during rest, in some cases even exceeds the static ones. This behavior is likely due to the high hydration capacity and to the mechanical

stress that promotes the redistribution of particles and gel structures into a more efficient configuration that enables higher particles hydration and disperse structures.

The experimental data of bentonite ID7 under mechanical stress are quite well fitted by the exponential model, as demonstrated by the good correlation value. The interpolation related to the 72 hours of hydration was not carried out due to the few measurements available.

Table 6.26 - Interpolation value and relative error

Hydration time (h)	τ (min)	$Mv_{,in}$ (s)	$Mv_{,inf}$ (s)	(RMSE)	Δ Marsh (%)	R^2
4h	1,7	330,00	196,18	79,7683	-40,55	0,97
24h	2,8	485,36	259,60	7,5527	-46,51	1,00
48h	4,5	637,00	321,64	45,6336	-49,51	1,00

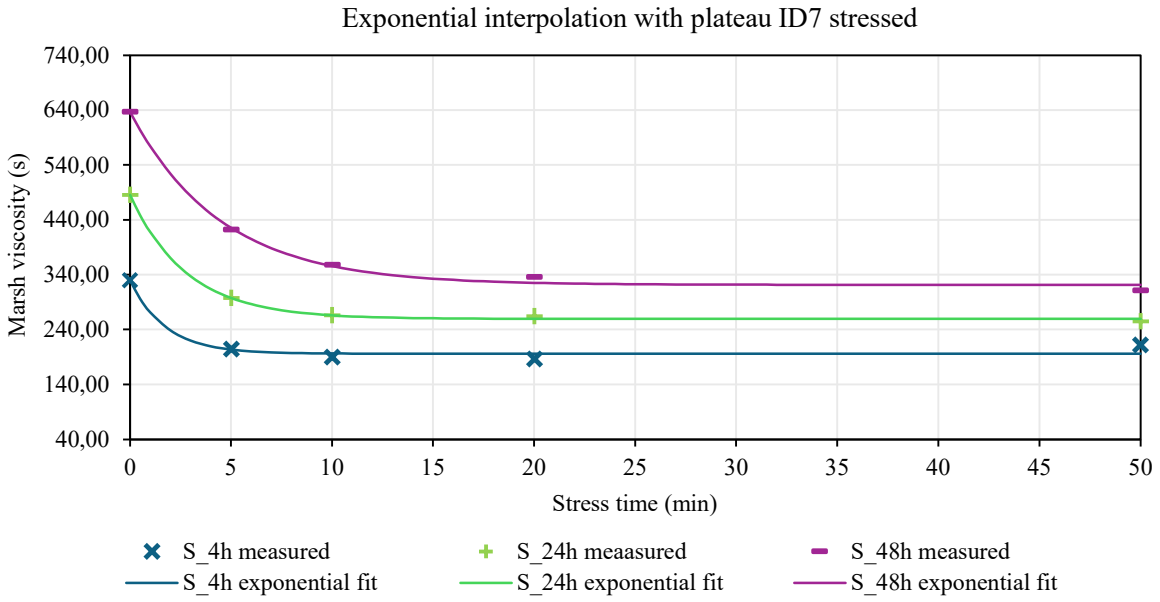

Figure 6.36 - ID7 70 kg/m³ graphical interpolation of the experimental result

Figure 6.36 shows that the time to reach the plateau is longer at higher hydration time and also highlights that viscosity decreases with increasing stress duration, indicating a moderate dependency from stress time. The plateau viscosity value changes with hydration time because the internal state evolves through time, the amount of hydration, thickness of the diffuse layer and strength between bonds between particles change as hydration progress. As result higher viscosity prestress values are observed followed by a constant decrease in viscosity under stress, converging to a different plateau equilibrium value.

6.1.30 ID8 - 60 kg/m^3 static

In table 6.27 and graphically in figure 6.37, are presented the results of the Marsh cone test carried out on slurry prepared with bentonite ID8 with concentration of 60 kg/m^3.

Table 6.27 - ID8 static Marsh cone test results

Hydration time (h)	$\mu_{Marsh\ viscosity}$ (s)	Relative variation (%)	$\sigma_{Marsh\ viscosity}$ (s)	γ (kg/L)	T (°C)
0	77,2	0%	2,2	1,04	24,8
1	101,3	23,81%	8,3	-	24,6
3	115,8	12,50%	9,6	-	24,2
4	115,1	-0,58%	9,0	1,04	24,0
24	148,5	22,49%	16,4	1,03	23,4
48	148,9	0,31%	18,1	1,04	23,3
72	132,8	-12,12%	11,7	1,04	23,2

Viscosity increments are moderate for slurry prepared with bentonite ID8, starting from a value of 77s to the maximum value of 148 s, measured at 48 hours. Relative variation underlines that viscosity is subjected to a higher increase after 1 hour and 4 hours of hydration, then remain stable, until a moderate reduction at 72 hours.

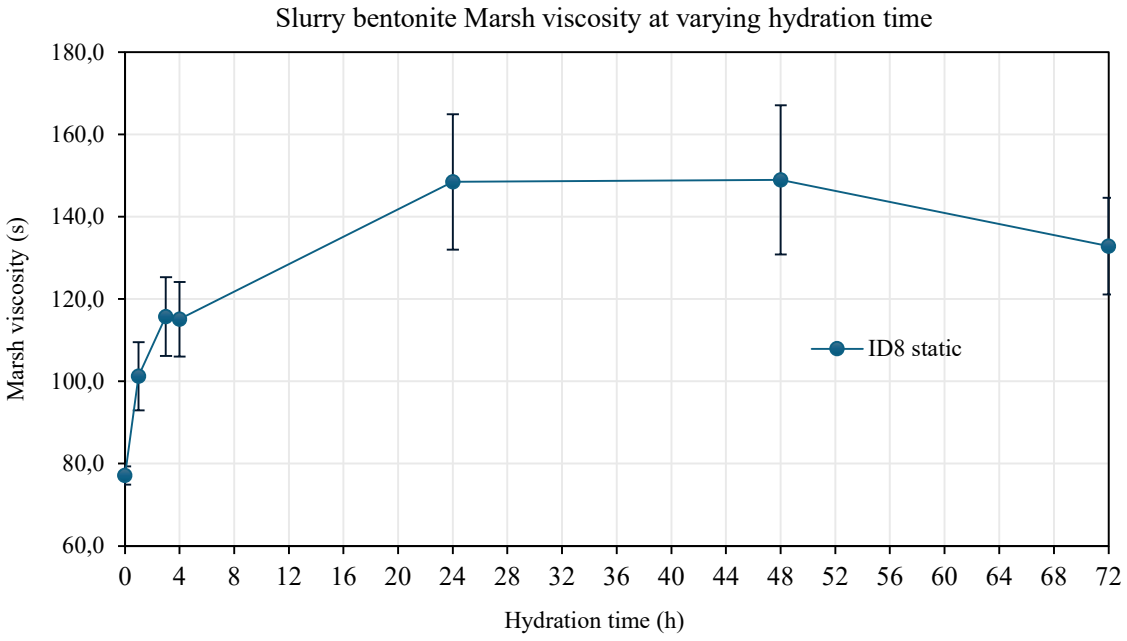

Figure 6.37 - ID8 graphical representation of the Marsh viscosity variation at each hydration time

In figure 6.37 the viscosity trend can be observed: the slurry exhibits a rapid initial increase up to 24 hours hydration, after which viscosity reaches a constant value, followed by a small decrease at 72 hours. A small drop is visible also at 3 hours of hydration.

6.1.31 ID8 - 60 kg/m^3 mechanically stressed

This section presents the Marsh cost test results for the slurry prepared with bentonite ID8 at a concentration of 60 kg/m^3, subjected to mechanical stress using a laboratory mixer, at a constant speed of 1000 rpm with progressively increasing stress duration. After each stressing phase, a Marsh cone test was performed to measure the corresponding change in slurry viscosity (table 6.28).

Table 6.28 - ID8 stressed Marsh cone test results

Hydration time (h)	stress time (min)	$\mu_{Marsh\ viscosity}$ (s)	relative variation (%)	$\sigma_{Marsh\ viscosity}$ (s)	SRI	γ (kg/L)	T (°C)
4	0	118,53	0,00%	11,6	100,00%	1,04	24,3
	5'	76,09	-55,78%	2,5	64,19%		
	5'+5'	72,86	-4,43%	3,0	61,47%		
	5'+5'+10'	72,43	-0,60%	2,1	61,10%		
	5'+5'+10'+30'	71,31	-1,56%	1,7	60,17%		
24	0	124,99	0,00%	15,9	100,00%	1,04	23,4
	5'	73,27	-70,58%	2,7	58,62%		
	5'+5'	71,05	-3,13%	3,1	56,84%		
	5'+5'+10'	69,88	-1,68%	1,3	55,90%		
	5'+5'+10'+30'	69,98	0,15%	2,9	55,99%		
48	0	106,39	0,00%	11,9	100,00%	1,04	23,6
	5'	68,44	-55,44%	1,7	64,33%		
	5'+5'	66,76	-2,52%	1,5	62,75%		
	5'+5'+10'	66,08	-1,03%	2,1	62,11%		
	5'+5'+10'+30'	65,00	-1,66%	2,0	61,10%		
72	0	93,77	0,00%	11,4	100,00%	1,04	23,2
	5'	64,91	-44,45%	0,8	69,23%		
	5'+5'	63,42	-2,35%	0,9	67,64%		
	5'+5'+10'	62,14	-2,07%	1,2	66,26%		
	5'+5'+10'+30'	62,49	0,57%	1,5	66,65%		

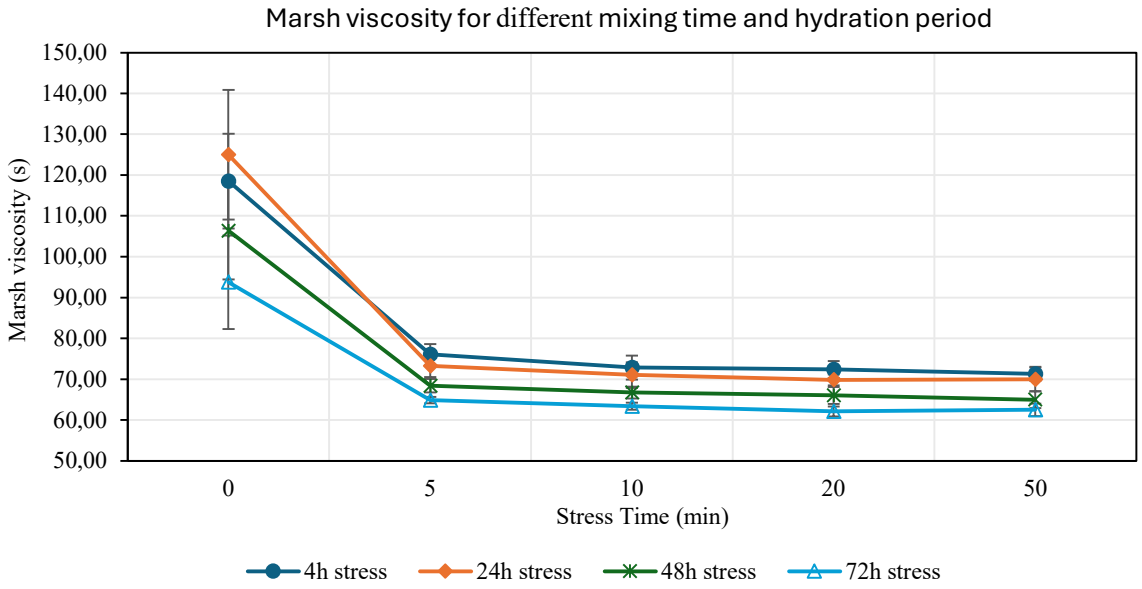

Figure 6.38 - ID8 graphical representation of Marsh viscosity variation after mechanical stress cycles

Across all hydration times, the rheological behavior remains essentially equal, showing a pronounced viscosity drop during the first 5 minutes stress, followed by small decreases at increasing stress time. The relative viscosity variation is also comparable among the different hydration stages, except at 4 hours hydration, during the 5 minutes stress, where the viscosity reduction reaches 70%, in all other cases, the decrease does not exceed 50%.

6.1.32 ID8 result analysis, stress vs static behavior

The Marsh viscosity value for bentonite ID8 shows non-constant hydration behavior. During the first 3 hours, viscosity increases by 50%, demonstrating a moderate hydration capacity, followed by a slight viscosity reduction, symptoms of a microstructure reorganization, likely due to the double diffuse layer expansion and to particles that became more dispersed, before the fully hydrated and more stable structures developed at longer hydration time. Full hydration is reached at 24 hours, confirmed also by the similar result obtained at 48 hours. At 72 hours, viscosity decreases by 12%, probably due to the over hydration phenomena, already seen in other bentonites, or again a structural reorganization.

The increase with longer hydration hours of the deviation indicates that once the structure is fully hydrated and forms a stable three-dimensional dispersed structure, it becomes more sensible to perturbation during measurements.

Under stressed conditions, Bentonite ID8 shows moderate mechanical degradation. The first 5 minutes of stress are responsible for the 50% viscosity loss, at all hydration time. At 24 hours when bentonite became fully hydrated, the disperse structure composed by edge-to-face bonds, led to higher susceptibility to mechanical stress, leading to an important loss of 70% of initial viscosity. During the additional stress cycles at each hydration time, slurry suffers of additional degradation, with small losses, which indicate a slight dependency between viscosity decrease and stress time. Although slurry keeps the SRI over 60 % for all hydration time except at 4 hours, maintaining good viscosity values.

In figure 6.39 are reposted all the Marsh cone test results both on static and stressed slurry. In the graph it is possible to observe good thixotropic behavior, with an important structure rebuild after stress, leading to a high viscosity recovery.

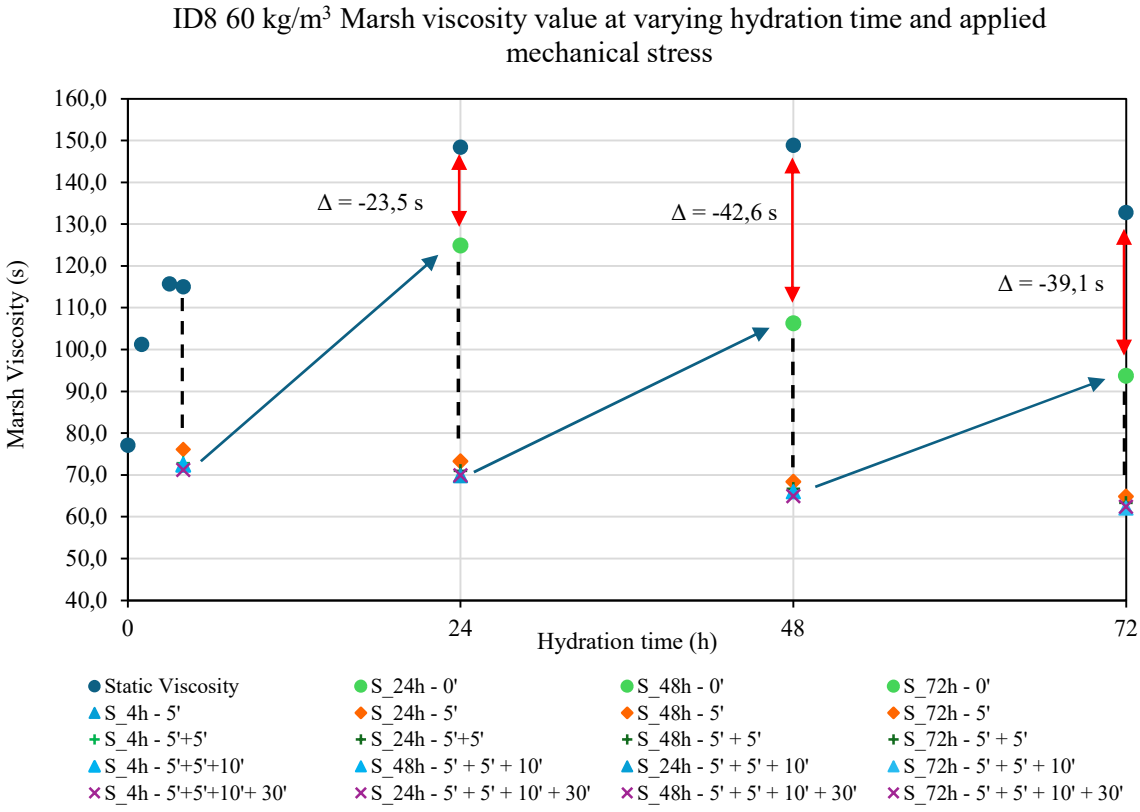

Figure 6.39 - Graphical visualization of the viscosity result of bentonite ID8 in static and stressed condition

Viscosity recovers decrease at longer hydration time, this is because at 24 hours the hydration is still ongoing, so the structure is easily reconstructed and subjected to change that increase the viscosity. At 48 and 72 hours the structure has already fully hydrated and developed, leading to a lower recovery after stress.

The experimental data of bentonite ID8 under mechanical stress are quite well fitted by the exponential model, demonstrate the correlation values are all equal to 1.

Table 6.29 - Bentonite ID8 interpolation value and relative error

Hydration time (h)	τ (min)	$Mv_{,in}$ (s)	$Mv_{,inf}$ (s)	(RMSE)	Δ Marsh (%)	R^2
4h	2,1	118,53	72,05	0,1766	-39,21	1,00
24h	1,7	124,99	70,22	0,1206	-43,82	1,00
48h	1,8	106,39	65,86	0,2634	-38,10	1,00
72h	2,0	93,77	62,59	0,1284	-33,25	1,00

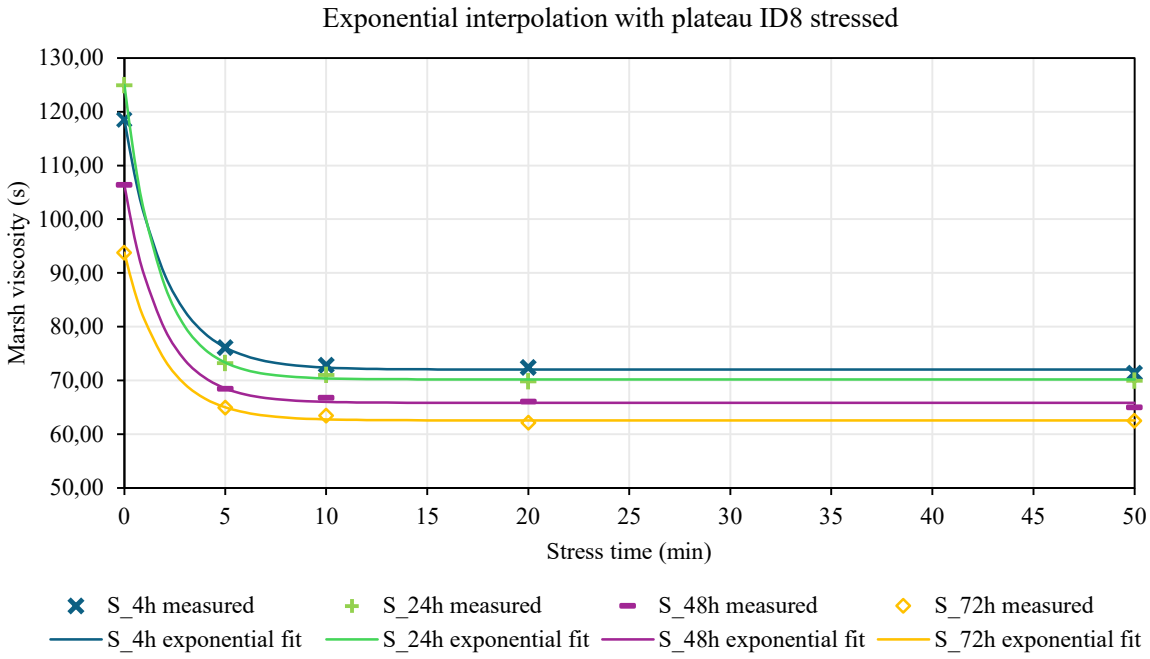

Figure 6.40 - ID8 graphical interpolation of the experimental result

Table 6.29 shows that the characteristic time to reach the plateau ranges between 1,7 to 2,1 minutes. This underlines that the greater part of viscosity loss occurs during the first minute of applied stress. From figure 6.40 it's possible to observe that the viscosity drop remains nearly constant, but the viscosity plateau value is different due to different recovery during resting phase. This behavior suggests that after full hydration is reached, bentonite structures in so longer able to efficiently reorganize after breakdown. The consequence is that the recovery capacity progressively leads to a lower plateau value at longer hydration times.

6.2 Viscometer results

In addition to the Marsh cone result, further rheological analyses were performed on bentonite ID7, using a rotational viscometer. The measurements were conducted on slurry at three different bentonite concentrations and increasing hydration time.

The viscometer directly provides viscosity measurement and the torque value (v), expressed as percentage of the full-scale torque range, of the different spindles. This value must be within 15 to 100% of the full-scale value, considering the measurement accurate and reliable.

In the following paragraph, the results of each measurement campaign are presented, divided for increasing bentonite concentration. For each hydration time, the following parameters are reported:

- $\mu_{viscosity}$ = the mean apparent viscosity value, calculated from all the available viscosity measurements, given by the instrument, along an established amount of time, at each tested rpm.
- $\sigma_{viscosity}$ = the standard deviation between the same viscosity measurements used to compute the mean, providing an indication of the viscosity variation during subsequent measurement at the same rpm.

At each hydration time, the viscosimeter measurements were performed by applying two sequences of decreasing and increasing rotational speed.

6.2.1 Bentonite ID7 - 45 kg/m^3

The following table presents the viscosity measurement for bentonite ID7 at a concentration of 45 kg/m^3. The measurements were performed at increasing hydration time, up to 24 hours, as the Marsh cone result highlights that period corresponds to the greatest hydration capacity. For measurement at this concentration, spindle L2, suitable for medium viscosity, were used, ensuring a torque value between 42-60%, within the optimal range for accurate measurement.

- **0 hours of hydration,** T = 20,1 C°

Table 6.30 - Viscometer result for bentonite ID7 45 kg/m³ after preparation

Cycle 1 - Decreasing		
RPM	**$\eta_{viscosity}$ (mPa*s)**	**$\sigma_{viscosity}$ (mPa*s)**
100	187,0	0,7
60	275,2	8,7
50	329,7	11,1
30	529,1	22,1
20	792,8	19,4
10	1464,2	0,5
6	2423,1	0,8
5	2922,1	0,2
4	3654,0	0,2
3	4800,2	0,1
2	6652,9	-
1	12942,0	-

Cycle 1 - Increasing		
RPM	**$\eta_{viscosity}$ (mPa*s)**	**$\sigma_{viscosity}$ (mPa*s)**
1	12645,0	-
2	6311,3	-
3	4017,0	0,4
4	3007,0	1,8
5	2368,3	7,4
6	2004,2	21,9
10	1152,8	100,1
20	654,3	32,1
30	433,8	3,5
50	293,9	10,4
60	247,0	0,3
100	166,2	0,1

Cycle 2 - Decreasing		
RPM	**$\eta_{viscosity}$ (mPa*s)**	**$\sigma_{viscosity}$ (mPa*s)**
100	161,5	0,0
60	262,1	4,2
50	323,3	6,8
30	503,9	2,3
20	759,5	6,2
10	1488,0	0,9
6	2313,7	14,0
5	2833,8	2,9
4	3459,0	0,1
3	4591,2	1,0
2	6411,0	-
1	12774,0	-

Cycle 2 - Increasing		
RPM	**$\eta_{viscosity}$ (mPa*s)**	**$\sigma_{viscosity}$ (mPa*s)**
1	12479,0	-
2	6568,0	-
3	4443,9	1,3
4	3066,7	0,4
5	2560,0	9,7
6	2129,1	27,8
10	1301,6	19,3
20	686,6	34,5
30	451,4	1,3
50	285,5	0,4
60	248,6	2,0
100	155,6	0,4

Viscometer results immediately demonstrate the typical shear-thinning behavior of slurry, with the viscosity progressively increasing as the rotational speed decreases. The apparent

viscosity ranged from approximately 155 to 12000 mPa*s, indicating a strong dependence with the applied shear rate. During the increasing branches in both cycles can be observed a decrease of viscosity revealing a hysteresis loop typical of thixotropic fluids.

The higher standard deviations are related to medium shear rate between 20 to 5 RPM, because there the breakdown at that speed is lower and happens slowly during the measurement, with viscosity measurement that decreases as the test time increases.

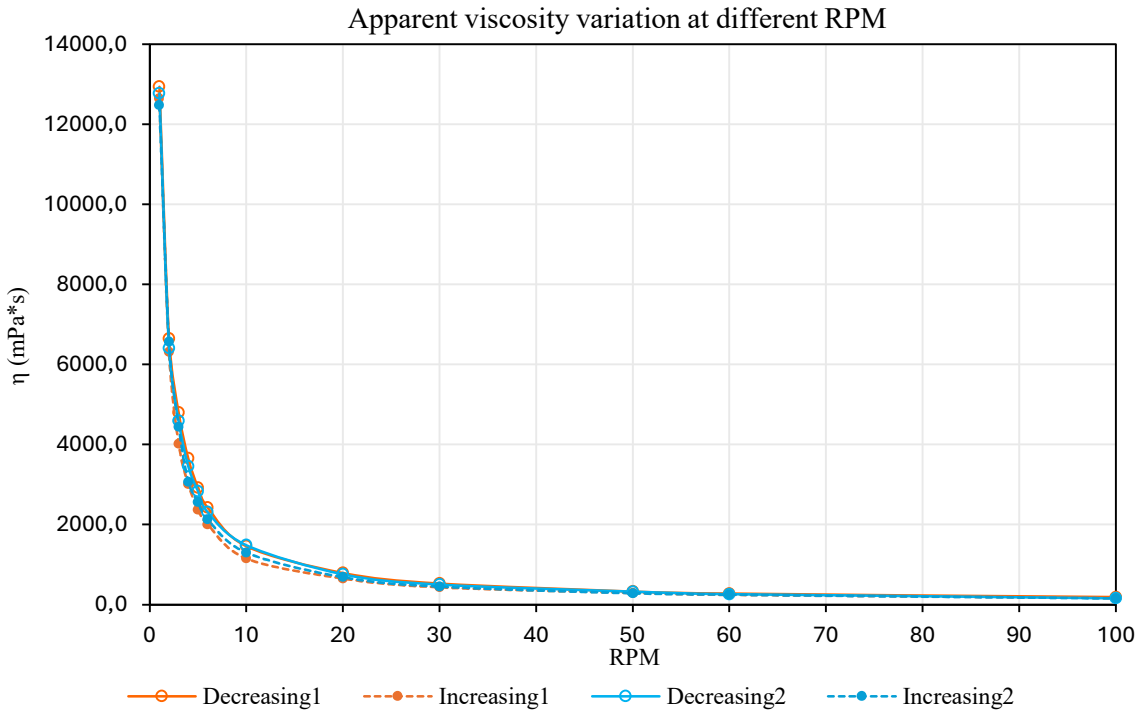

Figure 6.41 - Graphical representation of the viscometer result for bentonite ID7 45 kg/m³ after preparation

Figure 6.41 clearly shows the hysteresis loop between the increasing and decreasing branches in both test cycles. The two decreasing branches show almost comparable viscosity values, demonstrating a moderate thixotropic behavior that increases after the first cycle, due to a reorganization in the structure that reduces the susceptibility to mechanical degradation. The more pronounced hysteresis loop observed during the first cycles confirms a higher structure breakdown under shear, while the reduced loop area in the second cycle demonstrates a greater recovery capacity and ability form a more compact gel structure.

At higher rotational speed, 30 to 100 RPM, the shear stresses are so high that the microstructure of bentonite is disrupted immediately, and slurry almost behaves like a Newtonian fluid. This behavior indicates that at those speed slurry is not so affected by the shear variation, leading to almost null hysteresis and comparable value of viscosity. In contrast, at lower shear rate, the structure begins to rebuild, and the differences between the two curves become evident, revealing the thixotropic character of the slurry.

- **1 hour of hydration,** T = 20,1 °C

Table 6.31 - Viscometer result for bentonite ID7 45 kg/m³ at 1 hour of hydration

Cycle 1 - Decreasing		
RPM	**$\eta_{viscosity}$ (mPa*s)**	**$\sigma_{viscosity}$ (mPa*s)**
100	199,2	0,1
60	285,4	0,4
50	355,4	0,5
30	573,7	10,7
20	850,3	4,4
10	1672,1	0,7
6	2834,2	3,5
5	3248,4	0,7
4	3939,1	0,3
3	5041,6	0,1
2	7317,8	-
1	13814,0	-

Cycle 1 - Increasing		
RPM	**$\eta_{viscosity}$ (mPa*s)**	**$\sigma_{viscosity}$ (mPa*s)**
1	14019,0	-
2	7021,5	-
3	4531,3	0,8
4	3333,7	1,5
5	2607,1	2,1
6	2264,3	22,7
10	1320,8	75,4
20	710,0	38,3
30	482,6	0,1
50	312,6	1,1
60	270,1	0,2
100	172,3	0,0

Cycle 2 - Decreasing		
RPM	**$\eta_{viscosity}$ (mPa*s)**	**$\sigma_{viscosity}$ (mPa*s)**
100	163,6	std
60	286,7	0,1
50	342,9	0,4
30	536,0	0,5
20	823,4	10,7
10	1593,7	4,4
6	2532,5	0,7
5	3072,0	3,5
4	3746,8	0,7
3	4691,8	0,3
2	6918,8	0,1
1	13375,0	-

Cycle 2 - Increasing		
RPM	**$\eta_{viscosity}$ (mPa*s)**	**$\sigma_{viscosity}$ (mPa*s)**
1	13485,0	-
2	6816,1	-
3	4437,4	0,8
4	3500,3	1,5
5	2755,6	2,1
6	2248,4	22,7
10	1458,4	75,4
20	730,9	38,3
30	496,3	0,1
50	313,3	1,1
60	273,7	0,2
100	170,3	0,0

Increasing hydration time viscosity slightly increases, maintaining always its evident shear-thinning and thixotropic behavior. Viscosity at low rate reaches higher value to 14000 mPa*s

but also at higher shear rate the viscosity is higher, indicating a good hydration capacity and that the gel structure is progressively building.

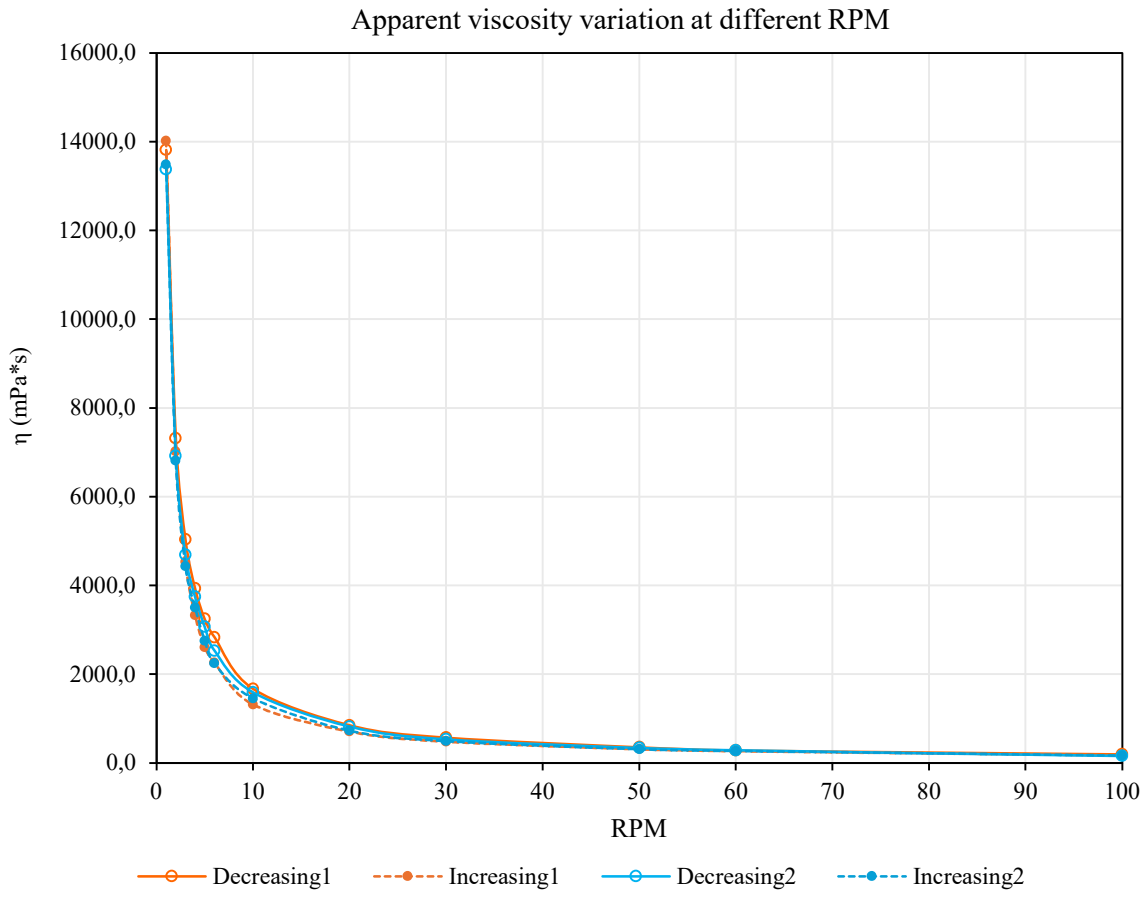

Figure 6.42 - Graphical representation of the viscometer result for bentonite ID7 45 kg/m³ at 1 hour of hydration

Figure 6.42 shows two different hysteresis loops with different dimensions. The first cycle is clearly visible with a marked difference between the decreasing and increasing branches, indicating an important breakdown during the decreasing phase and only partial recovery afterward. Unlikely the behavior observed immediately after preparation, the two decreasing branches do not overlap as the second decreasing curve shows an important drop in viscosity although still higher respect to increasing branches of the first cycle, showing that the partial recovery process continues between cycles. The second loop area is considerably smaller, indicating that some part of the structures was inevitably destroyed at higher shear rate. Nevertheless, the reorganization of bentonite particles after the first breakdowns leads to a more stable microstructure that shows lower susceptibility to mechanical degradation as demonstrated by the smaller loop area.

- **3 hours of hydration,** T = 20,4 °C

Table 6.32 - Viscometer result for bentonite ID7 45 kg/m³ at 3 hours of hydration

Cycle 1 - Decreasing		
RPM	**$\eta_{viscosity}$ (mPa*s)**	**$\sigma_{viscosity}$ (mPa*s)**
100	232,2	5,1
60	316,9	0,8
50	386,6	1,9
30	623,4	11,0
20	937,9	32,8
10	1868,4	11,8
6	3079,0	17,5
5	3534,1	1,7
4	4685,1	12,5
3	5987,9	3,4
2	8158,0	-
1	15456,0	-

Cycle 1 - Increasing		
RPM	**$\eta_{viscosity}$ (mPa*s)**	**$\sigma_{viscosity}$ (mPa*s)**
1	14947,0	-
2	7840,4	-
3	4912,0	0,5
4	3509,9	1,6
5	2943,3	17,2
6	2443,6	14,0
10	1459,3	44,4
20	748,4	41,6
30	515,4	11,4
50	328,8	5,6
60	288,7	0,3
100	176,2	0,5

Cycle 2 - Decreasing		
RPM	**$\eta_{viscosity}$ (mPa*s)**	**$\sigma_{viscosity}$ (mPa*s)**
100	171,8	1,6
60	300,4	20,8
50	350,8	5,6
30	571,1	3,6
20	885,5	20,6
10	1688,0	6,8
6	2755,2	1,9
5	3312,1	9,8
4	4011,3	0,1
3	4964,2	6,2
2	7318,1	-
1	14015,0	-

Cycle 2 - Increasing		
RPM	**$\eta_{viscosity}$ (mPa*s)**	**$\sigma_{viscosity}$ (mPa*s)**
1	14426,0	-
2	7353,9	-
3	4879,8	1,9
4	3658,6	0,5
5	3064,4	4,2
6	2388,6	0,5
10	1492,0	33,5
20	771,9	22,4
30	513,0	5,7
50	327,2	7,7
60	284,5	0,3
100	174,1	2,9

Table 6.32 shows important increase in viscosity respect to the previous result at 1 hour of hydration, with an increase of approximately 10%.

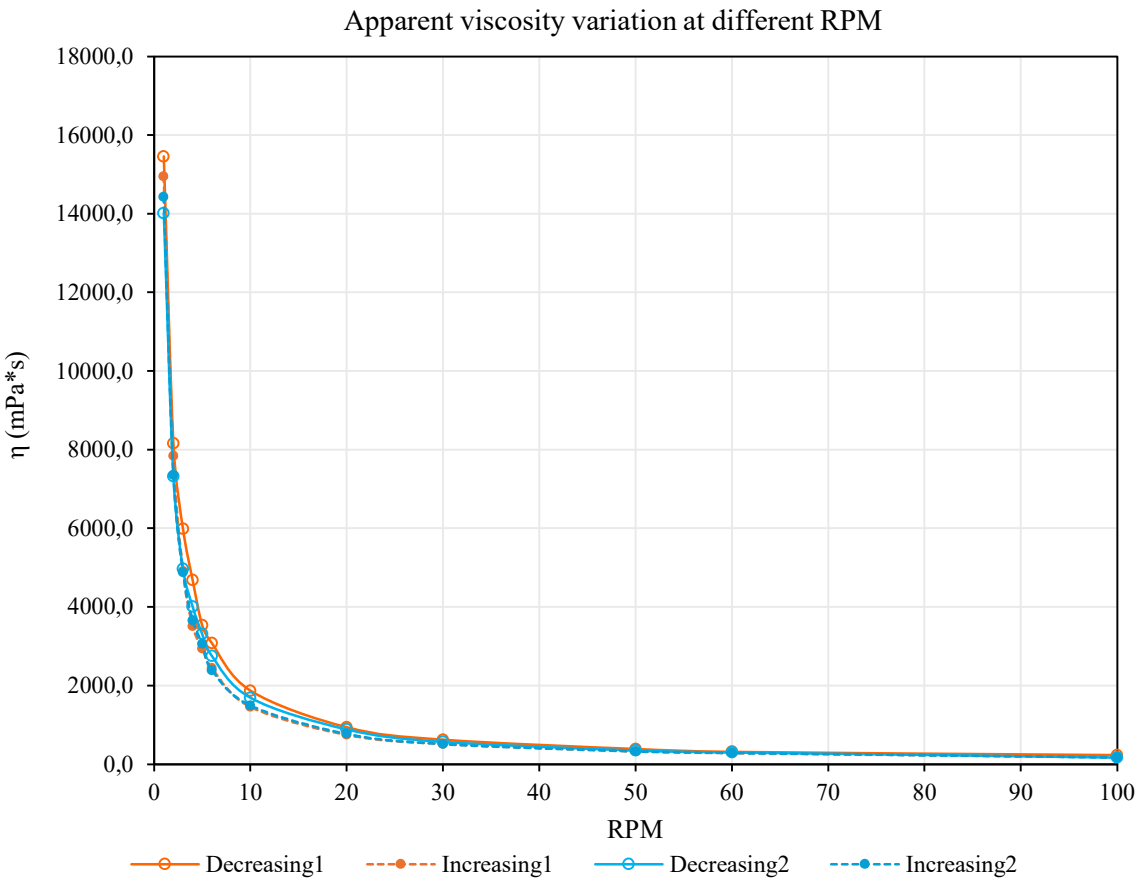

Figure 6.43 - Graphical representation of the viscometer result for bentonite ID7 45 kg/m³ at 3 hours hydration

At 3 hours of hydration, as shown in figure 6.43, the two-hysteresis loop presents different dimensions, mainly due to the lower viscosity value measured during the decreasing branch of the second cycle. This behavior demonstrates that, as hydration progresses, the slurry develops a more stable microstructure which, although still susceptible to mechanical stress, reaches a constant viscosity plateau. This indicated that regardless of the initial viscosity the residual viscosity after stress tends to a constant value. This feature is particularly important in excavation with SS-TBM, because maintaining an adequate residual viscosity, after being subjected to intense stress, is essential to continue without problem the excavation. The thixotropic behavior became lower as hydration increased, as demonstrated by a smaller recovery of the second cycle's decreasing curve.

- **4 hours of hydration,** T = 20,6 °C

Table 6.33 - Viscometer result for bentonite ID7 45 kg/m³ at 4 hours of hydration

Cycle 1 - Decreasing		
RPM	**$\eta_{viscosity}$ (mPa*s)**	**$\sigma_{viscosity}$ (mPa*s)**
100	241,6	10,6
60	314,5	3,9
50	387,7	2,0
30	631,0	12,8
20	941,7	23,1
10	1906,1	7,7
6	2904,7	1,3
5	3577,7	0,9
4	4404,9	6,2
3	5767,4	0,4
2	8406,6	-
1	15820,0	-

Cycle 1 - Increasing		
RPM	**$\eta_{viscosity}$ (mPa*s)**	**$\sigma_{viscosity}$ (mPa*s)**
1	16114,0	-
2	8309,3	-
3	5490,4	19,4
4	3852,2	2,6
5	3037,1	44,4
6	2515,1	16,9
10	1533,3	22,5
20	793,1	50,9
30	536,1	3,6
50	348,2	11,6
60	292,0	0,9
100	193,2	0,1

Cycle 2 - Decreasing		
RPM	**$\eta_{viscosity}$ (mPa*s)**	**$\sigma_{viscosity}$ (mPa*s)**
100	188,8	0,0
60	300,9	2,1
50	455,7	135,8
30	611,2	13,1
20	896,8	10,0
10	1673,3	0,2
6	2733,9	30,0
5	3392,8	0,2
4	4125,5	0,2
3	5218,6	0,1
2	7533,6	-
1	14857,0	-

Cycle 2 - Increasing		
RPM	**$\eta_{viscosity}$ (mPa*s)**	**$\sigma_{viscosity}$ (mPa*s)**
1	15209,5	-
2	7936,2	-
3	5181,0	0,3
4	3754,3	0,1
5	3044,1	0,4
6	2532,1	1,4
10	1619,6	17,1
20	814,5	45,0
30	535,1	5,9
50	339,9	4,1
60	300,7	21,9
100	191,6	0,0

Table 6.33 the results shows viscosity increases at a lower rate. At this point the increases in viscosity are limited to an approximate ranging between 2 to 8%, respecting the previous value.

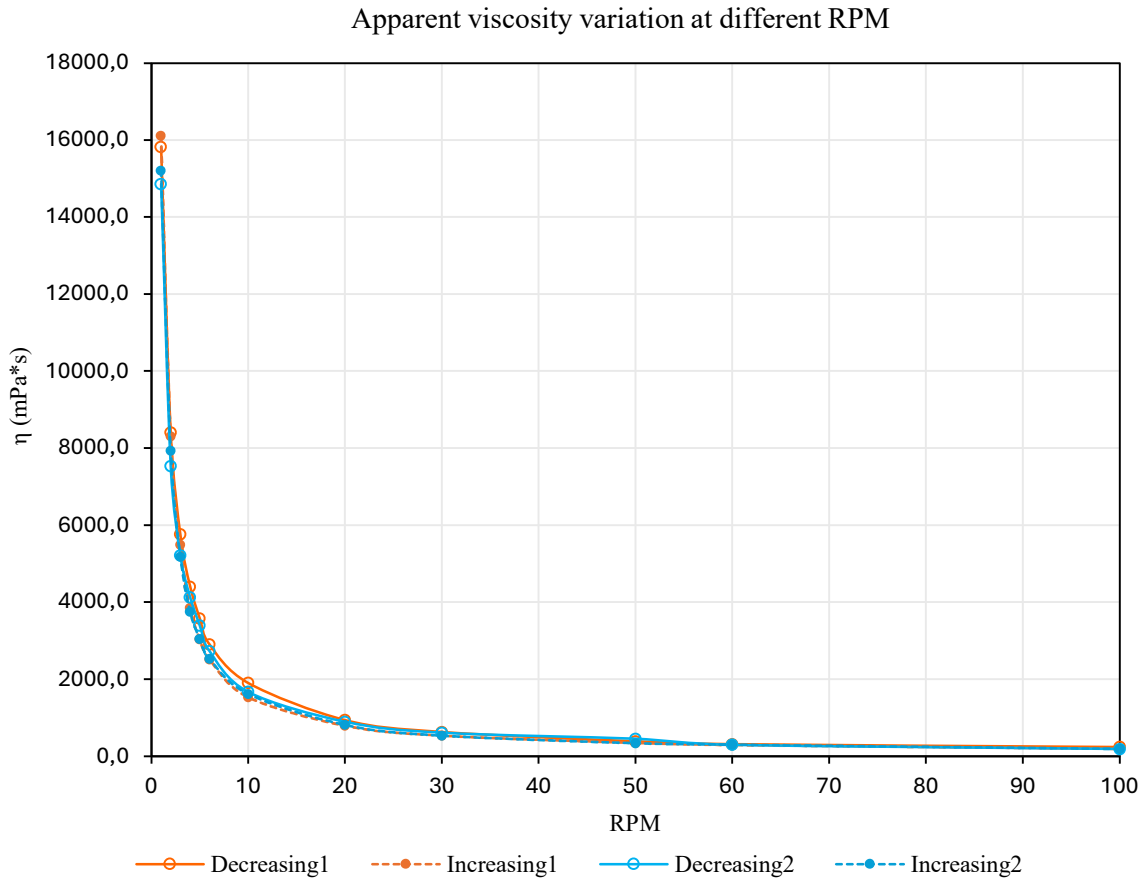

Figure 6.44 - Graphical representation of the viscometer result for bentonite ID7 45 kg/m³ at 4 hours hydration

The results presented in figure 6.44 are consistent with the rheological evolution of slurry during hydration. As hydration progresses, the viscosity increases in both cycle, but a clear decrease in thixotropic behavior is visible. After the first cycles, the blue curve representing the value measured during the second decreasing, presents small differences compared to the increasing curves, indicating difficulties in microstructure recovery, symptoms also of a lower hydration rate at this stage. The hysteresis loop became visible already at low shear rate, around 5-6 rpm, meaning that the structure breakdown starts even at small shear rate

- **24 hours of hydration,** T = 20,6 C°

Table 6.34 - Viscometer result for bentonite ID7 45 kg/m³ at 24 hours of hydration

Cycle 1 - Decreasing		
RPM	**$\eta_{viscosity}$ (mPa*s)**	**$\sigma_{viscosity}$ (mPa*s)**
100	283,1	7,7
60	402,2	6,7
50	481,7	12,7
30	792,2	39,3
20	1162,1	20,5
10	2474,6	64,9
6	3925,8	4,3
5	4582,6	1,0
4	5636,7	0,8
3	7114,5	0,7
2	10352,0	-
1	19994,0	-

Cycle 1 - Increasing		
RPM	**$\eta_{viscosity}$ (mPa*s)**	**$\sigma_{viscosity}$ (mPa*s)**
1	19641,5	-
2	10218,0	-
3	6459,9	0,4
4	4637,5	0,5
5	3911,0	11,9
6	3276,6	42,4
10	1884,9	115,1
20	943,5	50,3
30	618,2	18,4
50	392,4	0,1
60	335,1	6,2
100	207,3	0,4

Cycle 2 - Decreasing		
RPM	**$\eta_{viscosity}$ (mPa*s)**	**$\sigma_{viscosity}$ (mPa*s)**
100	203,7	2,6
60	347,3	3,7
50	422,6	1,4
30	687,8	18,1
20	1063,6	32,5
10	2109,6	12,3
6	3292,3	4,7
5	3951,7	10,8
4	4784,3	0,9
3	6365,6	0,2
2	9395,4	-
1	18609,0	-

Cycle 2 - Increasing		
RPM	**$\eta_{viscosity}$ (mPa*s)**	**$\sigma_{viscosity}$ (mPa*s)**
1	18183,0	-
2	8933,6	-
3	5639,8	92,3
4	4524,8	0,3
5	3686,7	145,6
6	3144,1	9,2
10	1765,8	86,0
20	938,2	70,6
30	625,0	0,4
50	397,1	4,0
60	327,1	2,2
100	195,7	0,6

At 4 hours hydration, the apparent viscosity reaches value above 19000 mPa*s at 1 rpm, decreasing to nearly 200 at 100 rpm, showing a clear shear thinning behavior. This large variation underlines the presence of a well-developed microstructure, but still fragile.

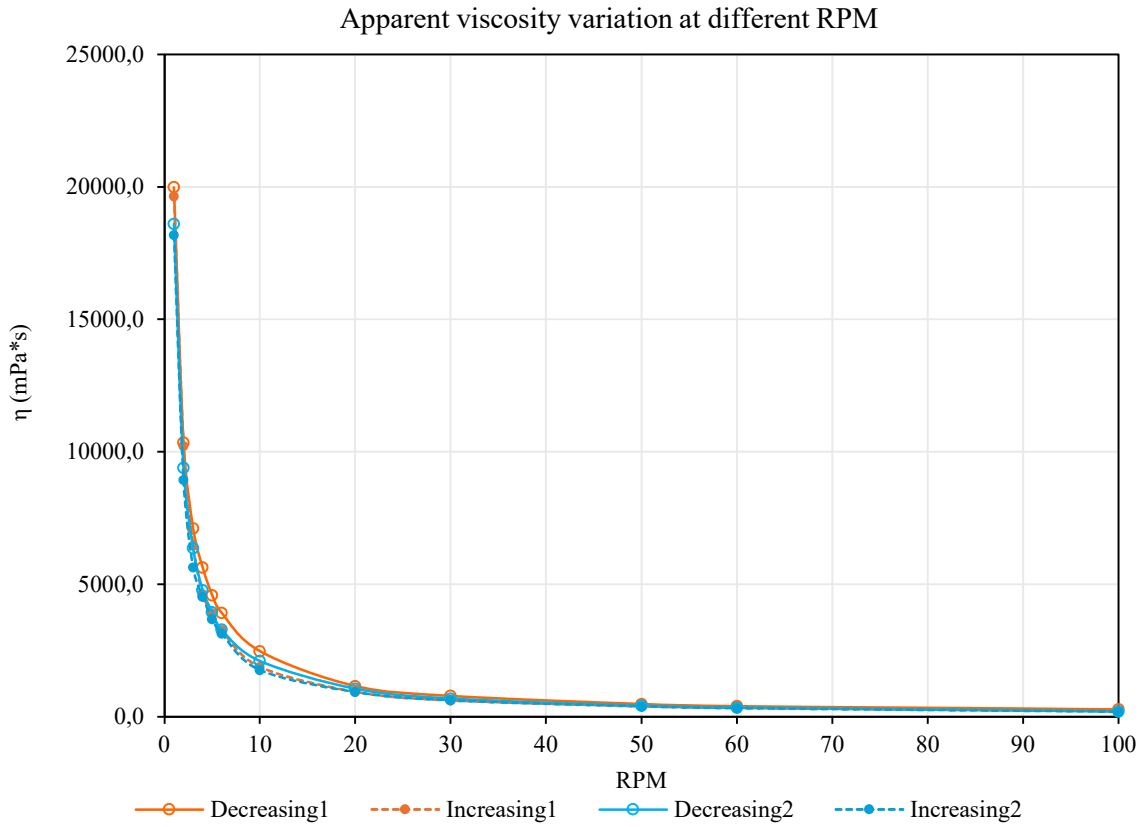

Figure 6.45 - Graphical representation of the viscometer result for bentonite ID7 45 kg/m³ at 24 hours hydration

The thixotropic behavior is moderate, as highlighted by the wide hysteresis loop observed by the first cycle more pronounced at lower shear rate. The second loop is significantly smaller confirming the decreased thixotropic response. The recovery between the two cycles is even lower at this hydration stage, as the three curves following the first decreasing branch are almost superimposed. This result suggests that part of the original structure was irreversibly destroyed during the first cycle. Overall, at this stage, bentonite exhibits dense and cohesive gel network capable with high viscosity value even after shear stress

6.2.2 Bentonite ID7 - 60 kg/m³

The following table presents the viscosity measurement for bentonite ID7 at a concentration of 60 kg/m³. The measurements were performed at increasing hydration time, up to 24 hours. Increasing concentration led to higher viscosity value, therefore the spindle used at lower concentration was no longer appropriate. Spindle L3, suitable for medium to high viscosity

was used, with torque percentage ranging between 30-60%, ensuring reliable viscosity measurement.

- **0 hours of hydration,** T = 22,6 C°

Table 6.35 - Viscometer result for bentonite ID7 60 kg/m³ after preparation

Cycle 1 - Decreasing		
RPM	**$\eta_{viscosity}$ (mPa*s)**	**$\sigma_{viscosity}$ (mPa*s)**
100	457,7	12,1
60	779,6	30,5
50	940,1	7,9
30	1582,4	1,7
20	2389,5	29,6
10	5066,9	171,3
6	-	-
5	8957,4	6,6
4	10495,0	0,0
3	12724,6	77,4
2	16768,0	-
1	25787,0	-

Cycle 1 - Increasing		
RPM	**$\eta_{viscosity}$ (mPa*s)**	**$\sigma_{viscosity}$ (mPa*s)**
1	31612,0	-
2	13958,0	-
3	11261,0	0,0
4	9290,5	12,8
5	7143,6	0,0
6	6032,2	0,0
10	4059,7	54,7
20	2273,6	251,1
30	1520,8	68,7
50	941,2	8,9
60	775,4	27,8
100	476,4	19,4

Cycle 2 - Decreasing		
RPM	**$\eta_{viscosity}$ (mPa*s)**	**$\sigma_{viscosity}$ (mPa*s)**
100	480,5	15,3
60	793,0	11,0
50	914,5	31,4
30	1619,7	139,1
20	2453,1	234,2
10	4867,7	146,3
6	7092,8	0,3
5	8132,2	12,0
4	9189,3	59,9
3	12363,0	15,5
2	17953,0	-
1	33313,0	-

Cycle 2 - Increasing		
RPM	**$\eta_{viscosity}$ (mPa*s)**	**$\sigma_{viscosity}$ (mPa*s)**
1	33403,0	-
2	17046,0	-
3	10789,6	272,6
4	9481,1	35,1
5	7687,9	20,2
6	6601,6	12,3
10	4133,5	103,7
20	2172,2	56,0
30	1484,0	15,4
50	898,0	3,4
60	772,1	28,9
100	482,7	10,0

The concentration increase is clearly observable from the viscosity result considerably higher respect to lower concentration. Viscosity value range between 500 mPa*s and 30000 mPa*s, highlighting that the higher quantity of disperse particles creates a greater number of edges to face bonds leading to a stronger hydrated three-dimensional network. The shear-thinning behavior is very pronounced, with a rapid decrease in viscosity, especially at low rpm. At higher rpm the phenomenon is less evident because the high shear rate disrupts a good part of the network and slurry starts to behave nearly as Newtonian fluid.

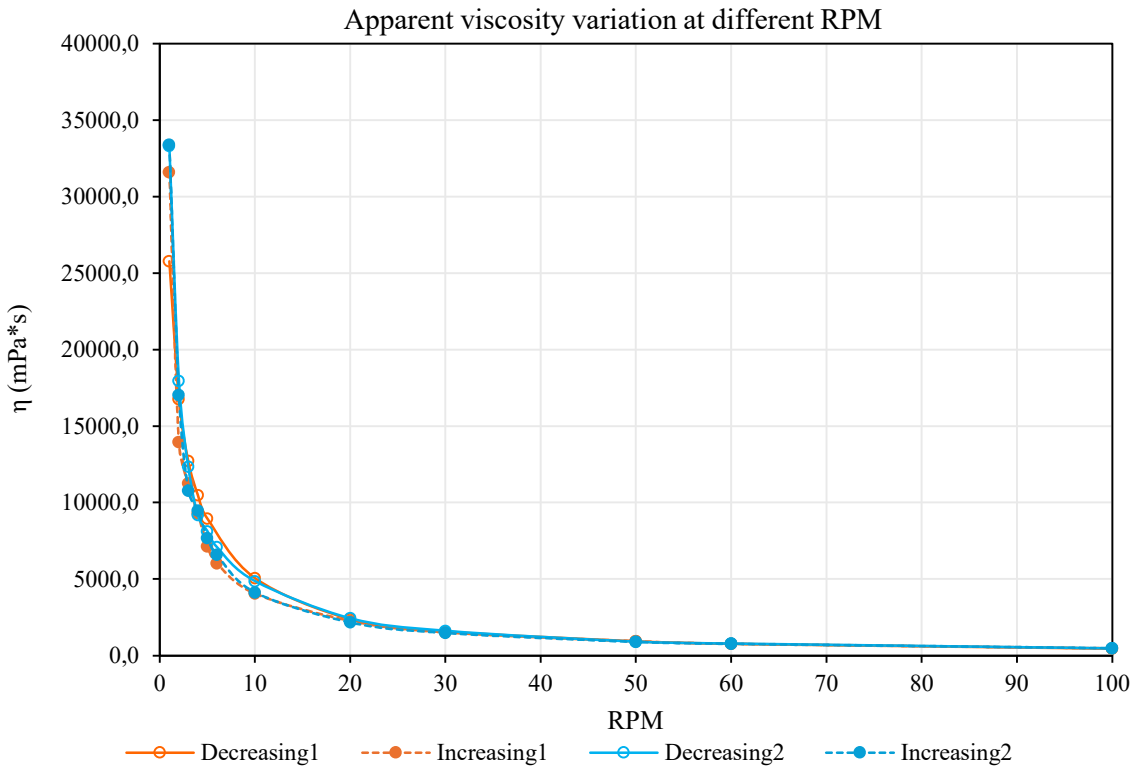

Figure 6.46 - Graphical representation of the viscometer result for bentonite ID7 60 kg/m³ after preparation

At this concentration, bentonite ID7 shows an important thixotropic behavior during the first cycle, with the hysteresis loop formed by the decreasing and increasing curve, considerably extended. This behavior represents a dispersed structure, highly subjected to mechanical degradation, that is not able to entirely recover its original structure at lower shear rate. Especially at lower rpm this behavior is clearly visible, while for higher rpm, above 30 the high stress destroys immediately the structure meaning null thixotropy. The second cycle presents different values due to small variation in bentonite structure which induces a more fragile behavior under mechanical stress also at low speed. also, high value of the standard deviation represents again the high thixotropy of the bentonite, showing dynamic behavior even during measurement, with continuous structure modification that led to lower viscosity during stress, and recovery at lower rpm.

- **1 hour of hydration,** T = 21,9 C°

Table 6.36 - Viscometer result for bentonite ID7 60 kg/m³ at 1 hour of hydration

Cycle 1 - Decreasing		
RPM	**$\eta_{viscosity}$ (mPa*s)**	**$\sigma_{viscosity}$ (mPa*s)**
100	550,8	8,6
60	882,8	46,6
50	1031,8	42,4
30	1798,7	25,9
20	2715,5	110,0
10	5510,4	20,5
6	8100,7	2,8
5	9167,0	0,1
4	11018,8	1,6
3	13719,6	29,6
2	18712,0	-
1	33154,0	-

Cycle 1 - Increasing		
RPM	**$\eta_{viscosity}$ (mPa*s)**	**$\sigma_{viscosity}$ (mPa*s)**
1	31113,0	-
2	14592,0	-
3	11872,2	86,5
4	10206,7	11,7
5	8177,0	11,6
6	6730,1	11,1
10	4211,0	125,6
20	2224,7	56,0
30	1553,0	62,5
50	1010,3	33,5
60	815,7	5,2
100	479,4	7,7

Cycle 2 - Decreasing		
RPM	**$\eta_{viscosity}$ (mPa*s)**	**$\sigma_{viscosity}$ (mPa*s)**
100	476,2	5,8
60	813,6	2,4
50	957,4	0,5
30	1579,9	44,9
20	2430,4	101,6
10	4798,4	14,4
6	7189,4	12,2
5	8352,1	0,8
4	10092,6	3,3
3	12572,0	8,2
2	15969,0	-
1	30653,0	-

Cycle 2 - Increasing		
RPM	**$\eta_{viscosity}$ (mPa*s)**	**$\sigma_{viscosity}$ (mPa*s)**
1	40741,0	-
2	17645,0	-
3	11635,8	146,2
4	9968,3	54,5
5	8443,2	9,1
6	7100,4	36,7
10	4489,8	60,7
20	2452,0	78,4
30	1674,1	137,7
50	1028,1	10,7
60	874,9	5,8
100	528,0	2,8

Increasing hydration time induces a slight increase in viscosity, maintaining always the slurry evident shear-thinning and thixotropic behavior. At this stage, bentonite presents high thixotropic behavior with a marked loop, especially in the first cycle, but also a good recovery after stress reduction. This behavior is clearly visible between 5 and 20 rpm, where structures break down faster, respect to the recovery. After 20 rpm, the higher shear destroys the entire structures with the two curves that became superimposed.

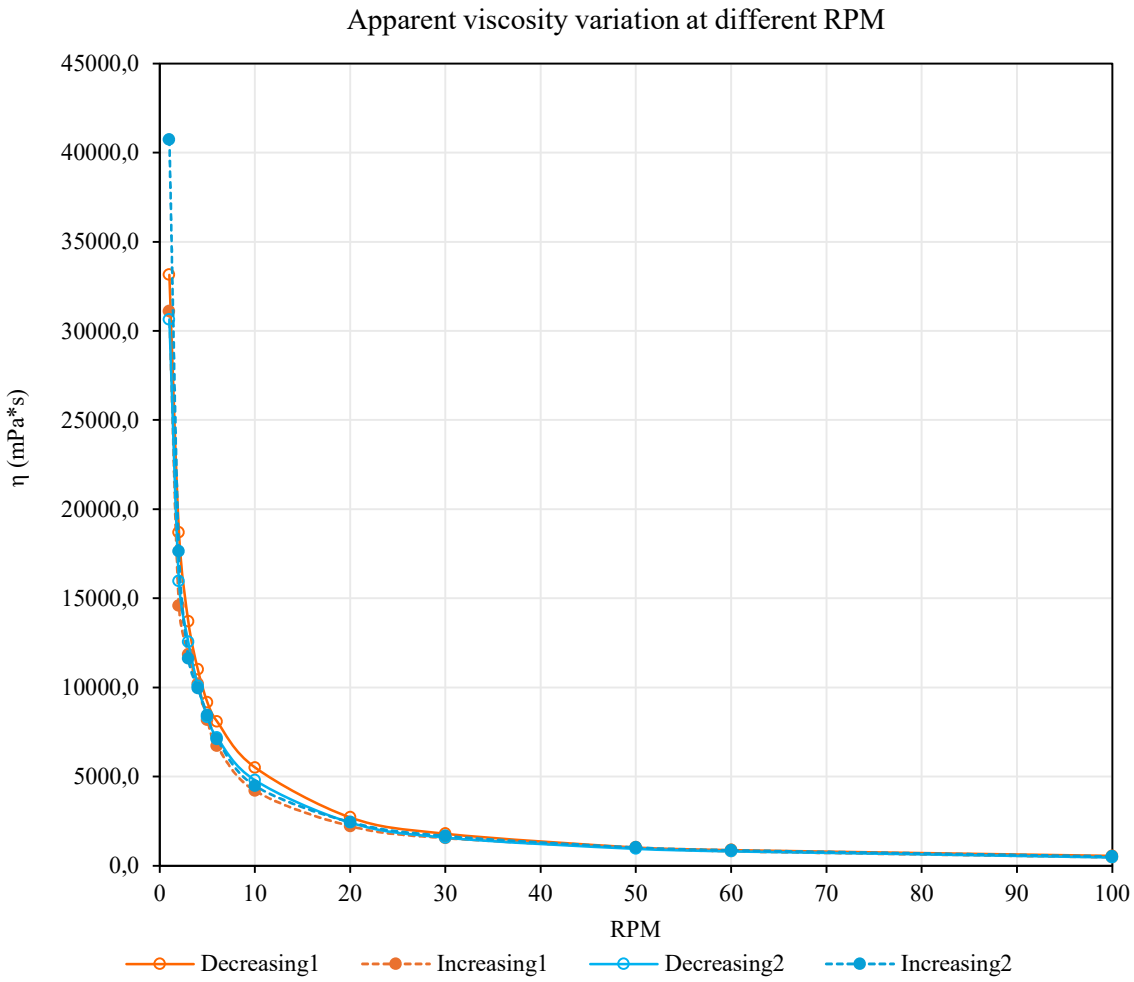

Figure 6.47 - Graphical representation of the viscometer result for bentonite ID7 60 kg/m³ at 1 hour of hydration

Figure 6.47 clearly shows the hysteresis loop of the first cycle is significantly larger than the one of the second cycle. The wider loop of the first cycle represents the behavior of the slurry still in early hydration phase, with a fragile microstructure under mechanical stress. In the second loop the hysteresis cycles became smaller, indicating a partial slurry structure reorganization, after the first breakdown in a more stable configuration. Although the rebuilt structures does not fully recover the original strength, the viscosity increase measured in the second increasing branch, demonstrates a good recovery capacity at lower shear rate.

- **3 hours of hydration,** T = 21,9 C°

Table 6.37 - Viscometer result for bentonite ID7 60 kg/m³ at 3 hours of hydration

Cycle 1 - Decreasing		
RPM	**$\eta_{viscosity}$ (mPa*s)**	**$\sigma_{viscosity}$ (mPa*s)**
100	606,8	1,1
60	987,3	25,2
50	1143,6	34,6
30	2006,6	52,7
20	3078,6	202,2
10	6279,1	73,2
6	8859,0	13,5
5	9705,5	7,4
4	10767,2	259,1
3	14562,6	117,6
2	19679,0	-
1	37652,0	-

Cycle 1 - Increasing		
RPM	**$\eta_{viscosity}$ (mPa*s)**	**$\sigma_{viscosity}$ (mPa*s)**
1	35607,0	-
2	19777,0	-
3	13494,4	204,4
4	11372,6	69,0
5	10163,9	14,3
6	8646,4	25,6
10	5334,2	113,8
20	2838,1	122,0
30	1923,3	107,1
50	1157,1	30,1
60	984,0	13,3
100	587,8	0,6

Cycle 2 - Decreasing		
RPM	**$\eta_{viscosity}$ (mPa*s)**	**$\sigma_{viscosity}$ (mPa*s)**
100	644,9	1,7
60	1056,1	8,5
50	1244,3	0,5
30	2135,0	148,6
20	3179,3	76,8
10	6297,0	14,1
6	9704,3	11,4
5	11237,6	16,3
4	13266,4	0,5
3	16175,4	188,7
2	22564,0	-
1	39088,0	-

Cycle 2 - Increasing		
RPM	**$\eta_{viscosity}$ (mPa*s)**	**$\sigma_{viscosity}$ (mPa*s)**
1	37045,0	-
2	18442,0	-
3	12848,0	221,4
4	10701,2	166,0
5	9487,0	46,8
6	8466,4	5,8
10	5248,1	157,3
20	2922,5	140,7
30	2053,8	109,8
50	1255,4	11,3
60	1064,7	5,9
100	641,7	8,4

Table 6.37 shows moderate increase in viscosity respect to the previous at 1 hour of hydration, with increases approximately of 10%. The shear thinning behavior becomes more evident especially at intermediate rpm. The slurry exhibits only a moderate thixotropy, the hysteresis loop is visible mainly between 20 and 5 rpm. Before and after that interval, the decreasing and increasing curves almost overlapped, indicating limited thixotropy. Different behaviors are observed during the second cycle, where the hysteresis loop became more pronounced with important differences between the increasing and decreasing curves already at higher rpm till low rpm. This result indicates an important thixotropic recovery between the two cycles, with the decreasing curve that in some cases shows higher viscosity respect to the corresponding values of the first cycle. This behavior can be associated with an important structure reorganization after the first breakdown, leading also to a marked susceptibility to mechanical stress.

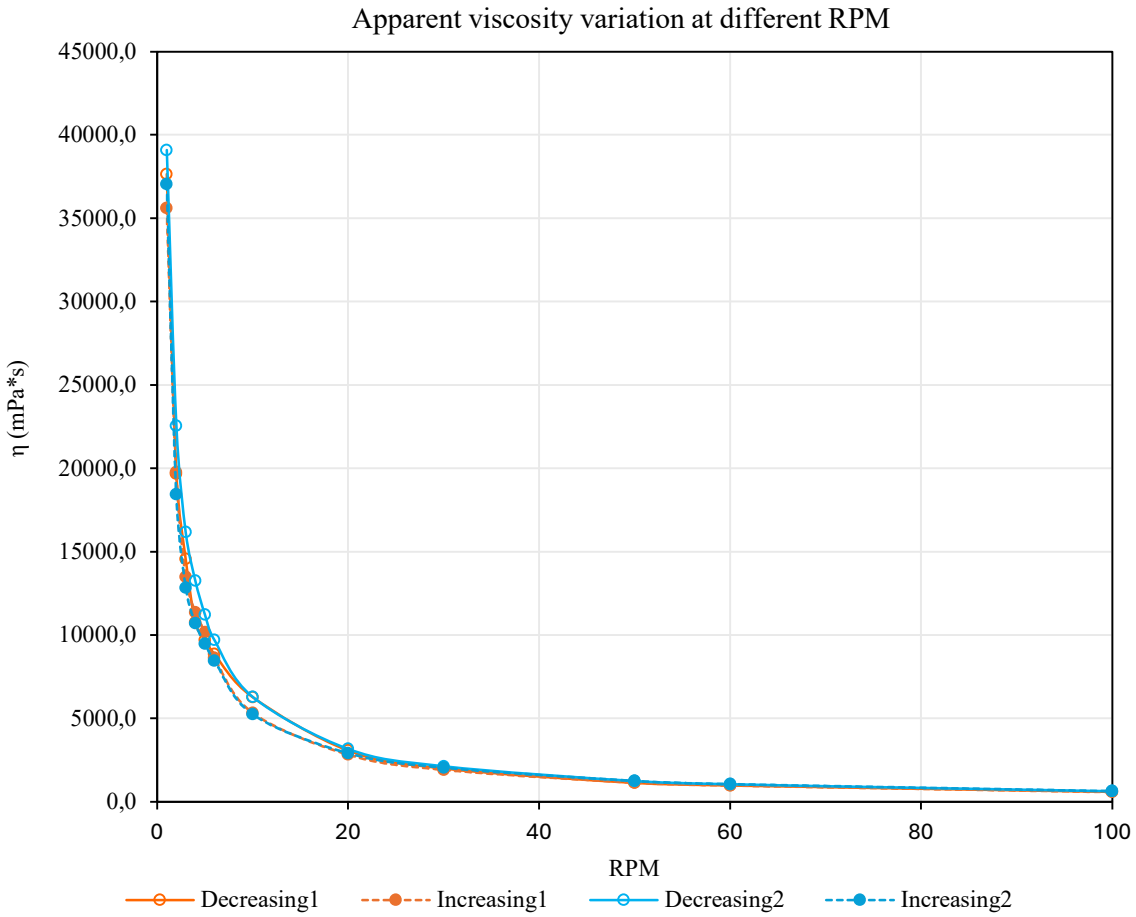

Figure 6.48 - Graphical representation of the viscometer result for bentonite ID7 60 kg/m³ at 3 hours hydration

In figure 6.48 the behavioural evolution between the two cycles is clearly highlighted. Typical behavior of bentonite at early hydration stage, where the first shear causes a collapse of the fragile gel network. While resting period promotes a more compact microstructure.

As consequence larger loop is observed in the second cycles and higher recovery under low stress.

- **4 hours of hydration,** T = 22 C°

Table 6.38 - Viscometer result for bentonite ID7 60 kg/m³ at 4 hours of hydration

Cycle 1 - Decreasing		
RPM	**$\eta_{viscosity}$ (mPa*s)**	**$\sigma_{viscosity}$ (mPa*s)**
100	639,6	1,3
60	1043,8	7,9
50	1207,1	0,7
30	2038,5	49,3
20	3131,3	110,2
10	6326,7	13,3
6	9630,0	0,9
5	10547,1	13,1
4	12693,0	0,0
3	15689,4	23,3
2	21165,0	-
1	41845,0	-

Cycle 1 - Increasing		
RPM	**$\eta_{viscosity}$ (mPa*s)**	**$\sigma_{viscosity}$ (mPa*s)**
1	40452,0	-
2	19493,0	-
3	13289,0	55,9
4	10041,1	136,8
5	9303,3	0,4
6	7978,9	13,5
10	4790,4	95,3
20	2554,1	93,7
30	1754,9	14,4
50	1092,6	7,6
60	930,2	3,2
100	574,7	0,1

Cycle 2 - Decreasing		
RPM	**$\eta_{viscosity}$ (mPa*s)**	**$\sigma_{viscosity}$ (mPa*s)**
100	519,6	6,5
60	908,5	0,4
50	1105,3	43,3
30	1803,3	23,0
20	2720,1	153,6
10	5326,2	7,5
6	7919,1	92,3
5	9169,3	6,9
4	10866,8	9,3
3	13530,6	61,7
2	19161,0	-
1	32540,0	-

Cycle 2 - Increasing		
RPM	**$\eta_{viscosity}$ (mPa*s)**	**$\sigma_{viscosity}$ (mPa*s)**
1	30035,0	-
2	14905,0	-
3	10716,0	252,7
4	9769,8	71,0
5	8336,2	10,2
6	7142,8	0,8
10	4437,2	44,5
20	2403,6	19,2
30	1684,9	2,0
50	1030,9	10,2
60	862,6	7,6
100	516,9	0,1

Table 6.38 shows a marked shear thinning behavior, with an important viscosity decrease as the shear rate increases. No huge increases in viscosity are visible with respect to the previous hydration phase, indicating a reduction in hydration capacity.

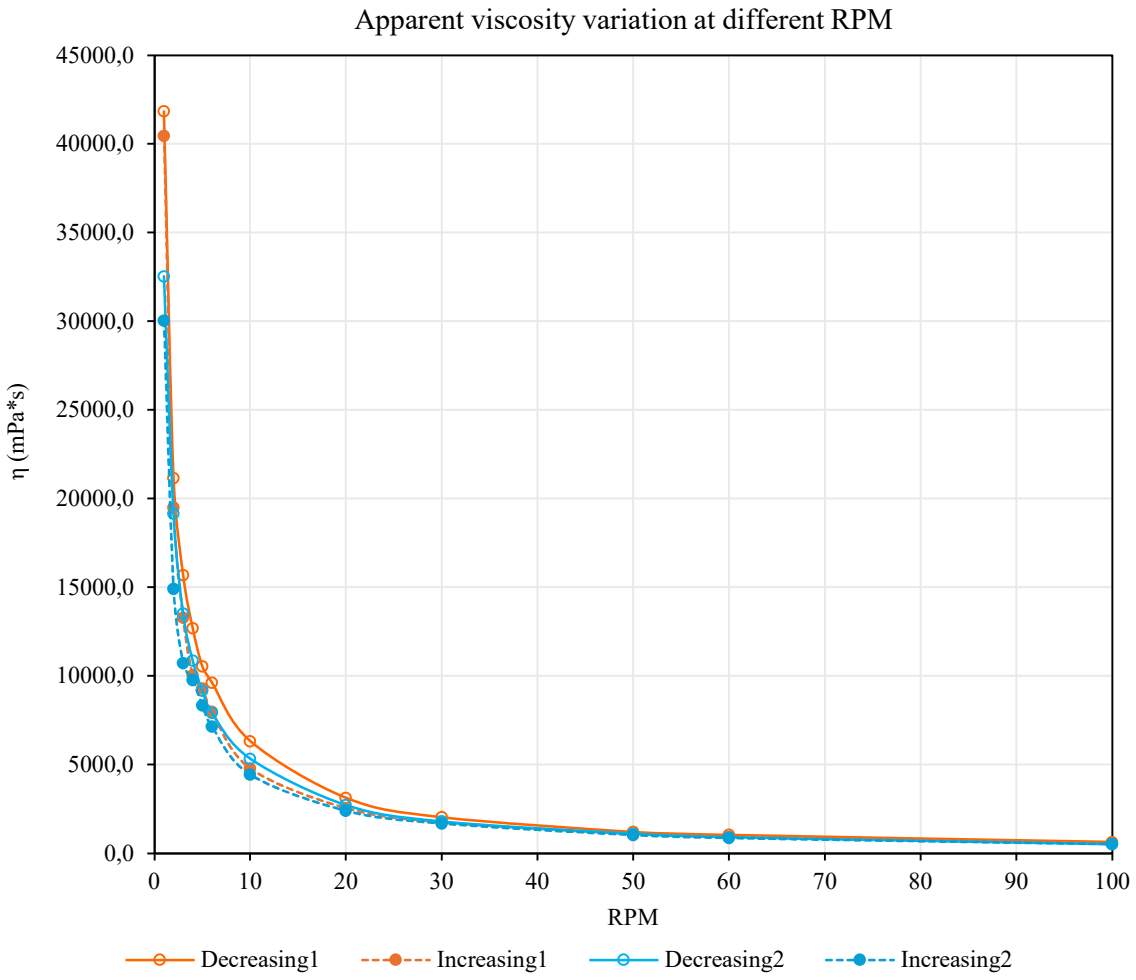

Figure 6.49 - Graphical representation of the viscometer result for bentonite ID7 60 kg/m³ at 4 hours hydration

The thixotropic behavior comeback evident at this hydration stage. The curve highlights large loops dimensions in both cycles. The different behavior between the increasing and decreasing curve became already visible at 60 rpm, indicating that during the decreasing curve the microstructure is not completely disrupted, while during the increasing branch, the slurry starts from a more degraded configuration and is not able to fully rebuild its structures, leading to a wider hysteresis area. This behavior becomes cleaner during the second cycle, where the decreasing curve shows lower viscosity compared to the first cycle, and even at low shear is not able to completely recover the original structures. The increasing branches lie consistently under the one of the first cycle, confirming that an additional breakdown occurred and small thixotropic recovery at low shear rate.

- **24 hours of hydration,** T = 20,6 C°

Table 6.39 - Viscometer result for bentonite ID7 60 kg/m³ at 24 hours of hydration

Cycle 1 - Decreasing		
RPM	**$\eta_{viscosity}$ (mPa*s)**	**$\sigma_{viscosity}$ (mPa*s)**
100	923,9	17,5
60	1181,5	10,5
50	1414,8	1,5
30	2323,4	37,0
20	3540,9	55,6
10	6736,4	4,9
6	10223,4	1,7
5	11634,7	1,3
4	14174,0	0,0
3	17232,0	11,2
2	24350,0	-
1	45610,0	-

Cycle 1 - Increasing		
RPM	**$\eta_{viscosity}$ (mPa*s)**	**$\sigma_{viscosity}$ (mPa*s)**
1	41968,0	-
2	20406,0	-
3	13384,2	86,5
4	10495,4	99,1
5	9351,3	58,1
6	8668,8	0,7
10	5345,7	33,9
20	2955,2	24,7
30	2025,2	2,0
50	1252,3	26,4
60	1041,7	0,3
100	687,1	6,8

Cycle 2 - Decreasing		
RPM	**$\eta_{viscosity}$ (mPa*s)**	**$\sigma_{viscosity}$ (mPa*s)**
100	669,2	0,8
60	1117,5	6,4
50	1338,0	40,8
30	2139,8	20,7
20	3152,5	302,1
10	5958,5	23,8
6	8817,9	9,2
5	9960,3	3,4
4	11559,4	6,0
3	14590,8	23,0
2	19509,0	-
1	36126,0	-

Cycle 2 - Increasing		
RPM	**$\eta_{viscosity}$ (mPa*s)**	**$\sigma_{viscosity}$ (mPa*s)**
1	32518,0	-
2	14859,0	-
3	10601,4	225,1
4	9494,1	163,7
5	8538,8	12,0
6	7242,7	14,2
10	4727,8	13,2
20	2683,8	24,7
30	1888,6	9,5
50	1160,8	10,1
60	989,2	0,9
100	613,9	0,1

At this hydration stage after 24 hours the hydration effect became more evident. Result shows viscosity increment of approximately 10-12%, respect to the previous hydration

phase. The shear-thinning behavior is underlined by the high viscosity variation at different rates, ranging between 700 mPa*s at 100 rpm to 40000 mPa*s at lower rpm.

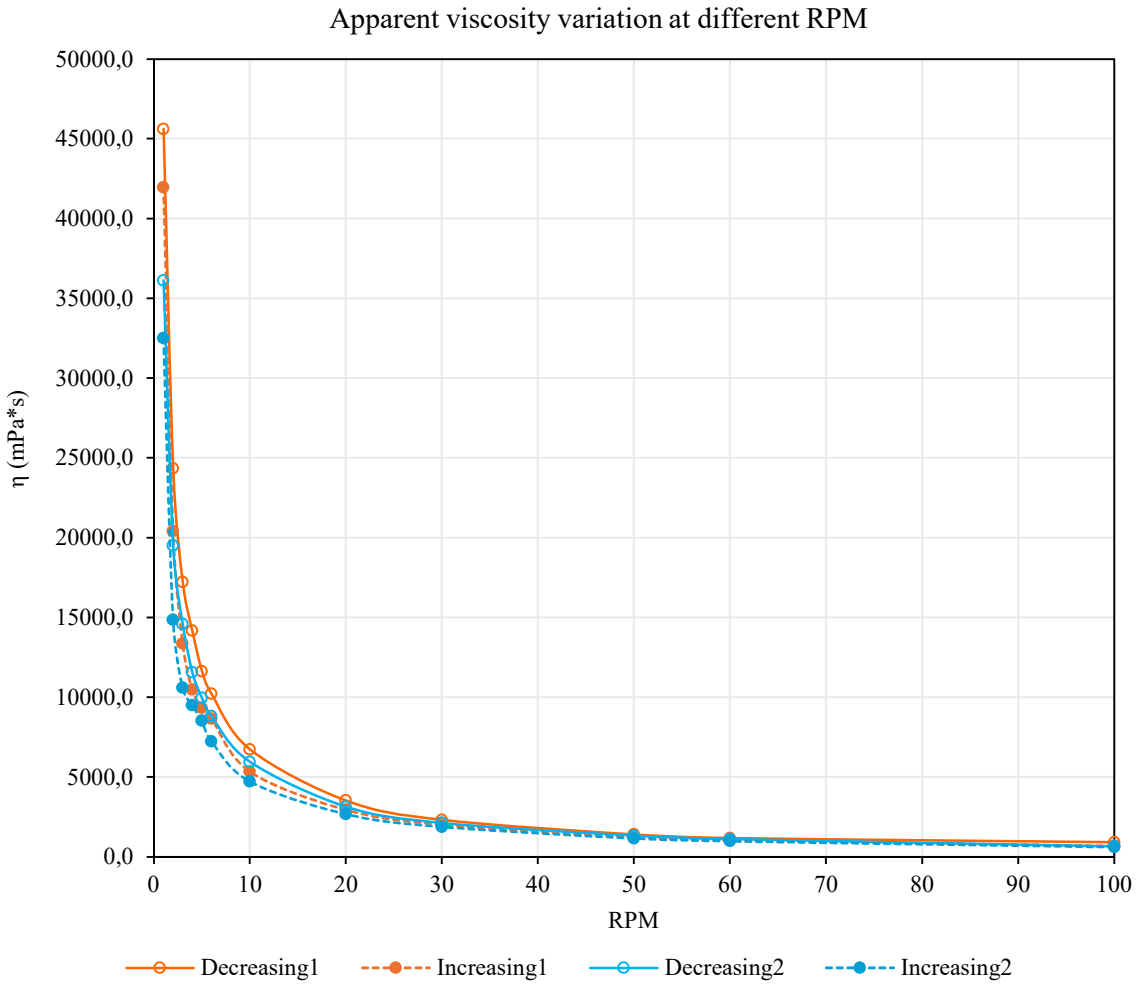

Figure 6.50 - Graphical representation of the viscometer result for bentonite ID7 60 kg/m³ at 24 hours hydration

Figure 6.50 shows a pronounced thixotropic behavior along the whole range of applied rpm, with clear differences between increasing and decreasing curves even at higher rpm. The decreasing curve of the first cycle is considerably above all the others, indicating that the following measurement starts from a more degraded structure, which results in additional viscosity loss. In both cycles, the increasing curve shows lower viscosity value with respect the decreasing one, producing large hysteresis loop. This behavior is likely due to the high degree of hydration reached at 4 hours, that creates a structure very sensitive to mechanical degradation. The decreasing curve of the second cycle lies always under the one of the first cycle, confirming a lower structure recovery at small rpm and that the initial colloidal net has lost its rigidity, becoming even more fragile. The second cycle increasing curve lies below the others, even at 100 rpm, highlighting the decreasing rebuilding capacity after the

first cycle symptoms of an additional quantity of internal bonds destroyed and not efficient structure reorganization at lower shear rate.

6.2.3 Bentonite ID7 - 80 kg/m^3

The following table presents the viscosity measurement for bentonite ID7 at a concentration of 80 kg/m^3. To observe the complete rheological evolution at different concentrations, tests were performed also on slurry with bentonite concentration of 80 kg/m^3. The problem arises, as highlighted during the Marsh cone measurement for slurry at 70 kg/m^3, from the large viscosity value reached almost immediately after preparation. The viscometer is not able to evaluate accurately viscosity value of that intensity.

Spindle L4, for high viscosity, was used, with torque percentage ranging between 9-30%, during the first hydration hour and even lower values at longer hydration hours. Due to the high viscosity, especially at 24 h, the torque percentage reduces to under 15% indicating low accuracy measurement, mainly at lower rpm. For this reason, the slurry was tested only on 0, 1, and 24 hours hydration, although the measured values were not highly accurate. These tests were nevertheless performed to obtain an indicative assessment of the slurry behavior under those conditions.

- **0 hours of hydration,** T = 23,3 C°

Table 6.40 - Viscometer result for bentonite ID7 80 kg/m³ after preparation

Cycle 1 - Decreasing		
RPM	**$\eta_{viscosity}$ (mPa*s)**	**$\sigma_{viscosity}$ (mPa*s)**
100	1841,9	103,5
60	3033,2	68,1
50	3480,7	87,3
30	6862,2	105,4
20	8828,7	594,0
10	17236,7	292,7
6	18443,6	93,1
5	21710,9	68,4
4	26175,6	137,5
3	29712,4	296,3
2	33674,0	-
1	56449,0	-

Cycle 1 - Increasing		
RPM	**$\eta_{viscosity}$ (mPa*s)**	**$\sigma_{viscosity}$ (mPa*s)**
1	69005,0	-
2	28619,5	-
3	22722,4	492,8
4	18381,4	162,1
5	16215,3	333,7
6	16656,1	189,1
10	11546,6	559,1
20	7411,7	193,6
30	5636,0	33,6
50	3392,5	94,7
60	2967,8	7,2
100	1818,7	142,1

Cycle 2 - Decreasing		
RPM	**$\eta_{viscosity}$ (mPa*s)**	**$\sigma_{viscosity}$ (mPa*s)**
100	1837,3	118,1
60	3108,0	62,3
50	3565,7	178,5
30	5854,7	173,4
20	8515,2	54,9
10	13761,4	542,9
6	17640,6	244,6
5	18920,3	1588,6
4	18917,2	220,7
3	33498,0	76,7
2	36069,0	-
1	65388,0	-

Cycle 2 - Increasing		
RPM	**$\eta_{viscosity}$ (mPa*s)**	**$\sigma_{viscosity}$ (mPa*s)**
1	58521,0	-
2	25475,0	-
3	22725,6	211,5
4	19229,8	135,3
5	17571,3	188,2
6	16719,0	23,6
10	11200,9	283,7
20	7360,2	103,5
30	5408,8	216,4
50	3456,3	275,7
60	3107,2	130,7
100	1921,3	8,3

Table 6.40 clearly shows the huge value of viscosity reached rapidly after preparation, remarkably higher respect to the previous concentrations. Now viscosity ranges from 2000 mPa*s to 65000 mPa*s, underlining much more the shear thinning behavior both at low and high shear rate.

At lower rpm the viscosity reaches enormous values, a sign of a highly concentrated suspension where the gel structure is forming, but not yet stable. The standard deviations are very high, signs of a continuous structure transformation during measurement, where both building construction and breakdown due to share stress, happen simultaneously

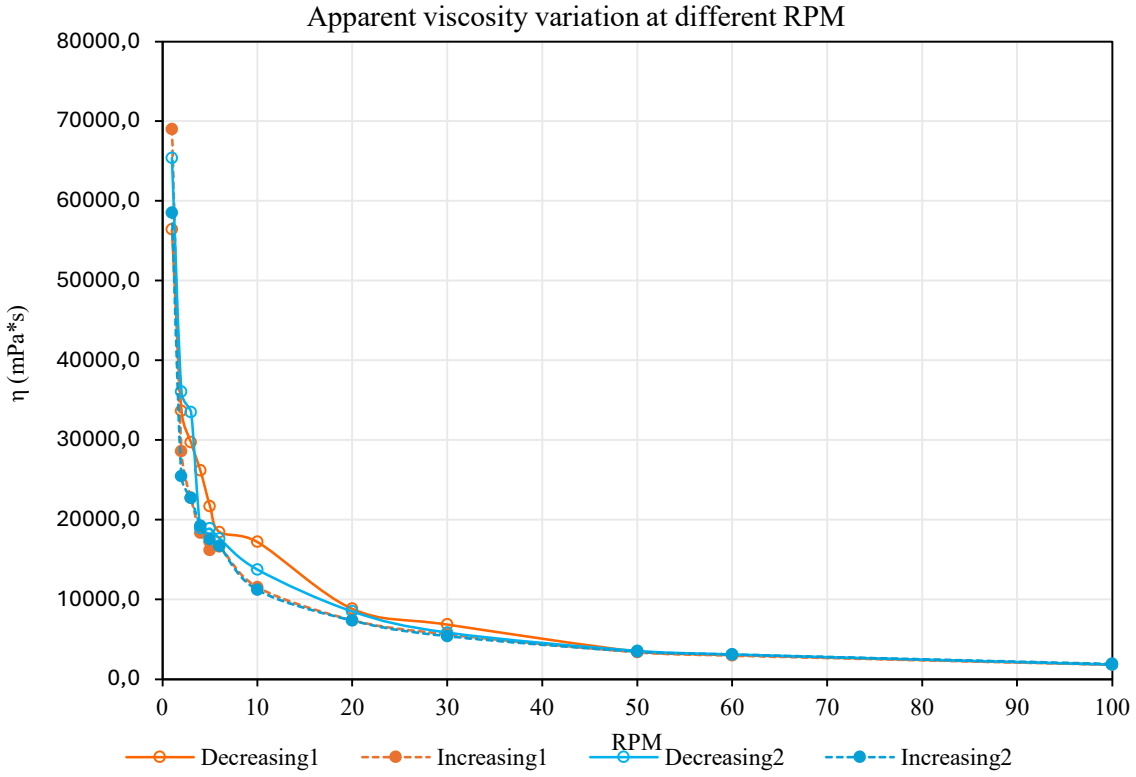

Figure 6.51 - Graphical representation of the viscometer result for bentonite ID7 80 kg/m³ after preparation

The thixotropic behavior of bentonite is clearly shown in figure 6.51, from the presence of two distinguishable hysteresis loops. The first loop is wide, showing the decreasing curve above the increasing one especially at 20 to 5 rpm, indicating an important structural breakdown and lower recovery at small shear rate. This behavior indicates a fragile structure that is partially broken during the first decrease, with a low recovery also due to a small hydration. The second cycle again underlines the previous behavior, with additional viscosity loss both during the decreasing phase and the increasing one. The hysteresis loop became smaller, not due to a lower thixotropy but due to the highly degraded structure. Some bounces or deviation from the expected path are evident in the graph, likely due to the

destruction of big, flocculated structure, or cluster of slurry, resulting in immediate viscosity variation. This phenomenon happens primarily at lower shear under 50 rpm.

- **1 hour of hydration,** T = 23 C°

Table 6.41 - Viscometer result for bentonite ID7 80 kg/m³ at 1 hour of hydration

Cycle 1 - Decreasing		
RPM	**$\eta_{viscosity}$ (mPa*s)**	**$\sigma_{viscosity}$ (mPa*s)**
100	2244,7	21,8
60	3459,2	33,0
50	4056,8	189,2
30	6683,8	328,0
20	9907,5	246,5
10	18136,2	134,2
6	20216,3	298,7
5	23430,9	107,7
4	25024,6	100,8
3	29912,2	72,0
2	43093,0	-
1	74410,0	-

Cycle 1 - Increasing		
RPM	**$\eta_{viscosity}$ (mPa*s)**	**$\sigma_{viscosity}$ (mPa*s)**
1	74333,0	-
2	31920,0	-
3	17750,6	126,6
4	17939,0	260,2
5	23531,1	189,2
6	18286,6	5,0
10	13436,8	756,6
20	9861,2	143,0
30	6592,0	97,5
50	4052,5	97,8
60	3456,2	26,0
100	2307,0	246,4

Cycle 2 - Decreasing		
RPM	**$\eta_{viscosity}$ (mPa*s)**	**$\sigma_{viscosity}$ (mPa*s)**
100	2231,3	68,7
60	3138,4	1054,9
50	4001,8	48,1
30	6561,1	71,1
20	9611,3	23,3
10	15618,1	631,4
6	21287,6	149,5
5	23225,6	102,1
4	27204,2	40,0
3	37110,0	71,6
2	45502,0	-
1	79293,0	-

Cycle 2 - Increasing		
RPM	**$\eta_{viscosity}$ (mPa*s)**	**$\sigma_{viscosity}$ (mPa*s)**
1	72836,0	-
2	31963,0	-
3	19545,4	258,0
4	14674,4	531,8
5	14956,3	624,6
6	16170,7	245,5
10	12133,2	509,2
20	8371,7	208,0
30	6019,6	174,9
50	3781,3	46,8
60	3290,2	38,7
100	2110,6	197,9

At 1 hour of hydration the viscosity increase is significant, with the doubling of all values respect to the previous hydration stage, in particular at low rpm, sign of a dense gel network. The shear-thinning behavior is evident with a rapid decrease of viscosity within the 1-10 rpm range, while more regular at higher speed, typical behavior of very dense suspension.

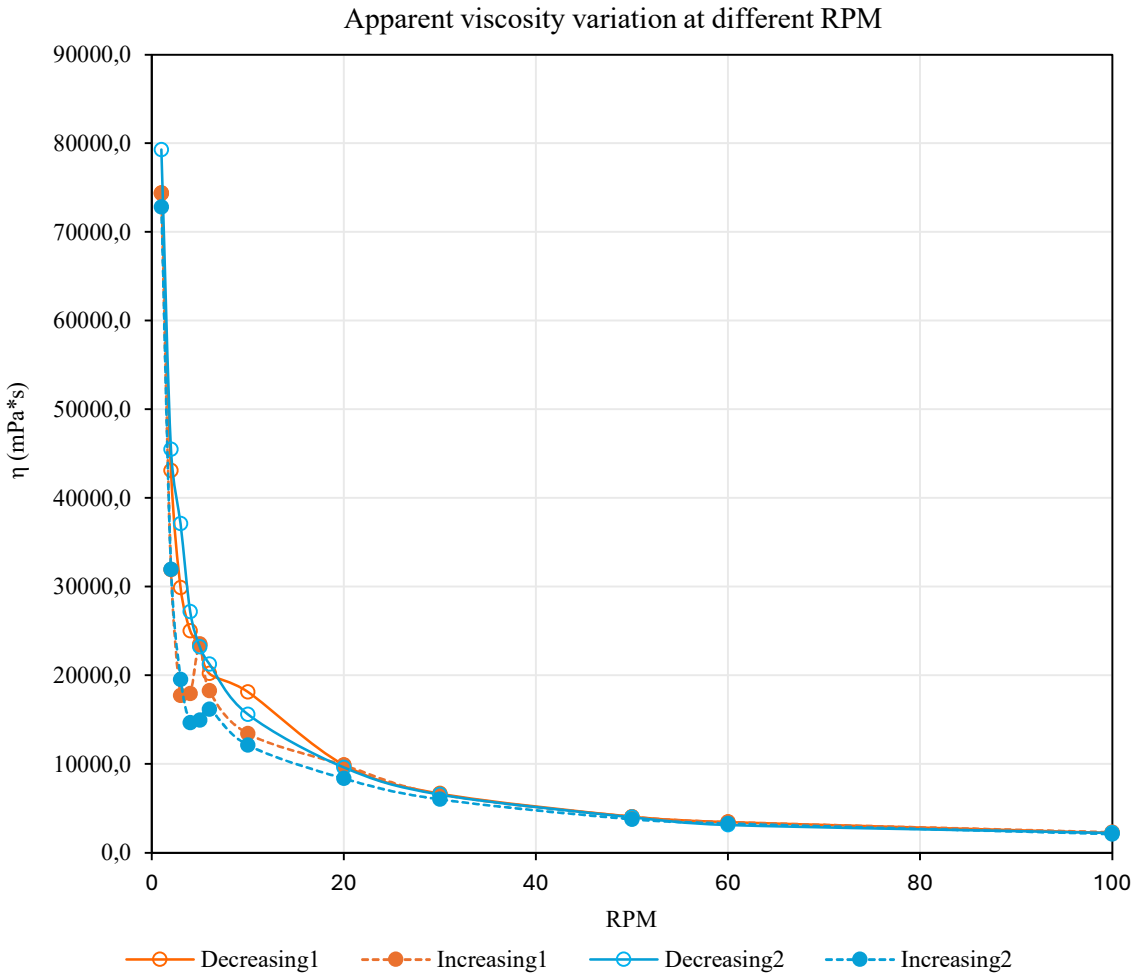

Figure 6.52 - Graphical representation of the viscometer result for bentonite ID7 80 kg/m³ at 1 hour of hydration

Figure 6.52 clearly shows the moderate thixotropic behavior of slurry, displaying marked differences between the first cycle's increasing and decreasing curves starting at about 20 rpm. At higher shear rates, values are almost comparable, indicating an important rupture of the structure and the absence of measurable thixotropy. The second cycle hysteresis loop is wider, although both decreasing curves are almost superimposed. This behavior suggests the ability to rebuild part of its structure at lower shear. Nevertheless, the second increasing curve lies far below the first one, underlining that the structure rebuilt was mainly due to the development of weak bonds between particles, more fragile under mechanical stress.

The graph highlights also a particular behavior between 5-6 rpm, already observed in the previous hydration stage, regarding a rapid decrease in both the increasing curve. This

phenomenon likely corresponds to the sudden rupture of small or large floccules within the bentonite structure, leading to an important and immediate decrease in viscosity. After those points at lower shear, the microstructure tends to rebuild again the flocculated structure, rising the viscosity. This behavior is usual for very concentrated slurry, where the large number of bentonite particles and their face-to-edge interaction generate a highly dense flocculated three-dimensional network, that is subjected to possible collapse.
As highlighted in the graph this phenomenon contributes to enlarging the hysteresis loop, especially at lower shear rates.

- **24 hours of hydration,** T = 20,4 C

Table 6.42 - Viscometer result for bentonite ID7 80 kg/m^3 at 24 hours of hydration

Cycle 1 - Decreasing		
RPM	**$\eta_{viscosity}$ (mPa*s)**	**$\sigma_{viscosity}$ (mPa*s)**
100	2133,0	12,8
50	3064,3	173,0
20	4697,1	273,7
6	7279,3	1275,8
4	6199,1	8,9
1	21471,0	-

Cycle 1 - Increasing		
RPM	**$\eta_{viscosity}$ (mPa*s)**	**$\sigma_{viscosity}$ (mPa*s)**
1	17095,0	-
4	6022,6	463,3
6	7321,9	716,4
20	4145,2	237,4
50	2683,4	5,5
100	1976,3	30,3

After 24 hours the hydration rise up the viscosity to very high level, making it difficult to measure with the viscometer, even with the spindle suitable for larger viscosity. For this reason, a fast evaluation of viscosity was caried out, only at low rpm stages and performing one cycle.
Although the results are not so reliable, due to low value of the torque percentage between 3 to 30%, the value gives important indication on the rheological behavior of slurry also at this hydration stage and high concentration.
The shear thinning behavior is still very marked especially under 20 rpm, where the viscosity variation reaches high value. At higher shear rate the variation is smoother.

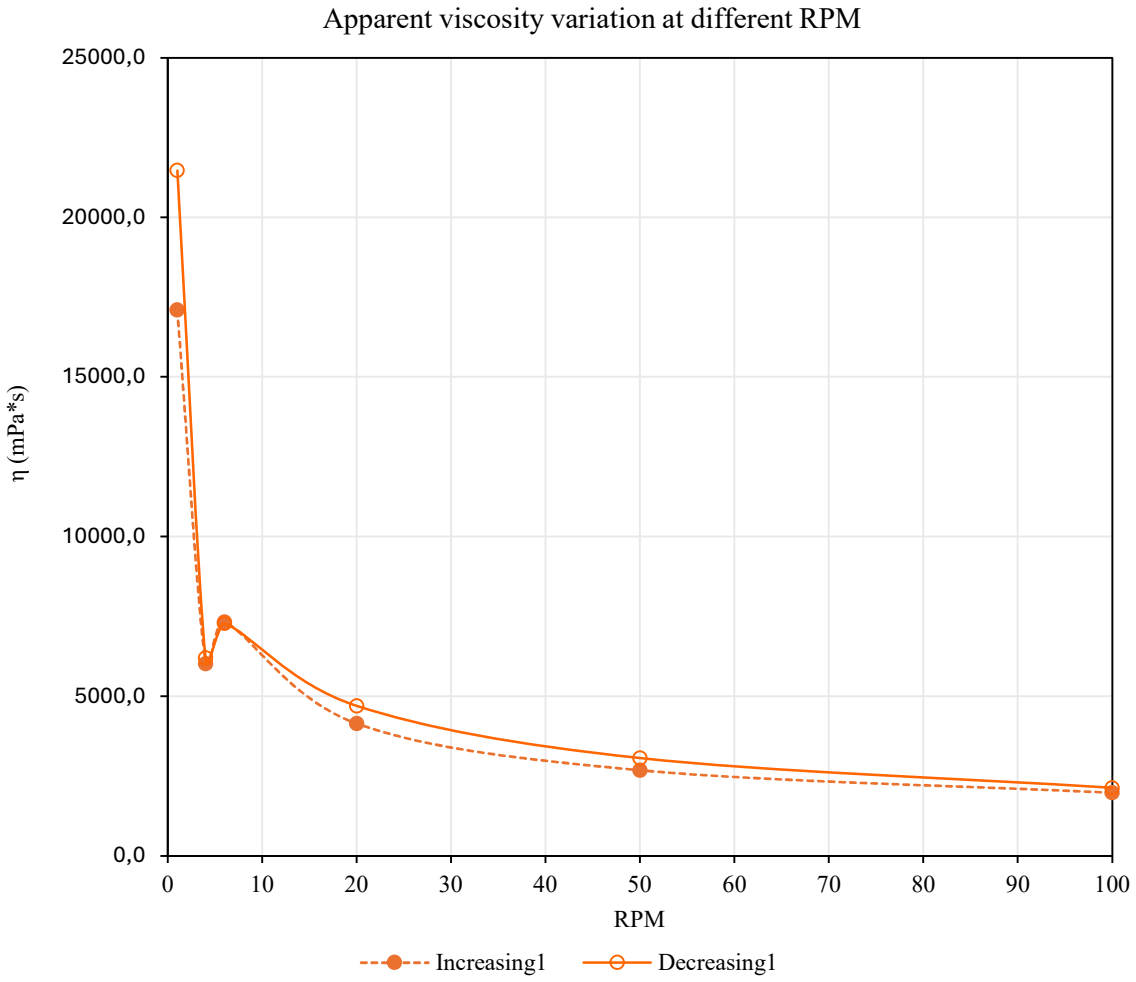

Figure 6.53 - Graphical representation of the viscometer result for bentonite ID7 80 kg/m³ at 24 hours hydration

Figure 6.53 shows very limited thixotropic behavior, underlined by the small hysteresis loop, symptoms of a more stable and fully hydrated microstructure, which undergoes a uniform breakdown under shear and minimal rebuilding at lower shear rate. At 6 rpm again, an abrupt collapse of some big, flocculated structure can be observed, in both increasing and decreasing branches, leading to a marked loss of viscosity.

6.3 Filter cake quality

The tests on the filter cake formation and quality were conducted using slurry prepared with bentonite ID7, studying the behavior variation of three different slurry bentonite concentrations: 45 kg/m^3, 60 kg/m^3 and 80 kg/m^3.

During the test it was evaluated the slurry interaction with two soils composed mainly of two particles granulometries as presented in table 6.43:

Table 6.43 - Grain-size compositions adopted to prepare synthetic soils for filter-cake tests

Terrain type	1 mm	0,5 mm	0,25 mm
T1	50%	50%	0%
T2	0%	50%	50%

6.3.1 Bentonite ID7 - 45 kg/m^3

The rotational viscometer at this concentration revealed very low viscosity value and limited hydration capacity due to the low number of particle bonds that composed its structure. This tests were therefore important to evaluate how the slurry's rheological properties influence the formation and quality of the filter cake.

Table 6.44 - Filter cake tests results ID7 45 kg/m^3

Terrain type	Filter cake formation	Thickness (mm)
T1	NO	-
T2	NO	-

During the test performed using bentonite slurry with a concentration of 45 kg/m^3, on both terrain types, no filter cake was developed, neither surface nor inner.

Once the manometer valve was opened and the pressure was transferred to the slurry inside the specimen cells, the whole slurry immediately penetrated through the soil. At the end of the 10 minutes test, opening the bottom valves, slurry rapidly flowed out of the cell, and no cake deposition was visible (figure 6.54).

Soil T1 is a coarse soil, comparable to very coarse sand, characterized by large pore spaces and high hydraulic conductivity. Both the high viscosity of the slurry and the soil characteristics hindered the filter cale formation

The same behavior occurred with Soil T2. Although T2 has a smaller grain size and lower porosity, slurry still penetrated the terrain without forming any filter cake. This result

indicates that, regardless of the soil characteristics, the slurry viscosity is the dominant factor governing the filter cake development.

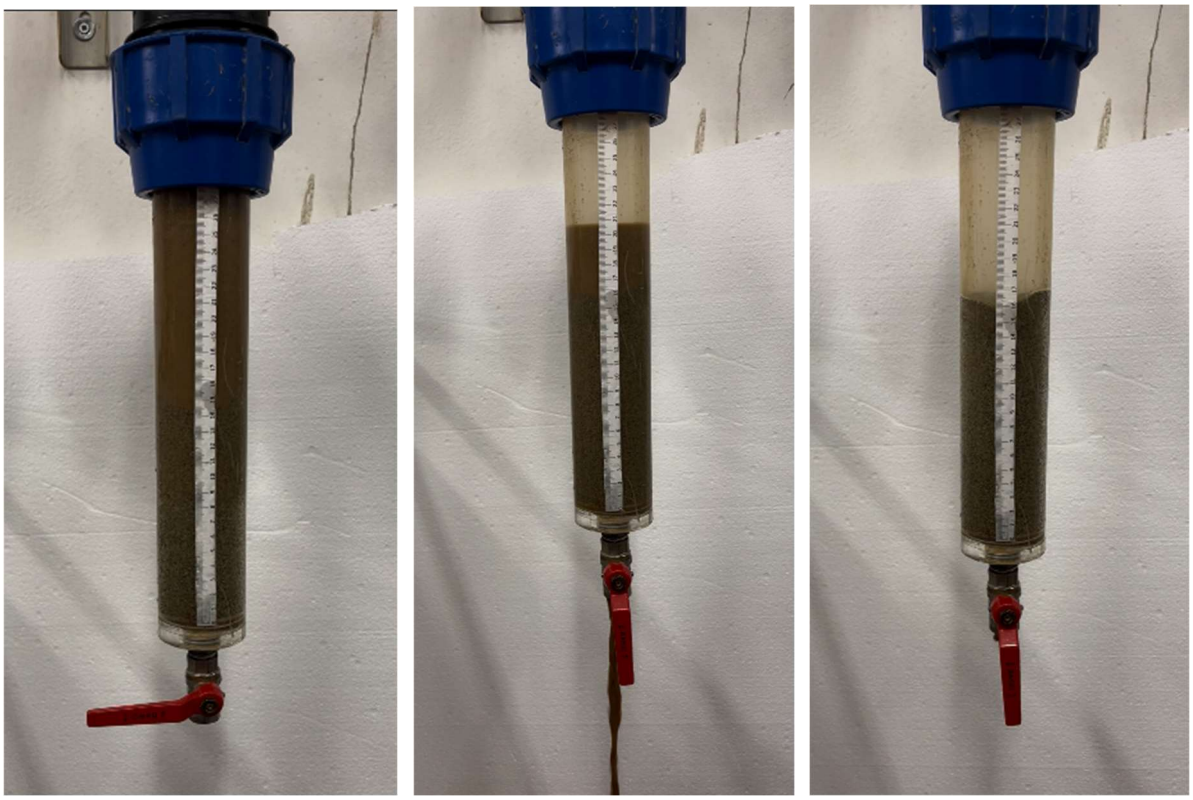

Figure 6.54 - Bentonite ID7, filter cake test

6.3.2 Bentonite ID7 - 60 kg/m^3

Increasing bentonite concentration leads to increased viscosity, as confirmed by both the Marsh cone result and viscometer measurements. At 60 kg/m^3 slurry starts to develop the typical behavior bentonite, hydration becomes more effective, and the particle's structure starts to become well dispersed three-dimensional network.

The results of the filter cake tests obtained at this concentration are summarized below:

Table 6.45 - Filter cake tests results ID7 60 kg/m^3

Terrain type	Filter cake formation	Thickness (mm)
T1	NO	-
T2	YES	1,4
	YES	1,4

The result in table 6.45 underlines that, despite bentonite rheology, the soil characteristic plays an important role in filter cake formation. For soil T1 also at this concentration, no

filter cake developed, confirming that pore size enhances slurry infiltration without particle deposition.

For soil T2, which is the more compact, a thin filter cake was developed. Two tests were carried out with the same soil T2, and same concentration produced the same cake thickness. This result confirms that at this concentration Bentonite ID7 demonstrates a good hydration capacity and swell, forming a colloidal network that is able to seal the terrain pore.

Figure 6.55 - ID7 60 kg/m³ filter cake

Figure 6.56 - ID7 60 kg/m³ filter cake and slurry penetration

Figure 6.56 shows the filter cake clearly visible together with the penetration depth, approximately 9 cm, recognizable by the colour difference between the saturated terrain with slurry and the unsaturated zone. Figures 6.55 and 6.57 show the extracted terrain sample with the filter cake clearly visible on the surface, appearing as a thin gelatinous layer that effectively inhibits water passage. The filter cake thickness was then measured using a ruler and a calliper.

Figure 6.57 - ID7 60 kg/m³ filter cake open and measured

6.3.3 Bentonite ID7 - 80 kg/m^3

The Marsh cone test result already underlines a rapid hydration capacity for bentonite ID7, leading to extremely high viscosity value. At this concentration, the viscosity is particularly elevated because the slurry structures start to become more flocculated due to the greater number of particle interactions that tend to compact the three-dimensional network.
The results of the filter cake test obtained at this concentration are the following:

Table 6.46 - Filter cake tests results ID7 80 kg/m^3

Terrain type	Filter cake formation	Thickness (mm)
T1	NO	-
T2	YES	4
	YES	2

The result in table 6.46 again demonstrates that terrain characteristic plays a key role in the correct filter cake formation, in fact for terrain T1 also at this concentration no filter cake developed. For terrain T2 instead, a good quality filter cake developed, with a medium thickness of 3 mm. This result indicates that higher concentration leading to greater viscosity and gel consistency helps develop a better and more resistant filter cake.

Figure 6.58 - ID7 80 kg/m^3 filter cake

Figure 6.59 - ID7 80 kg/m^3 filter cake and slurry penetration

Figure 6.59 highlights the filter cake clearly visible after cleaning the specimen cells together with the limited slurry penetration. Figures 6.60 and 6.61 show the extracted sample of terrain with the filter cake on the surface, appearing thicker and gelatinous with respect to the one at lower concentration that presents as a thin gel layer that inhibit the water pass. The thickness was then measured using a meter and a calliper.

Figure 6.60 - ID7 80 kg/m³ filter cake opened and measured

Figure 6.61 - ID7 80 kg/m³ caliper measurement of filter cake thickness

7 Conclusion

The eight bentonite slurries showed, as expected, the typical behavior of a non-Newtonian fluid, and in particular, follow very well the Herschel-Bulkley model. All the ID slurries present an increase in Marsh viscosity value with hydration time, showing higher rate in the first 4 hours and slower increase at longer hydration periods. The growth continues until reaching a stabilization point where the microstructure is almost fully developed and viscosity stabilized or in some cases, as for ID1, ID2, ID3 and ID8, slightly decreases, likely due to particle reorganization once full hydration is achieved (figure 7.1).

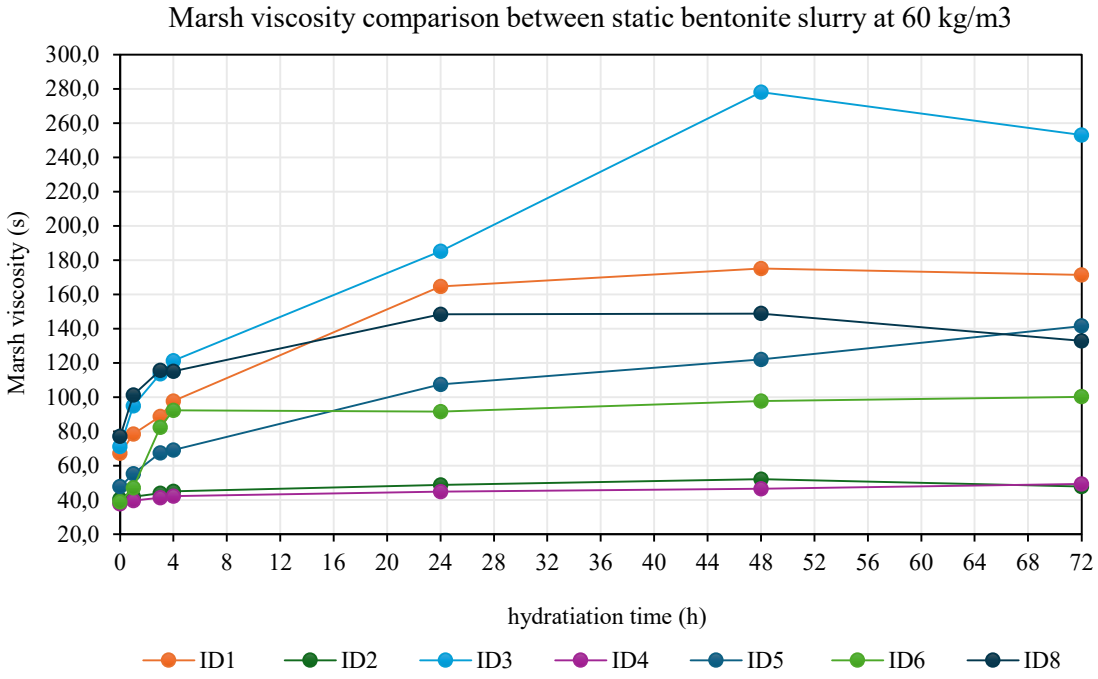

Figure 7.1 - Static marsh viscosity comparison between bentonite slurry at a concentration of 60 kg/m³

The distinct initial viscosity value highlights clear differences in hydration capacity, particle dispersion and microstructure development among the different bentonites, although their identical concentration.

The magnitude of viscosity value reached during hydration significantly varies between different bentonites, and no single index property can fully explain such variability.

Bentonite ID2 and ID4 reach very small Marsh viscosity values between 30 to 50 s. For bentonite ID4, this behavior is coherent with its relatively low swell index and lower expected montmorillonite content, which limit hydration and diffuse double layer expansion. However, bentonite ID2 represents an exception, despite having the highest swell index among the 8 bentonites, implying higher montmorillonite content and abundant sodium

cation, it develops very low viscosity value. This unexpected behavior suggests that viscosity is not only governed by swelling potential or hydration time, but mainly by the type of particle network formed during hydration.

Bentonite ID2, likely due to the high swelling potential and high montmorillonite content, developed an over dispersed structure characterized by an excessively expanded diffuse double layer and strong electrostatic repulsion between bentonite particles. In this condition particles remain too far apart, resulting in low viscosity.

Conversely, bentonite ID4 marsh seems to form a highly flocculated network, developed immediately after preparation, where the face-to-face interconnection between particles inhibits the hydration and prevents the development of a more dispersed and viscous structure.

At higher viscosity value lies all the other bentonites which developed more balanced microstructure. Their hydration capacity, swell index and mineralogic composition allow the formation of a more efficient particles network resulting in significantly higher viscosity value.

Bentonite ID3 develops the highest Marsh viscosity value among the whole tested bentonites at 60 kg/m^3, indicating an important hydration capacity, an optimal degree of dispersion and expansion of the diffuse double layer, sufficiently to support the formation of a strong and highly developed three-dimensional colloidal structure.

Overall, these results demonstrate that the key factors influencing bentonite viscosity are

- The microstructural arrangement developed during hydration
- The swell index and hydration potential
- The presence of divalent cations

Excessive flocculated structure (ID4, ID6) or excessive structure dispersion (ID2) both lead to low viscosity. Bentonite with moderate flocculation, good hydration capacity and ability to build an extended three-dimensional network (ID1, ID3, ID5, ID8), developing higher viscosity and most desirable rheological behavior for tunnelling applications.

Concentration influence

The result of the test performed on bentonite slurry at different concentrations underlines that bentonite concentration in the slurry is a significantly influential parameter for its rheological properties.

For all the bentonite tested at multiple concentrations (ID4, ID6, ID7), increasing concentration leads to higher viscosity and greater resistance to mechanical degradation, likely due to the larger number of particle-particle interactions that form the microstructure, which becomes progressively more difficult to fully breakdown under mechanical stress. A higher initial viscosity corresponds to a higher post stress viscosity plateau, resulting in more stable and effective viscosity values for engineering applications.

Mechanical degradation

Under mechanical stress, all eight bentonites demonstrate the characteristic thixotropic and shear-thinning behavior of non-Newtonian fluid and colloidal suspension. After the first 5 minutes of mechanical stress, all the slurries suffered significant degradation, with evident viscosity drop, at every hydration stage. As the stress duration increases, the viscosity loss remains nearly constant for all bentonites at all hydration times. This underlines a first important result, the duration of mechanical stress has a negligible influence on the additional viscosity decrease, confirming that most of the breakdown occurs within the first minutes of shear.

The influence of hydration time on mechanical degradation also appears limited. Figure 7.2 clearly shows that, at each hydration stage, the mean viscosity value after the mechanical stress remains almost constant for each bentonite. Only limited variations are observed, due to additional breakdown, lower rebuilding capacity, or in some cases, even slight increase due to particles reorganization and progressive hydration.

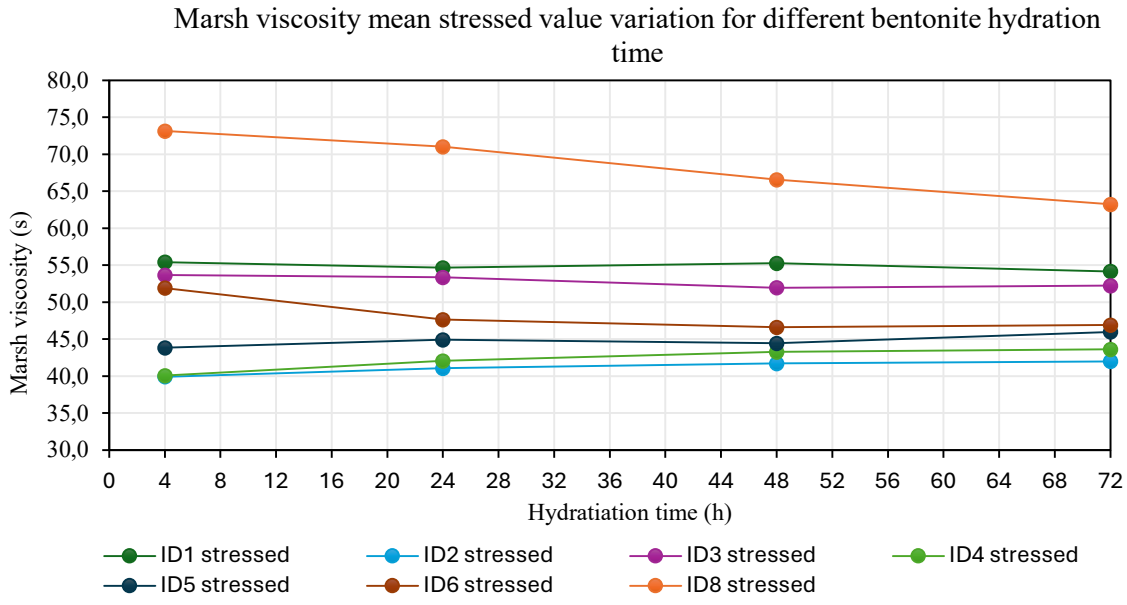

Figure 7.2 - Marsh viscosity mean stressed value variation for different bentonite hydration time

The result demonstrates that once bentonite reaches the stabilization point, meaning a fully hydrated and stable network development, it becomes less susceptible to mechanical degradation. In figure 7.2 all bentonites except ID8 show, after 24 hours of hydration, constant or even higher mean viscosity values after the stress cycle. This behavior indicates a lower viscosity reduction or a higher structure rebuild capacity.

However, the magnitude of the reduction varies considerably among bentonites, reflecting the robustness of the gel network. Figure 7.3 presents the comparative analysis of bentonites through the Marsh viscosity value measured at 48 hours of hydration:

- in static conditions, without being subjected to mechanical stress
- before stress, referring to the first Marsh viscosity measurement at 48 hours, representing the recovered viscosity value after the 24 hours stress phase and subsequent rest period
- after mechanical stressing, using the mean value among the whole viscosity results of each stress phase

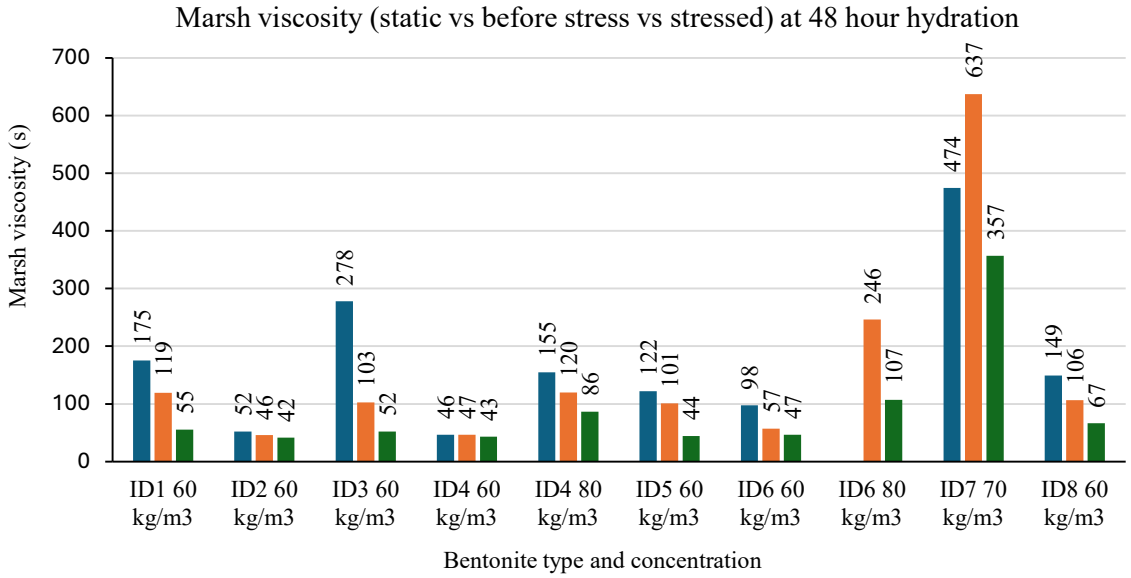

Figure 7.3 - Marsh viscosity variation measured at 48 hours, static, before stress and stressed

Figure 7.3 clearly shows that bentonite ID2, ID4 and ID6 maintain almost the same viscosity value in each condition, with very limited drop after stress, in line with the poorly developed or predominant flocculated structure, characterized by low thixotropy and rebuilding capacity. The other bentonite shows similar degradation after mechanical stress, converging toward comparable low viscosity values of approximately 45-55 s.

Bentonite ID1, ID5, ID8 fall into an intermediate category, showing moderate viscosity drop and good thixotropic response, reaching viscosity values close to those measured in static

conditions. Bentonite ID3 shows an important decrease in viscosity, leading to very low value respect to the static result, suggesting highly structure development but mechanically fragile. Bentonite ID6 80 kg/m^3 and ID7 70 kg/m^3 present high viscosity even after mechanical stress, confirming the more cohesive and resistant network that the concentration increase is able to develop.

Overall, the result demonstrates that for bentonites, the response to shear and ability to recover structure are both strongly controlled by slurry concentration and resulting microstructure. The best performing slurries are those combining high static viscosity value with good post-stress ability.

From a more operational perspective, the filter cake test underlines the major influence of slurry concentration on the development of good quality filter cake, demonstrating that higher concentration and viscosity are key parameters for efficient tunnelling operation.

The present research thesis has reached the proposed objective of evaluating the rheology of bentonite slurries prepared with different bentonites, highlighting significant variations in their behavior under mechanical stress. It is fundamental to underline the laboratory scale of this result, due to the very limited amount of mechanical stress that was possible to recreate in the laboratory, with respect to the one experienced during SS-TBM excavation.

For future research on this topic, it would be interesting to correlate these rheological results with more detailed structural analysis, starting from an evaluation of each bentonite composition, through XRD analysis. In addition, trying to recreate higher shear stresses closer to those experienced in the excavation site would provide a deeper understanding of slurry performances.

List of iconographic references

Figure 1.1 - Torino*Storia*. (2019). *Il Buco di Viso: il primo traforo delle Alpi*. Torino Storia. Retrieved August 20, 2025, from https://torinostoria.com/il-buco-di-viso-il-primo-traforo-delle-alpi

Figure 2.1 - The Robbins Company. (2025). *Single Shield TBMs* [Web page]. Retrieved October 18, 2025, from https://www.robbinstbm.com/products/tunnel-boring-machines/single-shield/

Figure 2.2 – Peila, D. (2022). L8 – Rock TBM (Power point slide lesson). Not public lesson, Tunnelling course, Polytechnic of Turin. Photo present in a slide, courtesy Herrenknecht AG.

Figure 2.3 - Herrenknecht AG. *Single Shield TBM* (web page with video). from: https://www.herrenknecht.com/en/products/productdetail/single-shield-tbm/ (retrived 14 ottobre 2025).

Figure 2.4 - Herrenknecht AG. *Single Shield TBM* (web page with video). from: https://www.herrenknecht.com/en/products/productdetail/single-shield-tbm/ (retrived 14 ottobre 2025).

Figure 2.5 - TunnelPro S.p.A. *Double Shield TBM.* Retrieved October 18, 2025, from https://tunnelpro.it/en/double-shield-tbm

Figure 2.6 - Herrenknecht AG. (s.d.). *Single Shield TBM* (web page with video). from: https://www.herrenknecht.com/en/products/productdetail/single-shield-tbm/ (retrived 18 ottobre 2025).

Figure 2.7 - Attewell, P. B., Yeates, J., & Selby, A. R. (1986). *Soil movements induced by tunnelling and their effects on pipelines and structures.* London: Blackie Academic & Professional.

Figure 2.8 - Zhao, C., Alimardani Lavasan, A., Barciaga, T., & Schanz, T. (2019). *Mechanized tunneling induced ground movement and its dependency on the tunnel volume loss and soil properties. International Journal for Numerical and Analytical Methods in Geomechanics, 43*(4), 781–800. https://doi.org/10.1002/nag.2890

Figure 2.9 - The Robbins Company. (2025). *Earth Pressure Balance TBM* [Web page]. Retrieved October 19, 2025, from https://www.robbinstbm.com/products/tunnel-boring-machines/single-shield/

Figure 2.10 - Herrenknecht AG. *EPB Shield.* Retrieved October 19, 2025, from https://www.herrenknecht.com/en/products/productdetail/epb-shield/

Figure 2.11 - Herrenknecht, M. (2011). *The development of earth pressure shields – from the beginning to the present*. *Geomechanics and Tunnelling, 4*(6), 469–481. https://doi.org/10.1002/geot.201100048

Figure 2.12- Budach, C., & Thewes, M. (2015). *Application ranges of EPB shields in coarse ground based on field tests*. Tunnelling and Underground Space Technology, 50, 296–304. https://doi.org/10.1016/j.tust.2015.07.010

Figure 2.13 - Qin, S., Cheng, Y., & Zhou, W.-H. (2023). State-of-the-art review on pressure infiltration behavior of bentonite slurry into saturated sand for TBM tunneling. *Smart Construction and Sustainable Cities, 1*(1), 14–36. https://doi.org/10.1007/s44268-023-00018-y

Figure 2.14 - Maidl, B., Thewes, M., & Maidl, U. (2004). *Handbook of Tunnel Engineering I: Structures and Methods*. Berlin: Ernst & Sohn.

Figure 2.15 - Thermosag India Pvt Ltd. *Hydrocyclone manufacturer in India*. Retrieved October 14, 2025, from https://thermosag.com/hydrocyclone-manufacturer/

Figure 2.16 - Kindle-Tech. (2024, January 1). *Understanding filter press: Function, components and applications*. Retrieved October 20, 2025, from https://kindle-tech.com/articles/understanding-filter-press-function-components-and-applications

Figure 2.17 - Peila, D. (2022). L8 – Soft ground mechanizes tunnelling TBM (Power point slide lesson). Not public lesson, Tunnelling course.

Figure 2.18 - Zhai, J., Wang, Q., Yuan, D., Zhang, W., Wang, H., Xie, X., & Shahrour, I. (2022). Clogging Risk Early Warning for Slurry Shield Tunneling in Mixed Mudstone–Gravel Ground: A Real-Time Self-Updating Machine Learning Approach. *Sustainability, 14*(3), 1368. https://doi.org/10.3390/su14031368

Figure 3.1 - Ontario: Marmora ash beds — Canada (Ontario) Beneath Our Feet. (2016, July 7). *Weathered volcanic ash bed within limestone* [Andy Fyon (July 7, 2016)]. Ontario: Marmora Ash Beds — Canada (Ontario) Beneath Our Feet. https://www.ontariobeneathourfeet.com/marmora-ash-beds

Figure 3.2 - Obsidian (volcanic glass) sample. From "Obsidian," Encyclopedia Britannica, last updated July 23, 2025. Retrieved September 1, 2025, from https://www.britannica.com/science/obsidian

Figure 3.3 - Brown, G. E., Jr., Post, J. E., & Komadel, P. (2020). *Bentonite*. In *Reference module in earth systems and environmental sciences*. Elsevier. https://doi.org/10.1016/B978-0-12-818805-7.00009-6

Figure 4.2 - R. Caenn, H. C. Darley, and G. R. Gray, Composition and Properties of Drilling and Completion Fluids, Gulf Professional Pub-lishing, 2011.

Figure 4.3 - Kube, S., Schoesser, B., & Thewes, M. (2019). *Penetration behaviour of slurry in saturated soil – analysis of particle deposition on the basis of electrical resistance.* Institute for Tunnelling and Construction Management, Ruhr University Bochum.

Bibliography

- TorinoStoria. (2019, January 9). *Il Buco di Viso: il primo traforo delle Alpi*. Torino Storia. Retrieved August 20, 2025, from https://torinostoria.com/il-buco-di-viso-il-primo-traforo-delle-alpi

- Herrenknecht AG. *Tunnelling – Products*. Retrieved December 3, 2025, from https://www.herrenknecht.com/en/products/tunnelling/

- Tanzini, M. (2008). *Scavo meccanizzato. Opere sotterranee e gallerie*. Palermo: Dario Flaccovio Editore.

- Herrenknecht AG. *Single Shield TBM* [web page with video]. from: https://www.herrenknecht.com/en/products/productdetail/single-shield-tbm/ (retrived 14 ottobre 2025).

- Zhao, C., Alimardani Lavasan, A., Barciaga, T., & Schanz, T. (2019). *Mechanized tunneling induced ground movement and its dependency on the tunnel volume loss and soil properties. International Journal for Numerical and Analytical Methods in Geomechanics, 43*(4), 781–800. https://doi.org/10.1002/nag.2890

- Bilgin, N., & Copur, H. (2023). *The effect of EPB face pressure on TBM performance parameters in different ground conditions*. *Tunnelling and Underground Space Technology, 141*, 105–142. https://doi.org/10.1016/j.tust.2023.105142

- Herrenknecht, M. (2011). *The development of earth pressure shields – from the beginning to the present*. *Geomechanics and Tunnelling, 4*(6), 469–481. https://doi.org/10.1002/geot.201100003

- Maidl, B., Thewes, M., & Maidl, U. (2004). *Handbook of Tunnel Engineering I: Structures and Methods*. Berlin: Ernst & Sohn.

- Wang, X., Zhang, L., Chen, H., & Liu, J. (2024). *Investigation into the properties of two-component backfilling grouts prepared by substituting bentonite with slurry from slurry shield tunnelling treated by a hydrocyclone. Tunnelling and Underground Space Technology,* 147, 105026. https://doi.org/10.1016/j.tust.2024.105026

- Zhai, J., Wang, Q., Yuan, D., Zhang, W., Wang, H., Xie, X., & Shahrour, I. (2022). Clogging Risk Early Warning for Slurry Shield Tunneling in Mixed Mudstone–Gravel

Ground: A Real-Time Self-Updating Machine Learning Approach. *Sustainability, 14*(3), 1368. https://doi.org/10.3390/su14031368

· Grim, R. E., & Güven, N. (Eds.). (1978). *Bentonites: Geology, Mineralogy, Properties and Uses* (Vol. 24, Developments in Sedimentology). Amsterdam; New York: Elsevier Scientific Publishing Co.

· Bentonite**.** (2025, August 19). In *Wikipedia*. Retrieved September 1, 2025, from https://en.wikipedia.org/wiki/Bentonite

· Thermo Fisher Scientific. (n.d.). *X-ray Diffraction (XRD): A non-destructive technique to study all types of material*. Retrieved September 3, 2025, from https://www.thermofisher.com/

· Shirazi, S. A., Kawasaki, S., & Sassa, T. (2010). *Permeability and swelling characteristics of bentonite*. *Journal of GeoEngineering, 5*(3), 119–126. https://doi.org/10.6310/jog.2010.5(3).4

· Salah, K., Agwah, A. K., & Elsersy, A. (2025). *The influence of bentonite content on the properties of its mixture with kaolinite*. *Geotechnical Research, 12*(2), 134–145. https://doi.org/10.1680/jgere.23.00080

· Mishra, A. K., Ohtsubo, M., Li, L., & Higashi, T. (2011). Controlling factors of the swelling of various bentonites and their correlations with the hydraulic conductivity of soil-bentonite mixtures. *Applied Clay Science*, *52*(1–2), 78–84. https://doi.org/10.1016/j.clay.2011.01.033

· Jeon, H. Y. (2014). Temperature Effects and pH Value on Free Swell Behaviors of Bentonite Solutions. *Advanced Materials Research*, 983, 44–51. https://doi.org/10.4028/www.scientific.net/AMR.983.44

· Nurmunira, M., & Siddiqua, S. (2021). *Calcium bentonite vs sodium bentonite: The potential of calcium bentonite for soil foundation*. In Materials Today: Proceedings (Vol. 48, Part 4, pp. 822–827). 2nd International Conference on Innovative Technology and Sciences (iCITES 2020), Chennai, India. Elsevier Ltd. https://doi.org/10.1016/j.matpr.2021.02.386

· CMS Industries. (2025, maggio 3). *What is bentonite swelling power and why it matters*. CMS Industries. https://www.cmsindustries.in/bentonite/what-is-bentonite-swelling-power-and-why-it-matters/

· Kelessidis, V. C., Tsamantaki, C., & Dalamarinis, P. (2007). *Effect of pH and electrolyte on the rheology of aqueous Wyoming bentonite dispersions*. *Applied Clay Science, 38*(1-2), 86–96. https://doi.org/10.1016/j.clay.2007.01.011

· Kube, S., Schoesser, B., & Thewes, M. (2019). *Penetration behaviour of slurry in saturated soil – analysis of particle deposition on the basis of electrical resistance.* Institute for Tunnelling and Construction Management, Ruhr University Bochum.

· Qin, S., Cheng, Y., & Zhou, W.-H. (2023). State-of-the-art review on pressure infiltration behavior of bentonite slurry into saturated sand for TBM tunneling. *Smart Construction and Sustainable Cities, 1*(1), 14–36. https://doi.org/10.1007/s44268-023-00018-y

· Luckham, P. F., & Rossi, S. (1999). The colloidal and rheological properties of bentonite suspensions. Advances in Colloid and Interface Science, 82(1–3), 43–92. https://doi.org/10.1016/S0001-8686(99)00005-6

· Di Giovanni, A., Carigi, A., Saltarin, S., Bogdana, R. M., Todaro, C., & Peila, D. (2024). *Bentonite slurry for TBM application: laboratory tests for rheological properties and soil interaction.* Geoingegneria Ambientale e Mineraria, 61(2–3), 37–43. https://doi.org/10.19199/2024.172-173.1121-9041.037

· British Standards Institution. (1990). *BS 1377-2:1990 – Methods of test for soils for civil engineering purposes – Part 2: Classification tests.* London: BSI.

· ASTM International. (2020). *ASTM D4380-20: Standard test method for density of bentonitic slurries used in civil engineering*. West Conshohocken, PA: ASTM International. https://doi.org/10.1520/D4380-20

· Fungilab S.A. *Alpha Series Rotational Viscometer: Instruction Manual* (Software Version 1.0). Sant Feliu de Llobregat, Barcelona: Fungilab S.A.

· American Petroleum Institute. (2017). *API Specification 13B-1: Recommended practice for field testing water-based drilling fluids* (5th ed.). Washington, DC: API Publishing Services.